Terms and Conditions of Use of Digitised Theses from Trinity College Library Dublin

Copyright statement

All material supplied by Trinity College Library is protected by copyright (under the Copyright and Related Rights Act, 2000 as amended) and other relevant Intellectual Property Rights. By accessing and using a Digitised Thesis from Trinity College Library you acknowledge that all Intellectual Property Rights in any Works supplied are the sole and exclusive property of the copyright and/or other IPR holder. Specific copyright holders may not be explicitly identified. Use of materials from other sources within a thesis should not be construed as a claim over them.

A non-exclusive, non-transferable licence is hereby granted to those using or reproducing, in whole or in part, the material for valid purposes, providing the copyright owners are acknowledged using the normal conventions. Where specific permission to use material is required, this is identified and such permission must be sought from the copyright holder or agency cited.

Liability statement

By using a Digitised Thesis, I accept that Trinity College Dublin bears no legal responsibility for the accuracy, legality or comprehensiveness of materials contained within the thesis, and that Trinity College Dublin accepts no liability for indirect, consequential, or incidental, damages or losses arising from use of the thesis for whatever reason. Information located in a thesis may be subject to specific use constraints, details of which may not be explicitly described. It is the responsibility of potential and actual users to be aware of such constraints and to abide by them. By making use of material from a digitised thesis, you accept these copyright and disclaimer provisions. Where it is brought to the attention of Trinity College Library that there may be a breach of copyright or other restraint, it is the policy to withdraw or take down access to a thesis while the issue is being resolved.

Access Agreement

By using a Digitised Thesis from Trinity College Library you are bound by the following Terms & Conditions. Please read them carefully.

I have read and I understand the following statement: All material supplied via a Digitised Thesis from Trinity College Library is protected by copyright and other intellectual property rights, and duplication or sale of all or part of any of a thesis is not permitted, except that material may be duplicated by you for your research use or for educational purposes in electronic or print form providing the copyright owners are acknowledged using the normal conventions. You must obtain permission for any other use. Electronic or print copies may not be offered, whether for sale or otherwise to anyone. This copy has been supplied on the understanding that it is copyright material and that no quotation from the thesis may be published without proper acknowledgement.

Numerical Methods for the High Speed Solution of Integral Equations in Wireless Communications

Eamonn Pol O Nuallain

Department of Electronic and Electrical Engineering

University of Dublin

Trinity College

Submitted for the Degree of

Doctor of Philosophy

2000

I, the undersigned, declare that this thesis is entirely my own work, except where otherwise accredited, and that it has not been submitted for a degree in any other university or institution. This thesis may be borrowed on application to the Dean of Graduate Studies, University of Dublin, Trinity College and with the written consent of the author.
It may be borrowed or copied from October 1st 2005 upon request with the permission of the Librarian, University of Dublin, Trinity College.

Signed on the 30th of September 2000.

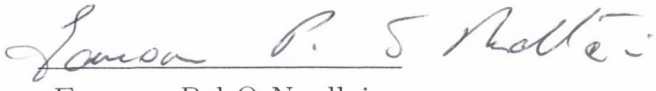

Eamonn Pol O Nuallain

DEDICATION

To my parents Bernadette and Eamonn.

SUMMARY

This thesis investigates the the appropriateness of integral equations for use in determining electric field coverage over sub-urban terrain which is illuminated by an arbitrarily placed transmitter.

Sub-urban terrain is the term used to describe undulating terrain with an homogeneous or piecewise homogeneous distribution of clutter (vegetation, buildings, rocks etc.).

The exact numerical solution for electric field coverage is given in the form of coupled integral equations.

These are the Coupled Electric Field Integral Equations (CEFIE) or the Combined Field Integral Equations (CFIE).

The field coverage is evaluated numerically using these equations over different terrain profiles consisting of various types of materials.

The CEFIE is reduced to a simpler Electric Field Integral Equation (EFIE) and its application in determining field coverage is justified mathematically and with field coverage results.

Published methods to speed up the calculation of coverage using the EFIE are implemented on various profiles at different frequencies.

These methods are the Natural Basis Method [57], the Green's Function Perturbation Method [58], the Fast Multipole Method/Fast Far Field Approximation [61]/[6] and the Tabulated Interaction Method [25].

These methods are then compared in terms of order of complexity of the algorithm, accuracy of results, memory requirement and complexity of code.

I introduce my own method, the Field Extrapolation Method (FEM) [62], and apply it as with the published methods.

By mathematical evaluation and comparison of results I note this method to have the lowest order of complexity, give the most accurate results, have the lowest memory re-

quirements and have the simplest code.

I conclude it is the most appropriate fast integral equation method to calculate field coverage over sub-urban terrain.

A statistical model for clutter is developed and the FEM is applied to this model over various profiles with varying degrees of clutter. The results confirm that the FEM is robust in its application to this type of terrain and the extent of signal distortion due to surface roughness mirrors the distortion of the original smooth surface.

Finally some of the better known non-integral equation methods for calculating field coverage are discussed.

These are the Physical Optics approximation [52], the Parabolic Equation Method [22], the Impedance Matrix Localisation Method [43], the Impedance Boundary Condition [21] and the Geometric and Uniform Theory of Diffraction [55].

The salient advantages and disadvantages of each of these methods are listed.

This thesis concludes that integral equation methods are an efficient means of estimating field coverage and that the FEM is the most appropriate of these methods for application to suburban terrain.

Having demonstrated its worth in sub-urban terrain the conclusion also expresses the author's belief that the FEM is the most promising integral equation method for coverage estimation in urban terrain and suggests this as a course for future research.

ACKNOLEDGEMENTS

I would like to thank Dr. Peter Cullen for his supervision and Teltec Ireland for funding this research. I would also like to thank my colleagues and the staff at the Department of Electronic Engineering for making my time here an enjoyable and memorable one. Particular thanks to Eamonn Kenny for his help with software.

GLOSSARY OF SYMBOLS

E	Electric Field Strength	V/m
E^I	Electric Field Incident from the Source	V/m
E^S	Scattered Electric Field	V/m
E^T	Total Electric Field	V/m
H	Magnetic Field Strength	A/m
J; J_s	Electric Current Density	A/m
M; M_s	Magnetic Current Density	A/m
F	Electric Vector Potential	C/m^2
A	Magnetic Vector Potential	T
ϵ	Electric Permittivity	F/m
ϵ_0	Electric Permittivity of Free Space	F/m
μ	Magnetic Permeability	H/m
μ_0	Magnetic Permeability of Free Space	H/m
σ	Conductance	Mhos
η	Intrinsic Impedance	Ohms
η_0	Intrinsic Impedance of Free Space	Ohms
ω	Angular Frequency	Radians/s
q	Charge Density	C/m^3
β	Propagation Constant	
ρ	Surface Position Vector to Source	
ρ'	Surface Position Vector to Observation Point	
ρ''	Position Vector to Observation Point (above Surface)	
i	Scattering Point	
j	Receiving Point	

G_l	Scattering Group
$G_{l'}$	Receiving Group
l	Centre Point of Scattering Group
l'	Centre Point of Receiving Group
∇_τ	Transverse Gradient Operator
i	$\sqrt{-1}$
C	Arbitrary Constant
G	Green's Function
$\mathcal{H}$	Hankel Function
$\bar{\mathcal{H}}$	Far-Field Approximation to the Hankel Function
$\mathcal{F}$	Fourier Transform Operator
$\hat{n}$	Unit Normal Vector
$\hat{t}$	Unit Tangent Vector
O	Order of Complexity
Δ_{xy}	$\mid xy \mid$ - the Euclidean Distance between points x and y

GLOSSARY OF ACRONYMS

EM	Electromagnetic
CC	Computational Cost
LHS	Left Hand Side
RHS	Right Hand Side
TM	Transverse Magnetic
PEC	Perfect Electrical Conductor
FT	Fourier Transform
FFT	Fast Fourier Transform
DFT	Discrete Fourier Transform
UHF	Ultra High Frequency
2-D	Two Dimensional
3-D	Three Dimendional
p.d.f.	Probability Density Function
w.r.t.	with respect to

CONTENTS

LIST OF FIGURES

LIST OF TABLES

LIST OF SYMBOLS

EFIE	Electric Field Integral Equation
MFIE	Magnetic Field Integral Equation
MoM	Method of Moments
PEC	Perfect Electric Conductor
CFIE	Combined Field Integral Equation
RWG	Rao-Wilton-Glisson
CG	Conjugate Gradient
CG-FFT	Conjugate Gradient-Fast Fourier Transform
FFT	Fast Fourier Transform
FAFFA	Fast Far-Field Approximation
TIM	Tabulated Interaction Method
UHF	Ultra High Frequency
ANIM	Analytical Interaction Method
NBS	Natural Basis Set
MLFAFFA	Multi-Level Fast Far-Field Algorithm
MLFMA	Multi-Level Fast Multipole Algorithm

INTRODUCTION

The need to effectively communicate using wireless systems is not easy to satisfy due to bandwidth limitations and to the complex behaviour of electromagnetic radiation as it propagates, scatters and attenuates.

Scattering and attenuation are more pronounced at higher frequencies posing severe problems in providing ubiquitous coverage for mobile communications providers whose bandvidth is at the upper end of the Ultra High Frequency (UHF) radio wave spectrum - (300 - 3000MHz).

The increased demand for better data transmission integrity, which is a current phenomenon in developed countries in the advent of the personal mobile phone and fax machines, means the provision of adequate field coverage via surface based transmitters will become an ever more challenging task.

It is conceivable, if not indeed likely, that these mobile devices will ultimately provide the services of a PC which will only exacerbate this demand.

Given the above demands, there is a relatively new interest in the use of integral equations in estimating field coverage because they are a form of the exact mathematical solution for this problem - which is to calculate the field coverage given by an arbitrarily based transmitter over an arbitrary surface profile.

To be in a position to offer a good mobile service, an effective transmitter network must be in place. For this network to be effective it must be derived from a suitable planning process (the alternative is an ad-hoc transmitter placement).

The purpose of this thesis is to aid this fast and accurate planning process by providing fast and accurate solutions for field coverage over sub-urban terrain.

The solution to this problem is slow by its very nature.

Popular solutions achieve their speed through a compromise in accuracy which is often unacceptable and leads to poor planning.

A concomitant fast and accurate planning tool can be provided using integral equation methods, the development of which is the focus of this thesis.

The propagation and scattering problem itself is expressed exactly as an integral equation and this provides the ideal starting point.

Elements of this integral equation can, *a priori*, be eliminated by virtue of their negligible contribution.

It is this feature of the integral equation formulation which makes it a suitable environment for finding fast computational methods which do not significantly compromise accuracy.

I am concerned with the computation of UHF radio wave propagation in a suburban environment with application to cellular radio systems planning.

By suburban environment I mean undulating terrain with an homogeneous or piecewise homogeneous distribution of clutter (vegetation, buildings, rocks etc.).

I wish to develop a fast, efficient deterministic approach to this problem, taking into account clutter as a paramaterised random (probabilistic) distribution of scatterers on the surface.

It must be pointed out that the integral equations describing the problem can be written in differential form and so the integral equation methods presented here have their analogy in the differential domain.

Integral equations are by their nature easier to conceive, being as they are, simply summations. They are therefore preferable to use in the search for fast means of solving this problem.

The exact numerical solution of the integral equations for the problem would take days to solve for a couple of kilometres of terrain, even on a high speed computer. Clearly this is the reason that until recently integral equation methods were not popular.

An important model is commonly used with this problem which speeds up the algorithm significantly. This is the PEC model.

Here the surface is assumed to be a PEC which allows use of the much simpler integral equation for PECs.

Another important assumption is the Forward Scattering Approximation which assumes that radiation propagates primarily in a forward direction away from the source.

Both give comparable results with the exact solution in the case of grazing incidence which implies a surface based transmitter on terrain which is gently undulating.

It should be noted that the computed coverage results presented in this thesis are derived assuming the atmosphere and terrain have, respectively constant electrical permittivities (ϵ_0 is used for the atmosphere).

Atmospheric effects such as poor weather, humidity and convection currents, to name but a few, will result in greater attenuation, fading and scintillation effects respectivley [1], [2].

Wet or snow/ice-covered terrain will yield different coverage results than when the terrain is dry [21].

Polarization effects are ignored; all scattered radiation is taken to have the same polarization as the incident field [5], and the possibility of resonance effects having a significant effect on coverage is discounted as being unlikley at the frequencies considered (144 and 970MHz).

However, this phenomenon would likely become a significant problem as service providers are forced to move up the UHF band. Here, raindrops and snowflakes would be likley to form resonant cavities in which case rain/snow fall may cause effective blackouts [3].

This thesis attempts to provide the reader with an intuitively acceptable means with which to understand integral equations in electromagnetics and the fast means used to solve them.

Research presented in this thesis justifies the PEC model and provides the fastest and most efficient method to date to calculate the field over sub-urban terrain.

The thesis will conclude with an analysis of coverage results which will be used as a base for the argument that integral equation methods offer the best means to address the terrain scattering problem.

ELECTROMAGNETIC SCATTERING THEORY

Modern Electromagnetic Scattering Theory is founded on the laws of Electromagnetism, which are Maxwell's Equations [5] and the constitutive relations for matter.

2.1 Maxwell's Equations

Maxwell's Equations are given here (a time dependence of $e^{i\omega t}$ is assumed) [52]:

$$\nabla \times H(\rho) = i\omega D(\rho) + J(\rho) \tag{2.1}$$

$$\nabla \times E(\rho) = -i\omega B(\rho) \tag{2.2}$$

$$\nabla \cdot D(\rho) = q(\rho) \tag{2.3}$$

$$\nabla \cdot B(\rho) = 0 \tag{2.4}$$

- where ω is the radiation frequency (rad/s), q is charge density and ρ is a position vector. They are respectively the laws of Ampere and Maxwell, Faraday and Lenz, Gauss and Biot and Savart.

Ampere's law was corrected by Maxwell to include the Displacement Current term $i\omega D$.

The above position-only vectors are complex quantities and are related to the original position and time dependent quantities by:

$$V(\rho, t) = Re\left[V(\rho)e^{i\omega t}\right] \tag{2.5}$$

2.2 The Constitutive Relations for Linear Matter

The following consituitive relations apply for linear matter - Harrington[19]:

$$D = \bar{\epsilon}E + \bar{\epsilon}_1\frac{\partial E}{\partial t} + \bar{\epsilon}_2\frac{\partial^2 E}{\partial t^2} + ... \tag{2.6}$$

$$B = \bar{\mu}H + \bar{\mu}_1\frac{\partial H}{\partial t} + \bar{\mu}_2\frac{\partial^2 H}{\partial t^2} + ... \tag{2.7}$$

$$J = \bar{\sigma}E + \bar{\sigma}_1\frac{\partial E}{\partial t} + \bar{\sigma}_2\frac{\partial^2 E}{\partial t^2} + ... \tag{2.8}$$

and can be approximated by:

$$D = \tilde{\bar{\epsilon}}E \tag{2.9}$$

$$B = \tilde{\bar{\mu}}H \tag{2.10}$$

$$J = \tilde{\bar{\sigma}}E \tag{2.11}$$

- where the tilde superscript denotes a complex quantity and the bar superscript denotes a tensor.

Empirically:

$$\tilde{\bar{\epsilon}} = \bar{\epsilon} + j\frac{\bar{\sigma}}{\omega} \tag{2.12}$$

Matter is termed 'simple' if the above complex quantities denoted with the tilde superscript can be replaced by scalars.

It is termed isotropic if the above tensors can be replaced by scalars.

2.3 The Vector Wave Equation

The Vector Wave Equations in E and H are derived from Maxwell's equations by taking the curl of (2.) and using the vector identity:

$$\nabla \times \nabla \times V = \nabla\nabla \cdot V - \nabla^2 V \tag{2.13}$$

- where V is an arbitrary vector.

The Vector Wave Equation for the Electric Field is:

$$\nabla \times \bar{\mu}^{-1} \nabla \times E(\rho) - \omega^2 \bar{\epsilon} \cdot E(\rho) = i\omega J(\rho) \tag{2.14}$$

- where $\bar{\mu}$ and $\bar{\epsilon}$, the magnetic permeability and electric permittivity, are rank 2 tensors.

In an homogeneous isotropic medium the Vector Wave equation becomes:

$$\nabla \times \nabla \times E(\rho) - \epsilon^2 E(\rho) = i\omega\mu J(\rho) \tag{2.15}$$

- which can bewritten

$$\nabla^2 E(\rho) + \epsilon^2 E(\rho) = -i\omega\mu \left(\bar{I} + \frac{\nabla\nabla}{\epsilon^2} \right) \cdot J(\rho) \tag{2.16}$$

-where $\bar{I}$ is theidentity operator and μ and ϵ are scalars.

By the DualityPrinciple [5], (2.16) can be written in terms of H and M.

The Vector Wave Equation is comprised of three coupled scalar wave equations.

The derivation of (2.16) is to be found in Chew[6].

The integral equations that describe the electromagnetic scattering problem we are about to investigate are derived from the wave equation via the application of the appropriate boundary conditions.

24 Green's Functions

A Green's Function is a physical system response to a Dirac delta type pulse.

The scalar Green's function, $g(\rho, \rho')$, is the solution to the Scalar Wave Equation where the current is the Dirac Delta function and it is:

$$g(\rho, \rho') = \frac{e^{i\beta|\rho-\rho'|}}{4\pi \mid \rho - \rho' \mid} \tag{2.17}$$

- where β is the wave number.

The Dyadic Green's Function, so named because it is a dyad or rank two tensor, is the analogous solution to the Vector Wave Equation.

For an homogeneous isotropic medium it is:

$$\bar{G}(\rho, \rho') = \left(\bar{I} + \frac{\nabla\nabla}{\epsilon^2}\right) g(\rho, \rho') \tag{2.18}$$

Derivations of (2.17) and (2.18) can be found in Chew[6] Because the Wave Equations are linear, the solution to an electromagnetic problem can be obtained by superposition.

2.5 Boundary Conditions

At the interface between two materials having relative permittivities ϵ_{r1}, ϵ_{r2} and permeabilities μ_{r1}, μ_{r2} and where there are no sources, the following conditions can be shown to hold at the boundary [5]:

$$\hat{n} \times (E_1 - E_2) = 0 \tag{2.19}$$

$$\hat{n} \times (H_1 - H_2) = 0 \tag{2.20}$$

$$\hat{n} \cdot (\epsilon_{r1} E_1 - \epsilon_{r2} E_2) = 0 \tag{2.21}$$

$$\hat{n} \cdot (\mu_{r1} H_1 - \mu_{r2} H_2) = 0 \tag{2.22}$$

- where $\hat{n}$ is the outward normal unit vector.

2.6 The Electric and Magnetic Vector Potentials

Consider Electric and Magnetic Fields E_A and H_A due to the Electric Current J only. Then [16] shows how:

$$E_A = \frac{\nabla\nabla \cdot A + \beta^2 A}{i\omega\epsilon} \tag{2.23}$$

- where A is the solution to:

$$\nabla^2 A + \beta^2 A = -J \tag{2.24}$$

which gives:

$$A = \int_V J_v(\rho') \frac{e^{-i\beta|\rho-\rho'|}}{4\pi \mid \rho - \rho' \mid} dv' \tag{2.25}$$

or

$$A = \int_S J_s(\rho') \frac{e^{-i\beta|\rho-\rho'|}}{4\pi \mid \rho - \rho' \mid} ds' \tag{2.26}$$

- depending on whether one is solving the Wave Equation in a volume or on a surface.

By exact analogy with the above it can be shown that

$$E_F = -\nabla \times F \tag{2.27}$$

- where F is the solution to:

$$\nabla^2 F + \beta^2 F = -M \tag{2.28}$$

which is:

$$F = \int_V M_v(\rho') \frac{e^{-i\beta|\rho-\rho'|}}{4\pi \mid \rho - \rho' \mid} dv' \tag{2.29}$$

or

$$F = \int_S M_s(\rho') \frac{e^{-i\beta|\rho-\rho'|}}{4\pi \mid \rho - \rho' \mid} ds' \tag{2.30}$$

A and F are the Magnetic and Electric Vector Potentials respectively.

By Superposition the total Electric Field is then:

$$E = E_A + E_F \tag{2.31}$$

Hence the general olution for the field radiated by a surface current is:

$$E^s(\rho) = \frac{\nabla\nabla \cdot + \beta^2}{\imath\epsilon} \int_S J_s(\rho') \frac{e^{-i\beta|\rho-\rho'|}}{4\pi \mid \rho - \rho' \mid} ds' - \nabla \times \int_S M_s(\rho') \frac{e^{-i\beta|\rho-\rho'|}}{4\pi \mid \rho - \rho' \mid} ds' \qquad (2.32)$$

Use of the Vector Potentials lead to intermediate differential equations which are uncoupled and simple. That i, each component, of say A, depends on the corresponding component of J only.

Use of A or F dos not decouple the original vector wave equation as can the use of Magnetic Current, which will be discussed in detail later.

Hence the only advantage in the use of A and F is in avoiding the use of complex operators (such as dyads) in olving the Vector Wave Equation.

2.7 Magnetic Current

The concept of Magnetic Current is to be used shortly in the Surface Equivalence Principle and the Coupled and Combined Field Integral Equations.

Magnetic current does not exist in the sense of electric current. I will devote some space here to explain what it is and where and why it should be used.

First it should be noted that magnetic current cannot be isolated because magnetic charges do not exist.

Secondly, magnetic current is used only as a mathematical convenience. It is an alternative representation for electric current.

In short, Magnetic Current (M) is an alternative representation in Faraday's Law for the Electric Current (J) which appears in Ampere's Law. There is thus a transform that relates both. Use of either or both is a question of convenience since the solution for the field is unaffected.

From Van Bladel [17] volume electric and magnetic currents are related by:

$$M_v(\rho) = -(\frac{1}{i\omega\epsilon})\nabla \times J_v(\rho) \tag{2.33}$$

and

$$J_v(\rho) = (\frac{1}{i\omega\mu})\nabla \times M_v(\rho) \tag{2.34}$$

A good example of the usefulness of Magnetic Current is in magnetic materials where rotating electric currents exist.

Applying the Continuity Equation to these electric currents yields:

$$\nabla \cdot J_v = i\omega q = 0 \tag{2.35}$$

- since there is no net inflow/outflow of charge.

Since any vector field is specified by its curl and divergence free components, this type of electric current can be completely described by a magnetic current M.

If the original electric current is a function of two orthogonal vectors - say $\hat{x}$ and $\hat{y}$ - then the equivalent magnetic current will be a function of the $\hat{z}$ vector only.

This means that the solution for J_v can be found by solving the Magnetic Vector Wave

Equation for M_v and converting the result to the equivalent J_v using (2.33).

The alternative to this would be having to solve the Electric Vector Wave Equation for J_v, which means solving two coupled scalar wave equations.

Hence, where J_v is rotating, does not diverge and is invariant in one direction, use of magnetic current allows one avoid the use of dyadic analysis in solving for J_v.

It should also be pointed out that if J varies in all directions $\hat{x}, \hat{y}$ and $\hat{z}$, conversion to magnetic current will result in having to solve two coupled scalar (magnetic) wave equations as opposed to three (electric).

In summary, appropriate use of magnetic current (i.e. where $\nabla \cdot J_v = 0$) reduces the dimensionality of solving the Vector Wave Equation by one.

The relations for surface electric and magnetic currents J_s and M_s are as follows [17]:

$$M_s = (\frac{1}{i\omega\epsilon})\hat{n} \times J\delta_s \tag{2.36}$$

and

$$J_s = -(\frac{1}{i\omega\epsilon})\hat{n} \times M\delta_s \tag{2.37}$$

where δ_s is defined by the functional:

$$< \delta_s, \phi >= \int_S \phi(\rho)dS = \int_V \delta_s\phi(\rho)dV \tag{2.38}$$

The notion of δ_s stems from the Dirac Delta Function, from whose definition the conversion of a line, surface or volume integral to a point value of a function is possible. This gives one the means to describe a distribution on a half-line or plane.

On the other hand, the definition of δ_s enables one to convert a volume integral to a surface integral. This gives one a tool to describe a distribution on a surface which is not necessarily planar.

The usefulness of surface magnetic current follows from its relation to surface electric current. That is, that a surface electric current which is a function of two orthogonal vectors may be described by a magnetic current which is a function of the third only.

It is immediately clear in this circumstance that if the Vector Wave Equation is to be solved on a surface, appropriate use of surface magnetic current gives the same advantages as the appropriate use of volume magnetic current above.

The key word here is 'appropriate'.

Above it was the use of volume magnetic current to describe a rotating electric current with zero divergence.

Here its use is in describing a surface electric current, which is a function of two orthogonal vectors, in terms of a surface magnetic current which is a function of the third orthogonal vector only.

2.8 The Surface Equivalence Principle

Consider the situation depicted in the figure below. Here we have two regions of space Γ_1 and Γ_2 separated by a mathematical surface S. One of the regions is unbounded.
Region 1 is homogeneous with electric and magnetic permeabilities ϵ_1 and μ_1 where Region 2 contains inhomogeneities that may include perfectly conducting materials.

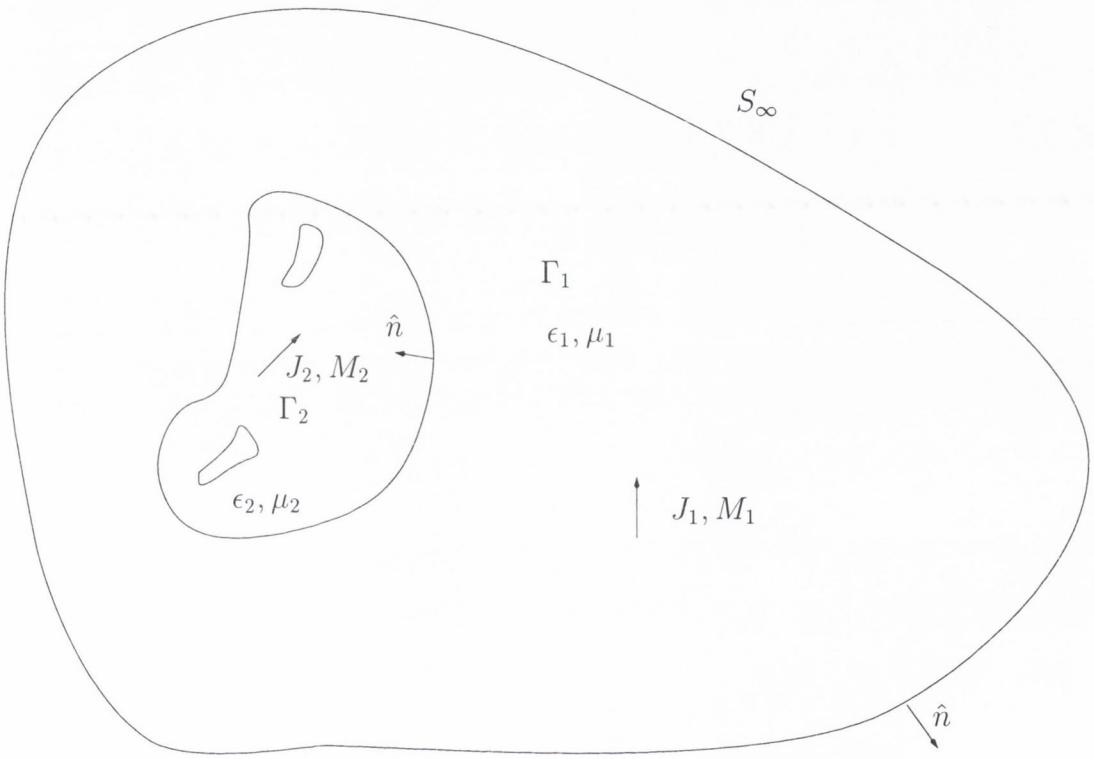

Figure 2.1: Two regions of space Γ_1 and Γ_2 separated by a mathematical surface S. Region 1 is homogeneous with (ϵ_1, μ_1) and Region 2 contains inhomogeneities that may include perfectly conducting materials. A source (J_2, M_2) in Region 2 produces fields (E_2, H_2) throughout Region 1. A second source (J_1, M_1) located in Region 1 radiates fields (E_1, H_1) throughout Region 1.

A source electric and magnetic current (J_2, M_2) is located in Region 2 and radiating in the presence of the inhomogeneities produces fields E_2 and H_2 throughout Region 1.
We postulate also a second source (J_1, M_1) located in Region 1 but radiating fields E_1 and H_1 in an homogeneous space having constitutive parameters ϵ_1 and μ_1.
The fields of both sources satisfy the Sommerfeld radiation condition [4] on the boundary at infinity (S_∞).

The Surface Equivalence Principle can be written as follows - Peterson [16]:

$$\hat{u} \cdot E_2(\rho) = \hat{u} \cdot \frac{\nabla\nabla \cdot + \beta^2}{i\omega\epsilon} \int_S (-\hat{n} \times H_2(\rho')) \frac{e^{-i\beta|\rho-\rho'|}}{4\pi \mid \rho - \rho' \mid} ds'$$
$$-\hat{u} \cdot \nabla \times \int_S (-E_2(\rho') \times \hat{n}) \frac{e^{-i\beta|\rho-\rho'|}}{4\pi \mid \rho - \rho' \mid} ds' \tag{2.39}$$

This equation is a statement that the field produced by (J_2, M_2) at some location outside of Region 2 can be expressed in the form of an integration over the tangential fields on the surface of Region 2.

The equation is of the form of (2.32) which is the general solution for the field radiated by a volume or a surface current.

For this reason we identify the tangential component of the magnetic field at the surface as a surface electric current and the tangential component of the electric field at the surface as a surface magnetic current.

The Surface Equivalence Principle makes it reasonable to postulate that the field scattered from a surface can be completely specified according to an equation of the form of (2.39).

Proof of the Surface Equivalence Principle is given in the Appendix A.

2.9 The Electric and Magnetic Field Integral Equations

The derivation of Electric Field Integral Equation (EFIE) is based on the following postulates - [5], [16]:

$$E^T(\rho) = E^I(\rho) + E^S(\rho) \tag{2.40}$$

That is, the total observed field at a point equals the sum of the field incident from the source plus the field re-radiated or scattered by the surface -
and

$$\begin{aligned} E^S(\rho) = \frac{\nabla\nabla\cdot + \beta^2}{i\omega\epsilon}\int_S(-\hat{n}\times H(\rho'))\frac{e^{-i\beta|\rho-\rho'|}}{4\pi\mid\rho-\rho'\mid}ds' \\ -\nabla\times\int_S(-E(\rho')\times\hat{n})\frac{e^{-i\beta|\rho-\rho'|}}{4\pi\mid\rho-\rho'\mid}ds' \end{aligned} \tag{2.41}$$

- which means the scattered field can be expressed in terms of the tangential components of the total electric and magnetic fields at the boundary, which is the Surface Equivalence Principle.
Identifying the surface integrals as Electric and Magnetic Vector Potentials, and substituting (2.32) into (2.40) yields:

$$E^I(\rho) = E^T(\rho) - \left(\frac{\nabla\nabla\cdot A + \beta^2 A}{i\omega\epsilon} - \nabla\times F\right) \tag{2.42}$$

Taking the tangential components of both sides yields:

$$\hat{n}\times E^I(\rho) = -M_s(\rho) - \hat{n}\times\left(\frac{\nabla\nabla\cdot A + \beta^2 A}{i\omega\epsilon} - \nabla\times F\right) \tag{2.43}$$

- which is the EFIE.
The Magnetic Field Integral Equation (MFIE) is derived in a similar fashion yielding:

$$\hat{n}\times H^I(\rho) = J_s(\rho) - \hat{n}\times\left(\frac{\nabla\nabla\cdot A + \beta^2 A}{i\omega\epsilon} - \nabla\times F\right) \tag{2.44}$$

For a PEC the EFIE and MFIE are simplified by noting the tangential component of the total electric field at the interface is zero.

COVERAGE ESTIMATION WITH INTEGRAL EQUATIONS

As outlined in the introduction, fast Integral Equation methods are the focus of this thesis. In this chapter, a formalised approach to solving integral equations exactly is examined along with the results this method gives with the Forward Scattering Approximation. These results are compared with the measured results in superimposed plots.
In Chapter 7, fast Integral Equation methods applied to the terrain profiles given here are examined chronologically, giving the reader an understanding of the evolution of the latest methods. The coverage results these fast methods give, will be compared with the results given here.

3.1 Surface Profiles, Terrain Composition and Transmitter Frequencies

The surface profiles used in this thesis are:
1) 11Km of gently undulating Danish (Hjorring) terrain. Profiles and measurements supplied by Prof. Anderson of Alborg University.
2) 6Km of gently undulating Danish (Jerslev) terrain. Profiles and measurements supplied by Prof. Anderson of Alborg University.
3) 3.8Km of mountainous German terrain provided by Deutsche Telekom AG (no measurements available).

The Danish profiles will be used to illustrate:
1) The Forward Scattering Model.
2) The EFIE (PEC) methods.

The German profiles will be used to illustrate:

1) The CFIE and CEFIE methods.

2) The EFIE (PEC) methods.

3) The effect of surface roughness on field coverage.

Dielectric terrain compositions considered are:

1) Dry clay with relative complex electrical permittivity 2.44-i0.098 at 970MHz.

2) Dry sand with relative complex electrical permittivity 2.55-i0.041 at 970MHz.

3) Dry loamy soil with relative complex electrical permittivity 2.48-i0.036 at 970MHz.

These values were obtained from [19].

The transmitter frequencies used in this thesis are 144MHz and 970MHz.

1) A 144MHz transmitter frequency will be used to illustrate all EFIE (PEC) methods.

2) A 970MHz transmitter frequency will be used to illustrate all methods.

The transmitters will be placed 10.4M above the starting point of the Danish profiles and 52M above the German profile.

In all cases the surface will be irradiated with TM_z radiation emanating from the source, an infinite 1A carrying strip transverse to the 2-D surface profile.

The discretisation length used for the numerical evaluation of the integral equations is $\lambda/4$ and $\lambda/15$ (λ is the wavelength of the radiation emanating from the source) for PEC and dielectric surfaces respectively.

The resultant field will be observed 2.4M above the terrain profiles.

In the FAFFA, TIM and FEM group sizes of 100.0 and 3.0 times the radiation wavelength are used for the Danish and German profiles respectively unless otherwise stated.

In the TIM the tabulation is performed at intervals of $\pi/500$.

All computations are coded in C^{++} and run on an IBM RS6000 computer. Computation times are given in seconds for all methods. This information is in itself immaterial since computation times will vary depending on coding language, coding methodology, compiler/optimiser used etc. They are included to provide a means of approximate com-

parison.

The important feature of each method is the order of complexity of the solution and the memory requirements. Coding complexity is also assessed. This is a relative assessment and somewhat subjective. The relative availability of library code such as the FFT is not given consideration.

The following are plots of the three profiles used.

3.1.1 Surface Profiles

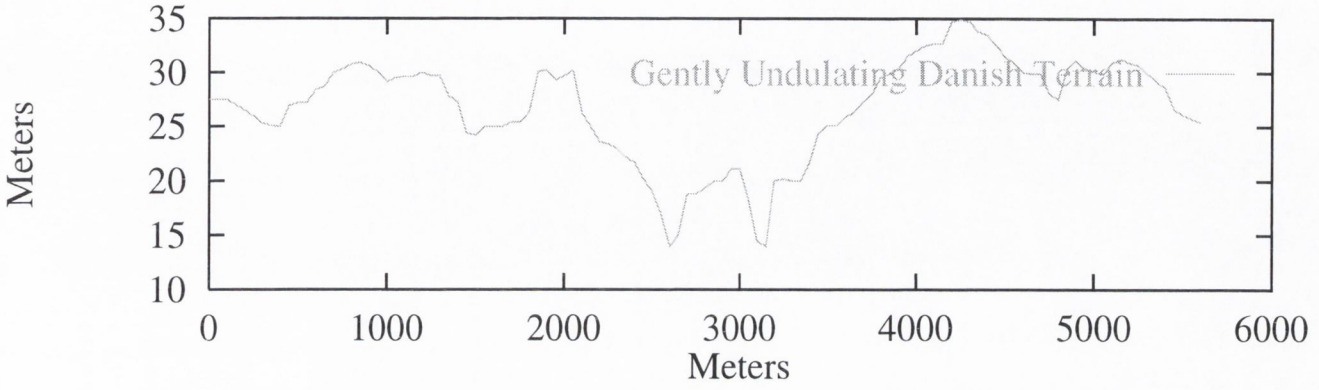

Figure 3.1: Danish (Jerslev) Terrain Profile. The surface co-ordinates are given at $50M$ intervals and are interpolated linearly.

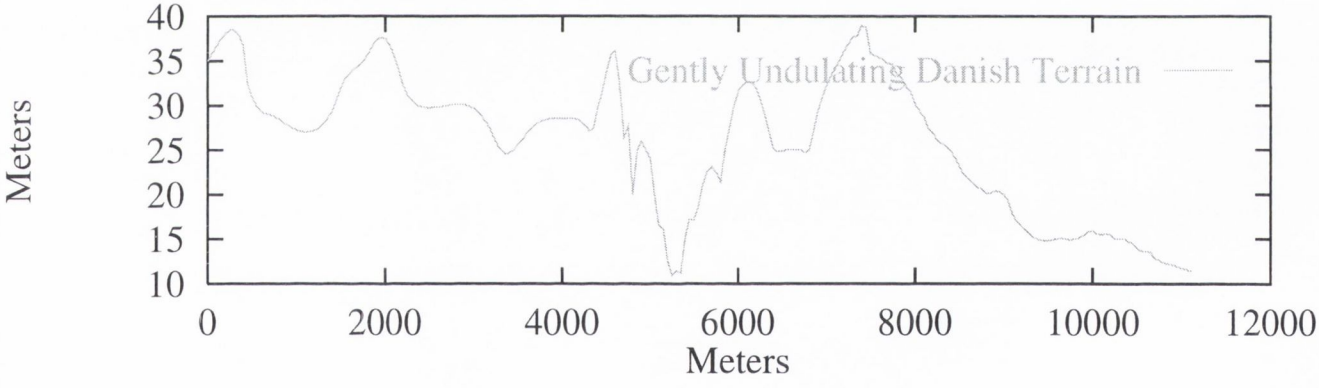

Figure 3.2: Danish (Hjorring) Terrain Profile. The surface co-ordinates are given at $50M$ intervals and are interpolated linearly.

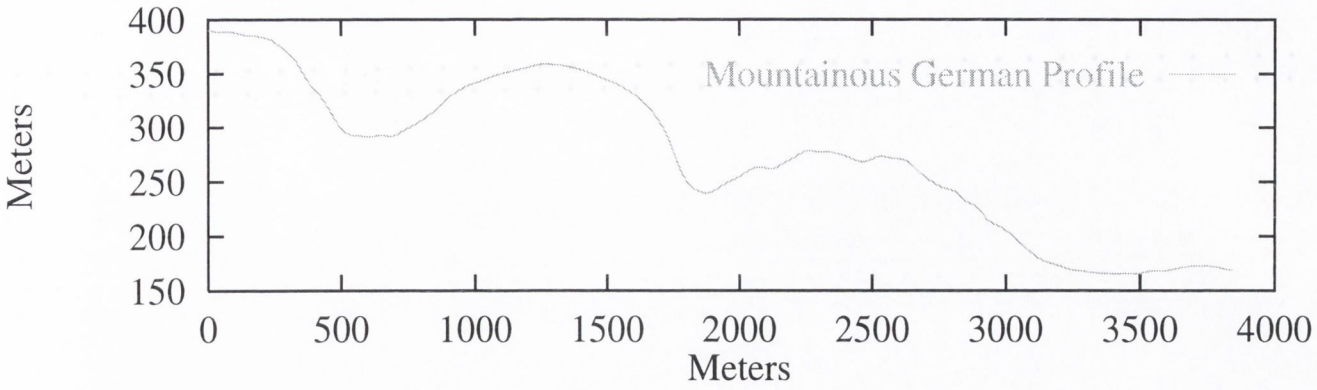

Figure 3.3: German Terrain Profile. The surface co-ordinates are given at $10M$ intervals and are interpolated linearly.

3.2 The Method of Moments (MOM)

This is a general method for reducing functional equations defined in a linear space to matrix equations - Harrington [18].

The EFIE is such a functional equation.

Consider the form of the EFIE over a surface S where source and observation points are ρ and ρ' respectively (I have ignored the constant factor $\beta\eta/4$ in the EFIE for simplicity):

$$E^I(\rho) = \int_S J(\rho')G(\rho, \rho')ds' \tag{3.1}$$

Discretising a $2-D$ surface into N segments allows us express the EFIE as a summation:

$$E^I(\rho) = \sum_{n=1}^{N} J(\rho'_n)G(\rho, \rho'_n)\Delta s'_n \tag{3.2}$$

To have the freedom to evaluate this summation and arrive at a general algorithm, which is the MOM, we express $J(\rho'_n)$ as a product $a_n g(\rho'_n)$, where a_n is a constant over the n^{th} domain. $g(\rho'_n)$ is referred to as a basis function.

We further enhance computational freedom by taking the inner product over each domain with functions w_n, called weighting functions.

That is, we allow ourselves apply weights at will should this be helpful to us in speeding up the summations:

$$\int_S w(\rho) \cdot E^I(\rho)ds = \int_S w(\rho) \cdot \sum_{n=1}^{N} J(\rho'_n)G(\rho, \rho'_n)\Delta s'_n ds \tag{3.3}$$

$$= \int_S w(\rho) \cdot \sum_{n=1}^{N} a_n g(\rho'_n)G(\rho, \rho'_n)\Delta s'_n ds \tag{3.4}$$

$$= \sum_{n=1}^{N} \int_{S_n} w_n \cdot a_n g(\rho'_n)G(\rho, \rho'_n)\Delta s'_n ds_n \tag{3.5}$$

If we assume a_n is constant over the n^{th} interval then a_n can be taken outside the integration to give:

$$\int_{S_n} w_n \cdot E^I(\rho_n)ds_n = \sum_{n=1}^{N} a_n \int_{S_n} w_n \cdot g(\rho'_n)G(\rho, \rho'_n)\Delta s'_n ds_n \tag{3.6}$$

There are N such equations, describing the incident field on the surface intervals, which can be expressed in matrix form:

$$[V] = [Z][J] \tag{3.7}$$

- where $[V]$, the supply vector, contains the fields from the source incident on each surface interval.

$[J]$, the current vector contains the surface currents on these intervals and $[Z]$, known as the impedance matrix, relates the two.

In $2-D$ the rank of $[Z]$ is $O(N^2)$ and in $3-D$ it is $O(N^3)$.

Should we choose the same weighting and testing functions, we have Galerkin's method. This often leads to simpler and symmetric impedance matrices [52].

If we choose the weighting functions to be Dirac Delta functions, we have what is known as the point matching method [52]. This method simplifies the calculation of $[Z]$.

3.3 The Forward Scattering Approximation (FSA)

The FSA assumes EM radiation propagates primarily in the forward direction (away from the source) i.e. backscattering effects are ignored.

This corresponds to setting elements in the upper-right triangle of the impedance matrix to zero, retaining the lower-left triangle and the upper-left to lower-right diagonal elements.

This approximation is good for undulating surfaces at grazing incidence where, due to the predominance of oblique angles of incidence of radiation on the surface, most radiation will not be reflected back towards the source.

The Forward Scattering Model is closely related to the PEC model in that oblique angles of incidence will give rise to total internal reflection.

Where the Forward Scattering model applies, so too does the PEC model and vice-versa. Both models are good approximations to the problem for slowly undulating terrain where the transmitter is surface based.

Evaluating the scattered field by the exact solution of the field integral equations without the use of the Forward Scattering model is cumbersome. The reason for this is not only that it is obviously more time-consuming but a very large amount of memory needs to be allocated to store the $N \times N$ impedance matrix. This is beyond the memory capacity of most computers for terrain profiles of length greater than 2Km.

The following plots are those of the electric field coverage measured and calculated using the forward scattering model at 144MHz and 970MHz.

The measured data (courtesy of Prof. Bach Anderson of Alborg University in Denmark) will obviously contain some backscattering effects which from viewing the superimposed plots for Jerslev profile are clearly negligible.

The FSA is assumed throughout the remainder of this thesis.

3.3.1 Results

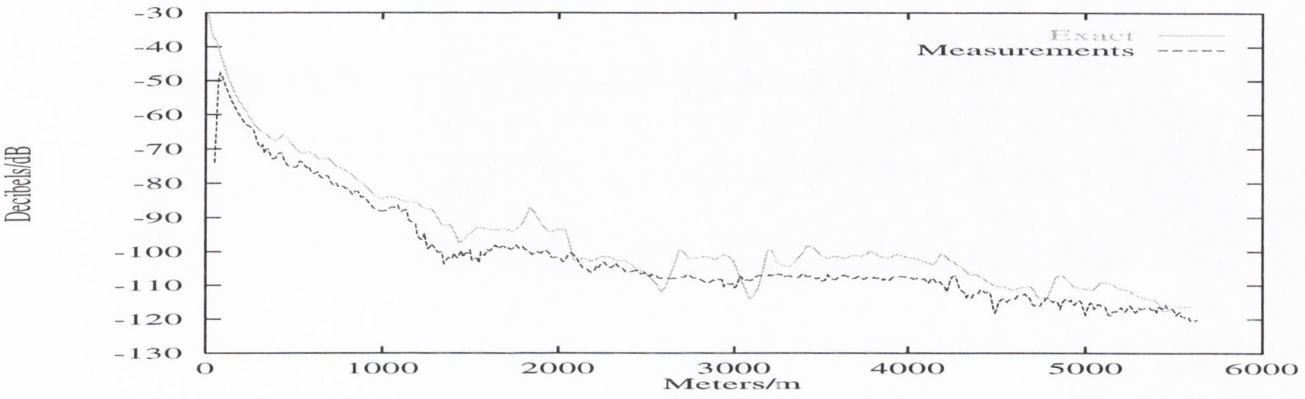

Figure 3.4: Electric Field coverage at 144MHz over the Jerslev profile.

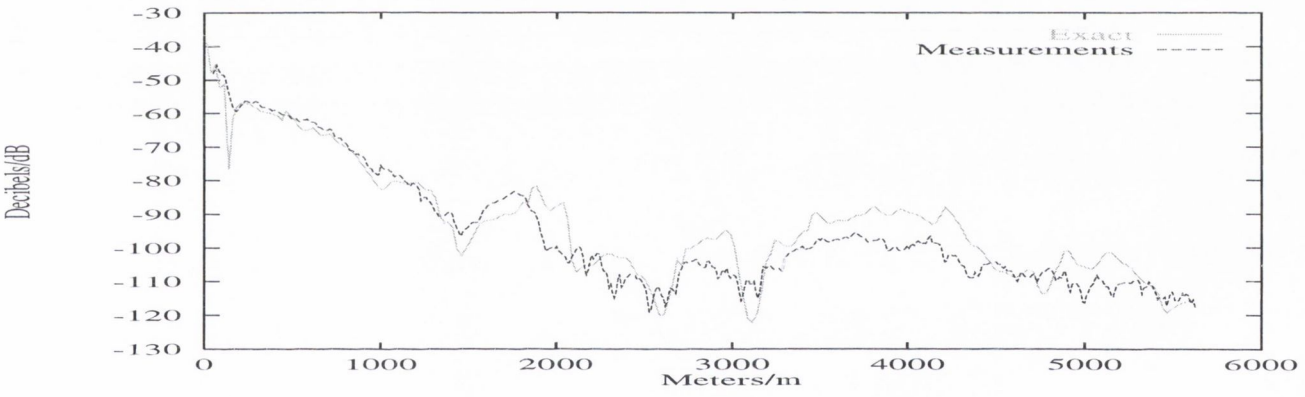

Figure 3.5: Electric Field coverage at 970MHz over the Jerslev profile.

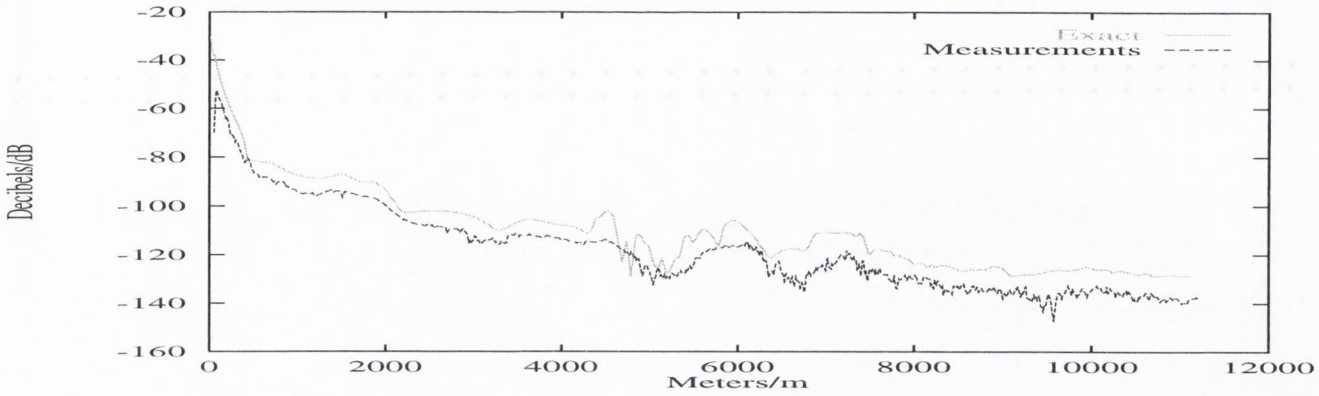

Figure 3.6: Electric Field coverage at 144MHz over the Hjorring profile.

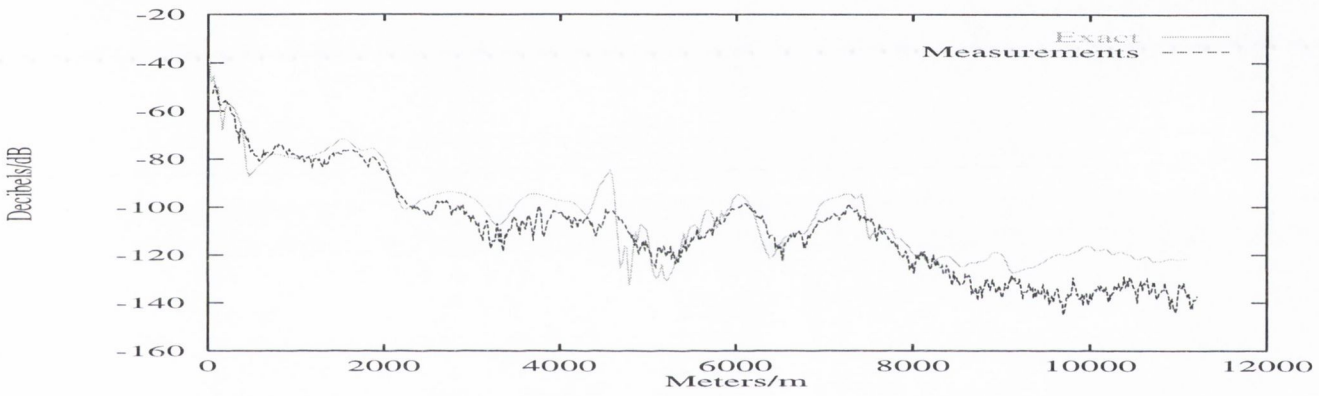

Figure 3.7: Electric Field Coverage at 970MHz over the Hjorring profile.

SCATTERING FROM DIELECTRIC SURFACES

The task is to calculate the total field in the $x - y$ plane in an homogeneous medium at a distance above a surface which is invariant in the z direction (2-D surface).

The surface is irradiated by an infinite unit amplitude current carrying line source in the z direction, a distance above the surface.

The problem geometry is illustrated in the following figure.

This figure will be referred to throughout this thesis

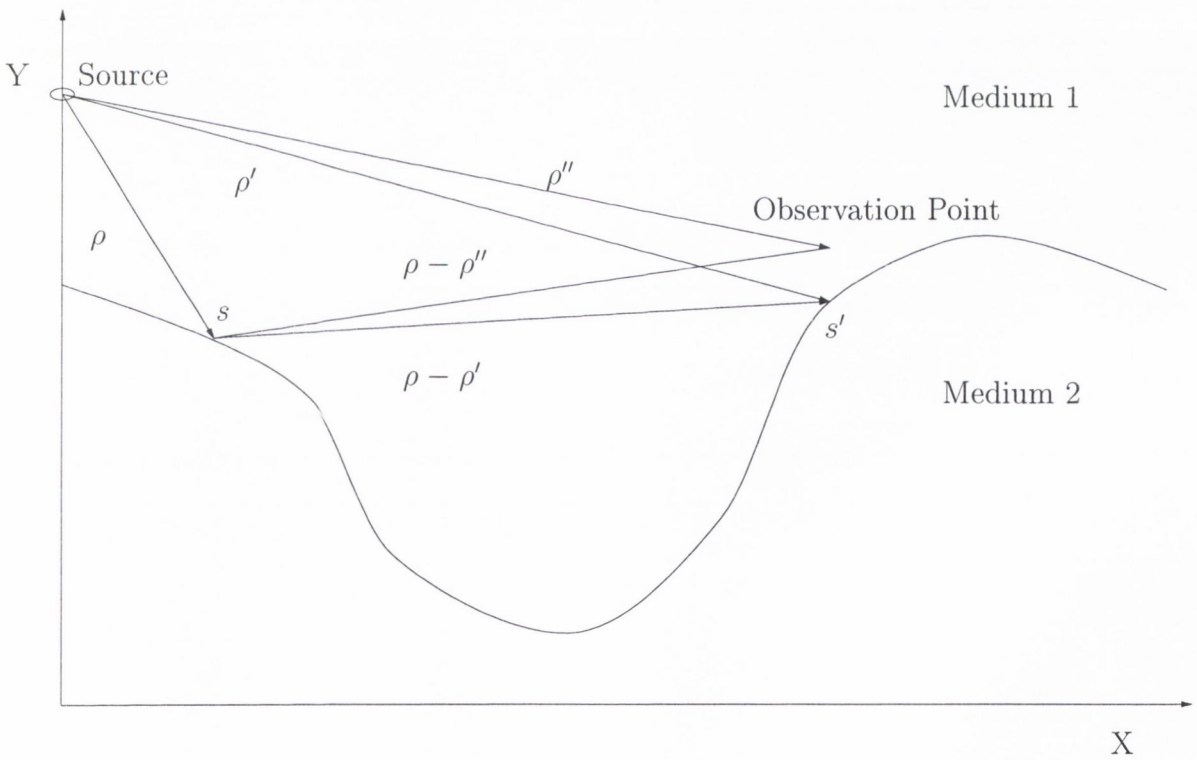

Figure 4.1: Terrain scattering geometry. The source, an infinite $1A$ carrying strip in the z direction, is placed above the starting point. Medium 1 is taken to be free space and Medium 2 is a solid dielectric or perfectly conducting material. The observation point is a distance above the surface. ρ, ρ' and ρ'' are position vectors.

4.1 Coupled Electric Field Integral Equations (CEFIE)

4.1.1 Theory

The Coupled EFIEs take the following form - Peterson [16]:

$$\hat{n} \times E^I(\rho) = -M_s(\rho) - \hat{n} \times \left(\frac{\nabla\nabla \cdot A_1 + \beta_1^2 A_1}{i\omega\epsilon_1} - \nabla \times F_1 \right)_{S+} \tag{4.1}$$

- evaluated just outside the surface.

$$0 = M_s(\rho) - \hat{n} \times \left(\frac{\nabla\nabla \cdot A_2 + \beta_2^2 A_2}{i\omega\epsilon_2} - \nabla \times F_2 \right)_{S-} \tag{4.2}$$

- evaluated just inside the surface.

Use of either the simpler EFIE or MFIE (these will be discussed in detail in subsequent chapters) alone necessitates evaluation of the fields at the surface. We may have good reason for not wanting to do this. Take for example the case of an infinitely thin PEC strip. Use of the EFIE for such a problem would be equivalent to imposing two conflicting boundary conditions:

One that the tangential magnetic field exists at the boundary and the other that it does not exist since the interior and exterior of the surface coincide.

In such a case one applies the EFIE simultaneously to the interior and exterior of the body [16].

Coupled EFIEs would normally be used however to calculate the surface currents on dielectric materials because unlike on a PEC, magnetic currents will exist on the surface and so with two unknowns, simultaneous integral equations must be applied to solve.

Coupled Magnetic Field Integral Equations can be stated in a similar fashion.

For the $2-D\ TM_z$ case the above equations become:

$$E^I(\rho) = M_s(\rho) + i\beta_1\eta_1 A_1 + \nabla_\tau \times F_1|_{S+} \tag{4.3}$$

- evaluated just outside the surface.

$$0 = -M_s(\rho) + i\beta_2\eta_2 A_2 + \nabla_\tau \times F_1|_{S-} \tag{4.4}$$

- where ∇_τ is the transverse gradient (in the $x-y$ plane) and :

$$A = \frac{1}{4i} \int J(\rho')\mathcal{H}_0^{(2)}(\beta\rho_{ll'})ds' \tag{4.5}$$

$$F = \frac{1}{4i} \int M(\rho') \mathcal{H}_0^{(2)}(\beta \rho_{ll'}) ds' \tag{4.6}$$

- where:

$$\mathcal{H}_0^{(2)}(\beta \mid \rho - \rho' \mid) = \int_{-\infty}^{+\infty} \frac{e^{i\beta|\rho-\rho'|}}{4\pi \mid \rho - \rho' \mid} dz \tag{4.7}$$

- is the $2-D$ Green's function.

From the MOM (4.1) and (4.2) can be written in matrix form thus:

$$[V] = [Z][J] \tag{4.8}$$

where each entry in the above is related by:

$$\begin{pmatrix} E \\ 0 \end{pmatrix} = \begin{pmatrix} A & B \\ C & D \end{pmatrix} \begin{pmatrix} J \\ M \end{pmatrix}$$

where

$$A_{mn} = \frac{\beta_1 \eta_1}{4} \int_{S_n} \mathcal{H}_0^{(2)}(\beta_1 \rho_{ll'}) ds' \tag{4.9}$$

$$B_{mm} = \frac{1}{2} \tag{4.10}$$

$$B_{mn} = \frac{\beta_1}{4i} \int_{S_n} cos(\phi_n - \phi_{ij}) \mathcal{H}_0^{(2)}(\beta_0 \rho_{ij}) ds' \tag{4.11}$$

- $m \neq n$

$$C_{mn} = \frac{\beta_2 \eta_2}{4} \int_{S_n} \mathcal{H}_0^{(2)}(\beta_2 \rho_{ll'}) ds' \tag{4.12}$$

$$D_{mm} = -\frac{1}{2} \tag{4.13}$$

$$D_{mn} = \frac{\beta_2}{4i} \int_{S_n} cos(\phi_n - \phi_{ij}) \mathcal{H}_0^{(2)}(\beta_2 \rho_{ij}) ds' \tag{4.14}$$

- $m \neq n$, from which J and M can be determined by the MOM.

The total field a distance above the surface is:

$$\begin{aligned} E(\rho'') &= E^I(\rho'') + \frac{\beta_0 \eta_0}{4} \int_{S_n} \mathcal{H}_0^{(2)}(\beta_0 \mid \rho_i - \rho'' \mid) ds' \\ &+ \frac{\beta_2}{4i} \int_{S_n} \cos(\phi_n - \phi_{il''}) \mathcal{H}_0^{(2)}(\beta_2 \mid \rho_i - \rho'' \mid) ds' \end{aligned} \tag{4.15}$$

The results which follow are those given by the Coupled EFIEs applied to the German terrain profile consisting of dry clay, sand and loam.

4.1.2 Analysis of Results

The most striking feature of the results which follow are how they are correlated with the surface profile.

This result is to be expected as radiation intensity will be lower in the troughs - a phenomenon referred to as 'shadowing'.

In the first and third troughs the radiation intensity increases noticably at the $500M$ and $3100M$ points where direct illumination by the source occurs.

The second trough is not directly illuminated at any point so over this region there is no sharp transition in radiation intensity except on entry to the trough. The fact that there is any radiation at all in this region is an illustration of the scattering phenomenon - i.e. that irradiated terrain acts as an antenna.

Another salient feature of these results is that there is little difference in the results given by terrain composed of dry clay sand and loam respectively.

This indicates that in calculating the field scattered by terrain it is not necessary to segment the surface profile and analyse on the basis of terrain composition unless very accurate results are required.

The results were obtained in 30 days.

4.1.3 Tabulated Characteristic Data

Computational Cost	Memory Requirement	Complexity of Code
$O(N^2)$	$O(N)$	Complex

Table 4.1: Computational Features of the CEFIE

4.1.4 Results

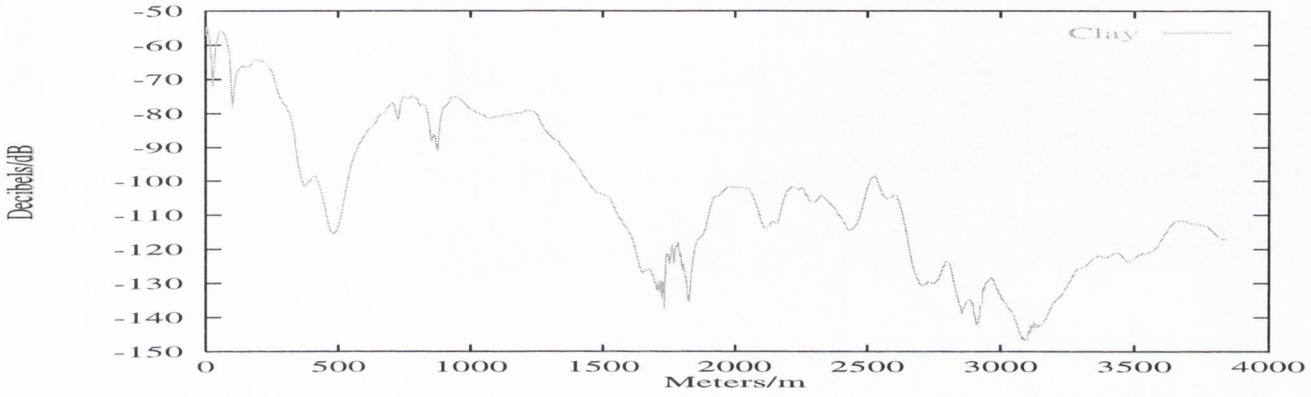

Figure 4.2: Electric Field Coverage at 970MHz over German Terrain consisting of Dry Clay ($\tilde{\epsilon_r} = 2.44 - i0.098$).

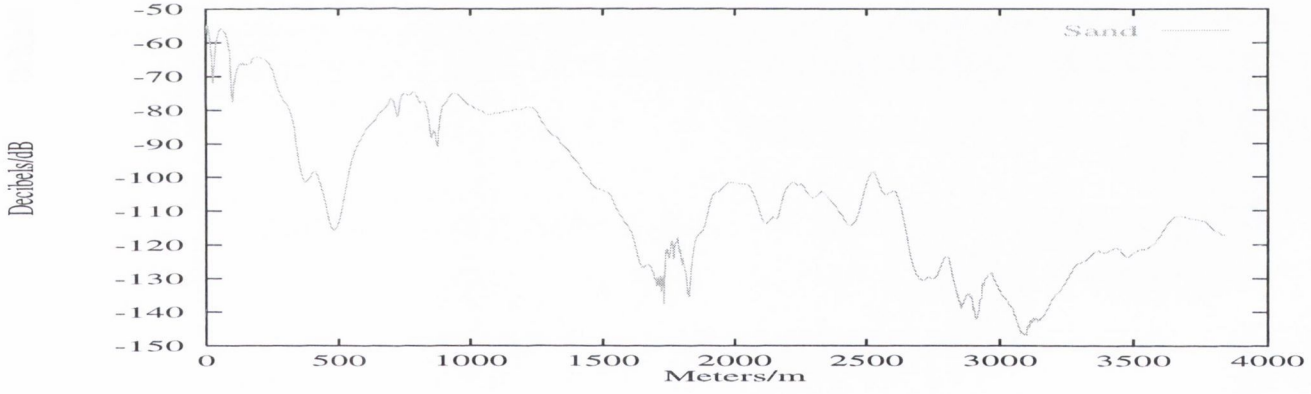

Figure 4.3: Electric Field Coverage at 970MHz over German Terrain consisting of Dry Sand ($\tilde{\epsilon_r} = 2.55 - i0.041$).

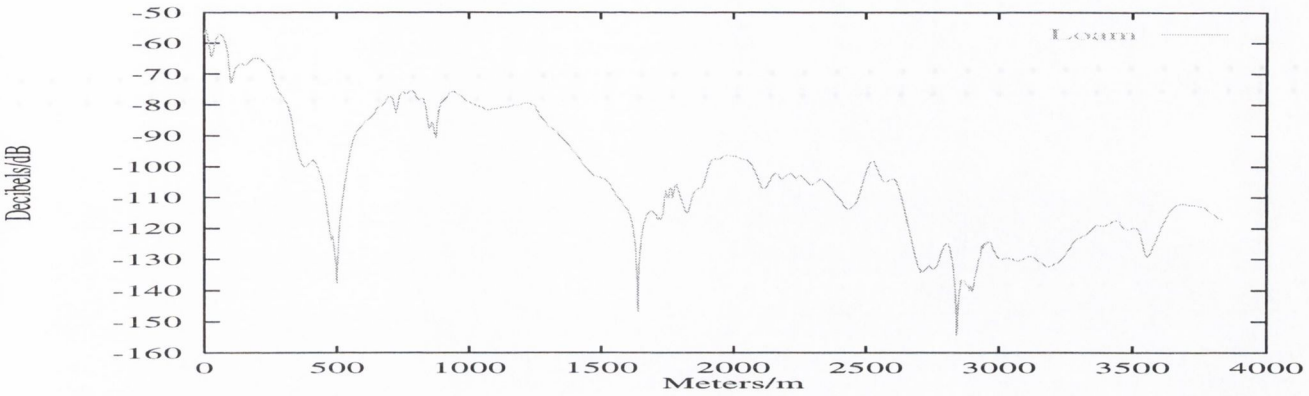

Figure 4.4: Electric Field Coverage at 970MHz over German Terrain consisting of Dry Loam ($\tilde{\epsilon_r} = 2.48 - i0.036$).

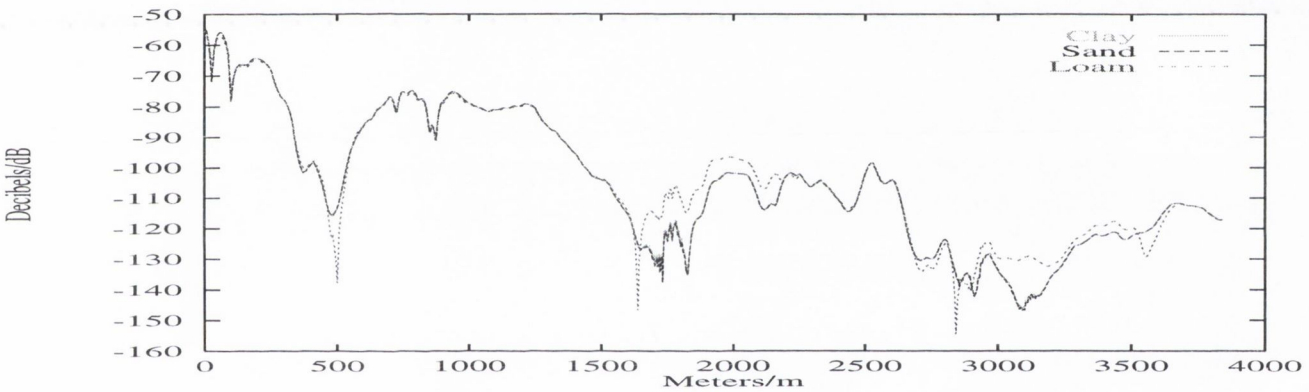

Figure 4.5: Comparative plot of Electric Field Coverage at 970MHz over German Terrain consisting of Dry Clay, Sand and Loam.

4.2 Combined Field Integral Equations (CFIE)

4.2.1 Theory

The Combined Field Integral Equations are used because of difficulties posed by the use of the EFIE or MFIE in obtaining a unique solution for bodies where resonance occurs [16]. The CFIE takes the following form [20]:

$$\hat{n} \times E^I(\rho) = \hat{n} \times \left(\frac{\nabla\nabla \cdot A_1 + \beta_0^2 A_1}{i\omega\epsilon_0} - \nabla \times F_1 + \frac{\nabla\nabla \cdot A_2 + \beta_2^2 A_2}{i\omega\epsilon_2} - \nabla \times F_2 \right)_S \quad (4.16)$$

$$\hat{n} \times H^I(\rho) = \hat{n} \times \left(\frac{\nabla\nabla \cdot F_1 + \beta_0^2 F_1}{i\omega\epsilon_0} - \nabla \times A_1 + \frac{\nabla\nabla \cdot F_2 + \beta_2^2 F_2}{i\omega\epsilon_2} - \nabla \times A_2 \right)_S \quad (4.17)$$

Obviously they are a couple comprised of a Combined EFIE and a Combined MFIE evaluated at the surface.

For the $2-D\ TM_z$ case the above equations become:

$$E^I(\rho) = i\omega\mu_0(A_0 + A_2) + \nabla_\tau \times (F_0 - F_2) \quad (4.18)$$

- evaluated just outside the surface.

$$H^I(\rho) = \nabla_\tau \times (A_0 - A_2) + i\omega\epsilon_0(F_0 + F_2) + \frac{\partial(\Psi_0 - \Psi_2)}{\partial s} \quad (4.19)$$

- where:

$$\Psi = \frac{1}{4\omega\mu} \nabla_\tau M(\rho') \mathcal{H}_0^{(2)}(\beta\rho_{il}) ds' \quad (4.20)$$

(4.16) and (4.17) can be written in matrix form thus:

$$\begin{pmatrix} E^I \\ H^I \end{pmatrix} = \begin{pmatrix} A & B \\ C & D \end{pmatrix} \begin{pmatrix} J \\ M \end{pmatrix}$$

where

$$A_{mn} = \frac{\beta_0\eta_0}{4} \int_{S_n} \mathcal{H}_0^{(2)}(\beta_0\rho_{ij}) + \mathcal{H}_0^{(2)}(\beta_2\rho_{ij}) ds' \quad (4.21)$$

$$B_{mm} = 0 \quad (4.22)$$

$$B_{mn} = \frac{\beta_1}{4i} \int_{S_n} \cos(\phi_{n'} - \phi_{ij})(\mathcal{H}_0^{(2)}(\beta_0\rho_{ij}) + \mathcal{H}_0^{(2)}(\beta_0\,\rho_{ij})) ds' \quad (4.23)$$

- $m \neq n$

$$D_{mm} = 0 \tag{4.24}$$

$$C_{mn} = \frac{\beta_1}{4i} \int_{S_n} \cos(\phi_n - \phi_{ij})(\mathcal{H}_0^{(2)}(\beta_0 \rho_{ij}) + \mathcal{H}_0^{(2)}(\beta_0 \rho_{ij}))ds' \tag{4.25}$$

$$\begin{aligned} D_{mn} = \frac{\omega\mu}{4} \int_{S_n} \cos(\phi_{n'} - \phi_n) \left(\epsilon_0 \mathcal{H}_0^{(2)}(\beta_0 \rho_{ij}) + \epsilon_2 \mathcal{H}_0^{(2)}(\beta_2 \rho_{ij}) \right) ds' \\ + \frac{\partial}{\partial s} \int_{S_n} \frac{\partial}{\partial s'} \frac{1}{4\omega\mu} \left(\mathcal{H}_0^{(2)}(\beta_0 \rho_{ij}) + \mathcal{H}_0^{(2)}(\beta_0 \rho_{ij}) \right) ds' \end{aligned} \tag{4.26}$$

- $m \neq n$, from which J and M can be determined by the MOM.

The derivatives are calculated using the finite difference method.

The total field a distance above the surface is as before:

$$\begin{aligned} E(\rho'') = E^I(\rho'') + \frac{\beta_0 \eta_0}{4} \int_{S_n} \mathcal{H}_0^{(2)}(\beta_0 \mid \rho_i - \rho'' \mid) ds' \\ + \frac{\beta_2}{4i} \int_{S_n} \cos(\phi_n - \phi_{il''}) \mathcal{H}_0^{(2)}(\beta_2 \mid \rho_i - \rho'' \mid) ds' \end{aligned} \tag{4.27}$$

The results which follow are those given by the CFIE applied to the German terrain profile consisting of dry clay, sand and loam.

4.2.2 Analysis of Results

The results obtained for the field coverage using the CFIE are identical to those given by the CEFIE and were obtained in a somewhat longer time of $3.08 \times 10^6 s$.

This not only serves to confirm the results obtained using the CEFIE but also to deduce that internal resonance is not a feature of irradiated terrain in that it effects the results for coverage - Peterson [16]. This is not surprising since terrain is an open surface.

However it is useful to note that pockets of resonance are not occurring where the surface is partially closed, say within a peak or a trough - a fact that will be underlined later in calculating the field coverage over rough surfaces.

The CEFIE is somewhat a less complex formulation than the CFIE.

The CFIE is used to calculate the scattered field in cases where resonance is likely to occur (i.e. from closed surfaces) - Peterson [16], Umashankar [20].

It may thus be safely said that the CEFIE is an appropriate algorithm with which to establish field coverage over terrain.

This fact will be used as a starting point in the justification of the use of the Electric Field Integral Equation (EFIE) - the PEC Model, in estimating coverage.

4.2.3 Tabulated Characteristic Data

Computational Cost	Memory Requirement	Complexity of Code
$O(N^2)$	$O(N)$	Complex

Table 4.2: Computational Features of the CFIE

4.2.4 Results

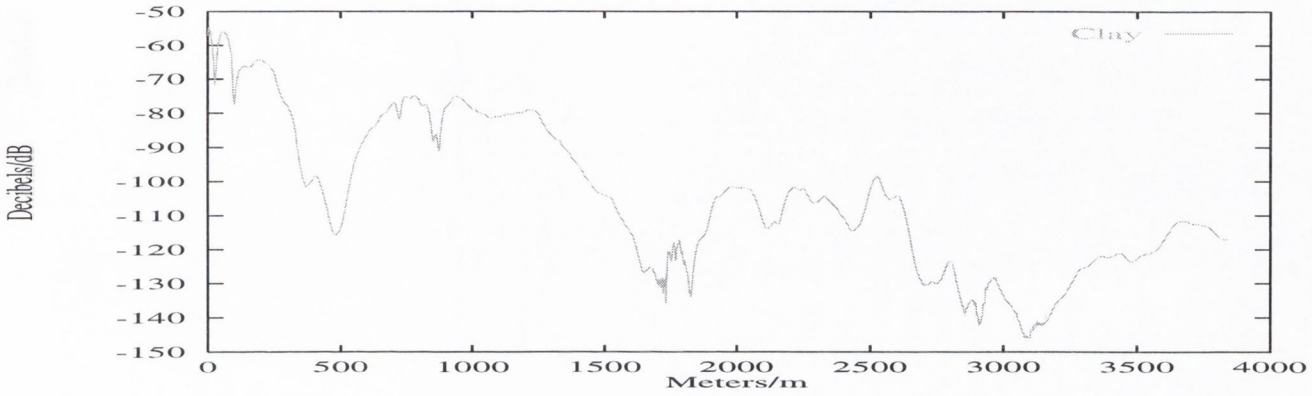

Figure 4.6: Electric Field Coverage at 970MHz over German Terrain consisting of Dry Clay ($\tilde{\epsilon_r} = 2.44 - i0.098$).

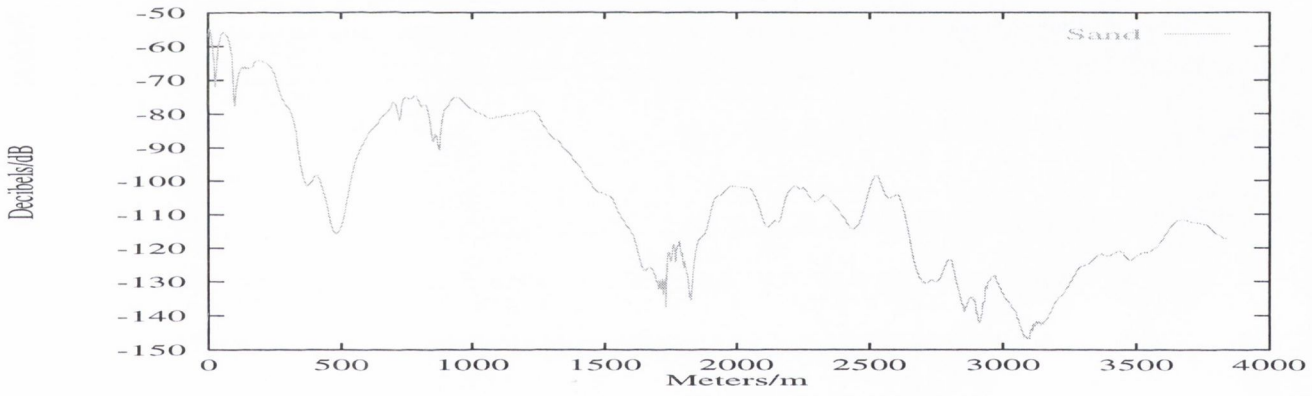

Figure 4.7: Electric Field Coverage at 970MHz over German Terrain consisting of Dry Sand ($\tilde{\epsilon_r} = 2.55 - i0.041$).

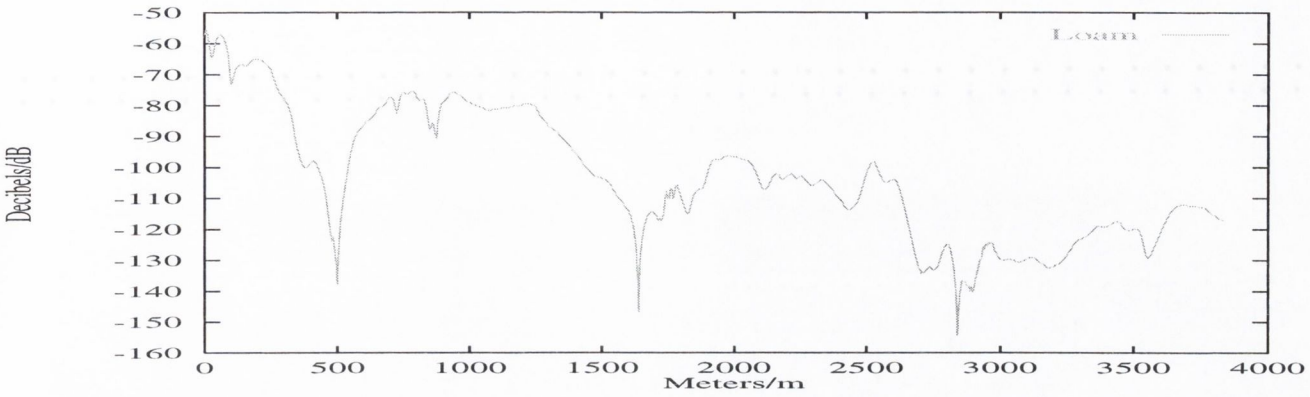

Figure 4.8: Electric Field Coverage at 970MHz over German Terrain consisting of Dry Loam ($\tilde{\epsilon_r} = 2.48 - i0.036$).

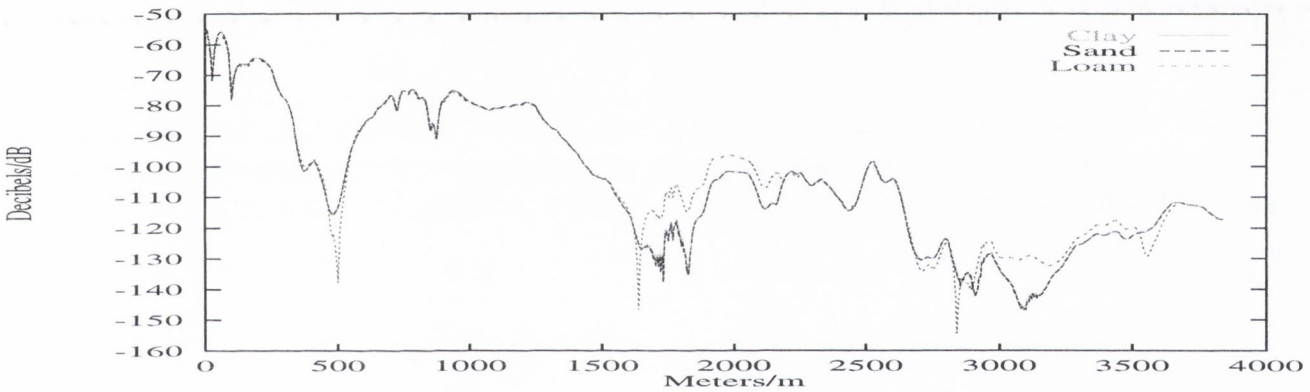

Figure 4.9: Comparative plot of Electric Field Coverage at 970MHz over German Terrain consisting of Dry Clay, Sand and Loam.

THE PEC MODEL

5.1 Introduction

Solving the Combined Field integral Equation and the Coupled Field Integral Equations is computationally extremely intensive.
The reasons for this are as follows:

1) The problem is $O(N^2)$ in two dimensions and $O(N^3)$ in three dimensions where N is the number of discretisations taken on the surface.
2) To guarantee a convergent solution the discretisation length must be at least one quarter of a wavelength.

While there is no escaping the physics of the problem which implies **1)**, there is something we can do about **2)**.
In **2)** it is necessary to take the discretisation length as one quarter the shortest wavelength.
In the dielectric problem two radiation wavelengths exist, that of the incident field in Medium 1 and that radiation which penetrates Medium 2.
These wavelengths are related by:

$$\frac{\lambda_1}{\lambda_2} = \sqrt{\frac{\epsilon_2}{\epsilon_1}} \tag{5.1}$$

For the dielectric media we are considering (dry clay, sand and loam) this means the wavelength of the radiation in these media is three to four times shorter than the incident radiation.
Were we able to consider the surface to be a PEC we could use a discretisation length that many times larger than for the equivalent dielectric problem. Also, the resulting integral

equation is a single integral equation in one unknown by virtue of the fact that no fields exist inside the surface of a PEC and the total electric field on the surface of a PEC is zero.

Assuming the surface to be a PEC is equivalent to assuming all radiation incident on the surface is reflected.

Recalling the Forward Scattering Approximation, where radiation is assumed to propagate away from the source, this model and the PEC model are valid where the radiation incident on the surface is largely at grazing incidence. This corresponds to total internal reflection in the case of a dielectric surface which is equivalent to assuming a PEC model. The PEC model is justified here mathematically for terrain and results are presented to validate the analysis and its conclusion.

5.2 Mathematical Justification of the PEC Model Terrain

5.2.1 Theory

Consider the sum of the coupled EFIEs:

$$\hat{n} \times E^I(\rho) = \hat{n} \times \left(\frac{\nabla\nabla \cdot A_1 + \beta_0^{(2)} A_1}{i\omega\epsilon_0} - \nabla \times F_1 \right)_{S^+} + \hat{n} \times \left(\frac{\nabla\nabla \cdot A_2 + \beta_2^2 A_2}{i\omega\epsilon_2} - \nabla \times F_2 \right)_{S^-} \tag{5.2}$$

where:

$$A_1 = \int_{S^+} J_s(\rho') G_1(\beta_0 \mid \rho - \rho' \mid) ds' \tag{5.3}$$

$$A_2 = \int_{S^-} J_s(\rho') G_2(\beta_2 \mid \rho - \rho' \mid) ds' \tag{5.4}$$

$$F_1 = \int_{S^+} M_s(\rho') G_1(\beta_0 \mid \rho - \rho' \mid) ds' \tag{5.5}$$

$$F_2 = \int_{S^-} M_s(\rho') G_2(\beta_2 \mid \rho - \rho' \mid) ds' \tag{5.6}$$

and the Greens' Functions are:

$$G_1 = \frac{1}{4i} \mathcal{H}_0^{(2)}(\beta_0 \mid \rho - \rho' \mid) \tag{5.7}$$

$$G_2 = \frac{1}{4i} \mathcal{H}_0^{(2)}(\beta_2 \mid \rho - \rho' \mid) \tag{5.8}$$

- for 2-D TM_Z.

I do not expect significant resonance problems with irradiated terrain because the surface is not closed which means I am not obliged to use the Combined Field Integral Equations [16].

Now, I will simplify the above for the 2-D TM_Z case.

Note in (5.2):

$$\nabla\nabla \cdot A = 0 \tag{5.9}$$

because:

$$\begin{aligned}\nabla\nabla\cdot A &= \nabla\nabla\cdot\int_{S^{\pm}}(-\hat{n}\times H(\rho'))G(\mid\rho-\rho'\mid)ds'\\ &= \nabla\int_{S^{\pm}}\nabla\cdot(-\hat{n}\times H(\rho'))G(\mid\rho-\rho'\mid))ds'\\ &= \nabla\int_{S^{\pm}}\Big((\hat{n}\times H(\rho'))\cdot\nabla G(\mid\rho-\rho'\mid)+G(\mid\rho-\rho'\mid)\nabla\cdot(\hat{n}\times H(\rho'))\Big)ds'\\ &= 0\end{aligned} \tag{5.10}$$

because ∇G is a vector in the $\hat{x}-\hat{y}$ plane and $\hat{n}\times H(\rho')$ is a vector in the $\hat{z}$ direction. Therefore their dot product is zero.

Also

$$\nabla\cdot(-\hat{n}\times H(\rho'))=0 \tag{5.11}$$

- by the continuity equation.

Therefore (5.2) becomes:

$$\hat{n}\times E^{I}(\rho)=\hat{n}\times\left(\frac{\beta_0^2}{i\omega\epsilon_0}A_1-\nabla\times F_1\right)_{S+}+\hat{n}\times\left(\frac{\beta_2^2}{i\omega\epsilon_2}A_2-\nabla\times F_2\right)_{S-} \tag{5.12}$$

- which if evaluated at the surface becomes:

$$\begin{aligned}\hat{n}\times E^{I}(\rho)=\hat{n}\times i\omega&\int_{S}(\hat{n}\times H(\rho'))(\mu_0G_1+\mu_2G_2)ds'\\ &+\hat{n}\times\int_{S}(\hat{n}\times E(\rho'))\times(\nabla' G_1+\nabla' G_2)ds'\end{aligned} \tag{5.13}$$

Note:

$$\nabla' G=\frac{\partial G}{\partial x'}\hat{x'}+\frac{\partial G}{\partial y'}\hat{y'} \tag{5.14}$$

$\equiv$

$$\nabla' G=(x-x')\mathcal{H}_0^{(2)}(\beta\mid\rho-\rho'\mid)\hat{x'}+(y-y')\mathcal{H}_0^{(2)}(\beta\mid\rho-\rho'\mid)\hat{y'} \tag{5.15}$$

- for $2-D\ TM_z$.

The slope of this vector is clearly $\frac{x-x'}{y-y'}$ which is in the direction of $\rho-\rho'$.

Hence:

$$\begin{aligned}\hat{n}\times E^{I}(\rho) &= \hat{n}\times i\omega\int_{S}(\hat{n}\times H(\rho'))(\mu_0G_1+\mu_2G_2)ds'\\ &+ \hat{n}\times\int_{S}\hat{z}\mid E(\rho')\mid\mid\nabla' G_0+\nabla' G_2\mid\sin(\theta)ds'\end{aligned} \tag{5.16}$$

- from the definition of the cross product where θ is the angle between $\hat{n} \times E(\rho')$ and $\rho - \rho'$.

This equation could have been written here as a single integration over S but I choose to express it as two because the second integral is of significance for terrain.

Obviously the above equation has an infinite number of solutions (because it is a single equation in two unknowns) but the contribution of the second integration will be small.

If it is small enough we can ignore it and we are left with the following approximation:

$$\hat{n} \times E^I(\rho) = \hat{n} \times i\omega \int_S (\hat{n} \times H(\rho'))(\mu_0 G_1 + \mu_2 G_2) ds' \tag{5.17}$$

- which for non-magnetic materials is:

$$\hat{n} \times E^I(\rho) = \hat{n} \times i\omega\mu_0 \int_S (\hat{n} \times H(\rho'))(G_1 + G_2) ds' \tag{5.18}$$

- and so (5.2) and (5.13) take the form of the EFIE.

I will refer to this formulation as the Combined Electric Field Integral Equation Approximation (CEFIEA).

For materials encountered in terrain $\tilde{\epsilon}$ will normally have a small imaginary part.

This means $G_2 \rightarrow 0$ for $i \neq j$.

Then:

$$\hat{n} \times E^I(\rho) = \hat{n} \times i\omega\mu_0 \int_S (\hat{n} \times H(\rho')) G_1 ds' \tag{5.19}$$

This is the EFIE for a PEC which was arrived at by eliminating relatively insignificant quantities from the Coupled EFIEs for terrain.

To see how the second integral in (5.13) above may be ignored for terrain, consider first a flat dielectric surface.

In this case $\sin\theta$ will be zero and so the above approximation of (5.17) is exact. Should the surface undulate, θ varies positive and negative w.r.t. the tangential component of the electric field at the surface.

This means the second integral in (5.13) is not monotonically cumulative and as a result the overall value of this integral will be small in comparison with the first integral.

The EFIE for a PEC is formally derived from the Coupled EFIEs by noting the tangential field on the surface is zero and no fields exist inside a PEC.

To illustrate the validity of the assumptions made above the following are plots of the field

coverage obtained using (5.17) superimposed on plots of the field coverage obtained using the EFIE and the Coupled EFIEs and CFIE for the German profile consisting of clay. This is followed by a superposition of results obtained using dielectric methods on clay, sand and loam and the PEC model.

5.2.2 Analysis of Results

Figure 5.1 is a graphical representation of the progression from the CEFIE to the EFIE via the CEFIEA. The results given by the CEFIEA for the most part lie somewhere between the other two validating the assumptions which led to the CEFIEA formulation and ultimately the EFIE approximation.

The comparative plots of coverage illustrate the accuracy of the PEC model for terrain. The PEC model is a better approximation for terrain consisting of dry clay or sand than for loam though not greatly so.

It is however to be concluded from this plot that the PEC model varies in its agreement with the exact results depending on terrain composition.

With both plots it is clear that transmission is taking place through the surface and it is significant. This is particularly apparent in the second and third troughs where shadowing is much less pronounced in the dielectric results in comparison with those given by the PEC model where no transmission through the surface is possible from Faraday's law.

It is interesting to note that the results given by dielectric terrain are somewhat more closely correlated with the surface profile though this feature of the field results is not investigated in this thesis.

5.2.3 Results

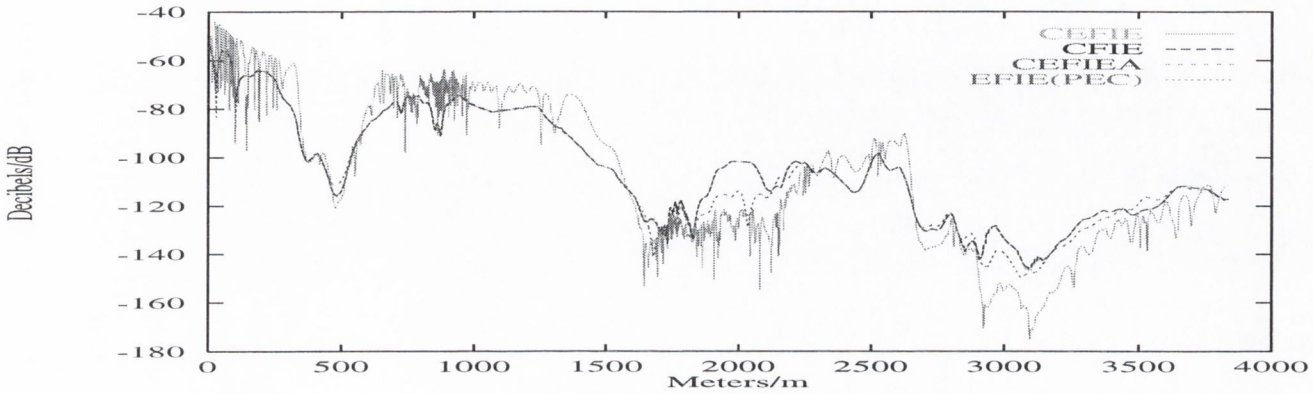

Figure 5.1: Comparative Plot of Electric Field Coverage at 970MHz over German Terrain consisting of Dry Clay.

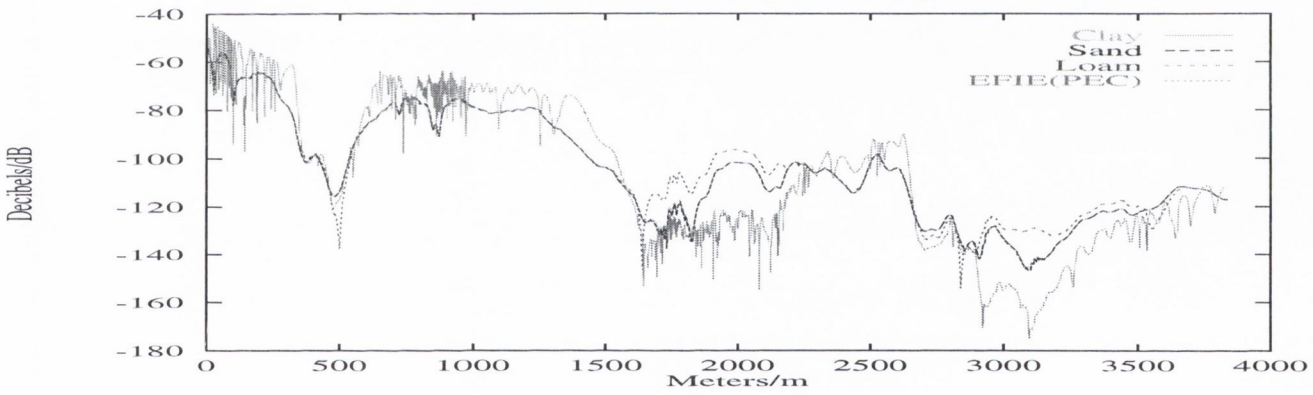

Figure 5.2: Comparative Plot of Electric Field Coverage at 970MHz over German Terrain consisting of Dry Clay, Sand, Loam and the PEC Model.

SCATTERING FROM PEC SURFACES

6.1 Introduction

Here the terrain is considered to be a PEC.

This difference simplifies the problem because:

1) Fields do not exist in the terrain.

2) Only surface electric (no magnetic currents) are induced at the terrain boundary.

3) Greater length surface discretisations can be taken.

4) There is only one unknown involved in the problem - electric current - and so only a single field integral equation is required to solve.

It is for the reason of the above simplifications the PEC model for terrain is popular.

To solve we may use the EFIE or MFIE.

6.2 The Electric Field Integral Equation (EFIE)

6.2.1 Theory

The EFIE for the problem is:

$$E^I(\rho) = \frac{\beta\eta}{4} \int_S J(\rho')\mathcal{H}_0^{(2)}(\beta \mid \rho - \rho' \mid)ds' \tag{6.1}$$

where

$$E^I(\rho) = -\frac{\beta^2}{4\omega\epsilon}\mathcal{H}_0^{(2)}(\beta\rho) \tag{6.2}$$

Hence:

$$\mathcal{H}_0^{(2)}(\beta\rho) = -\int_S J(\rho')\mathcal{H}_0^{(2)}(\beta \mid \rho - \rho' \mid)ds' \tag{6.3}$$

The total field a distance d above the surface is then:

$$E^T(\rho'') = E^I(\rho'') + E^S(\rho'') \tag{6.4}$$

which is:

$$E^T(\rho'') = -\frac{\beta^2}{4\omega\epsilon}\left(\mathcal{H}_0^{(2)}(\beta\rho'') + \int_C J(\rho')\mathcal{H}_0^{(2)}(\beta \mid \rho' - \rho'' \mid)ds'\right) \tag{6.5}$$

-[5].

Using unit weights and pulse basis functions, the Method of Moments [18] allows us express the EFIE in matrix form thus:

$$(E) = (Z)(J) \tag{6.6}$$

where (E) and (J) are rank N column vectors and (Z) is an $N \times N$ matrix where N is the number of discretisations taken of the surface (normally of length $\frac{\lambda}{4}$ to ensure convergence). The entries in (E) and (J) are:

$$E^I(\rho_j) \tag{6.7}$$

and

$$J(\rho_i') \tag{6.8}$$

for $i, j = 1 \ldots N$

The entries in (Z) are:

$$Z_{ij} \approx -\frac{\beta\eta}{4}\mathcal{H}_0^{(2)}(\beta \mid \rho_j - \rho_i' \mid)\Delta s_i \tag{6.9}$$

for $i, j = 1 \ldots N; i \neq j$.

The diagonal entries in the impedance matrix require special attention because the Hankel

function is singular at zero.

For small arguments the Hankel function can be replaced by a power series expansion [16]:

$$\mathcal{H}_0^{(2)}(x) \simeq \left(1 - \frac{x^2}{4}\right) - i\left(\frac{2}{\pi}\ln(\frac{\gamma x}{2}) + \left(\frac{1}{2\pi} - \frac{1}{2\pi}\ln(\frac{\gamma x}{2})\right) + O(x^4)\right) \tag{6.10}$$

- where $\gamma = 1.781072418\ldots$

Assuming the curvature of the segment is small enough that it can be considered flat, the dominant terms in (6.10) can be retained to give:

$$\int_{S_n} \mathcal{H}_0^{(2)}(\beta x)dx \approx 2\int_0^{S_n/2}\left(1 - i\frac{2}{\pi}\ln(\frac{\gamma\beta x}{2})\right)dx \tag{6.11}$$

which gives:

$$Z_{ij} \approx -\Delta s\frac{\beta\eta}{4}\left(1 - i\frac{2}{\pi}\ln\left(\frac{1.781\beta\Delta s}{4e}\right)\right) \tag{6.12}$$

for $i = j$.

The solution for the current is obtained by inverting (Z).

Following an analysis, the field coverage results for the Danish and German profiles obtained using the EFIE (PEC Model), are presented.

6.2.2 Analysis of Results

The results for the Danish profiles are important in that they exhibit clearly field decay with distance from the source on the fashion of the inverse square root of this distance. The reason for this clarity is that most or all the surface is irradiated directly by the source and the surface profiles are relatively flat in comparison with the German profile.
Having previously noted the correlation between the coverage results and the surface a good 'rule of thumb' in estimating field coverage over terrain is to correlate the field decay given by the inverse root of distance from the source with the surface profile.
The results obtained for the Danish and German profiles at $144MHz$ and $970MHz$ all indicate that shadowing is more pronounced at higher frequencies.

6.2.3 Tabulated Characteristic Data

Computational Cost	Memory Requirement	Complexity of Code
$O(N^2)$	$O(N)$	Simple

Table 6.1: Computational Features of the EFIE

Jerslev	Hjorring	German
900	3400	410

Table 6.2: Computation times for Electric Field Coverage at 144MHz over the Jerslev (Danish), Hjorring (Danish) and German profiles.

Jerslev	Hjorring	German
45000	170000	20500

Table 6.3: Computation times for Electric Field Coverage at 970MHz over the Jerslev (Danish), Hjorring (Danish) and German profiles.

6.2.4 Results

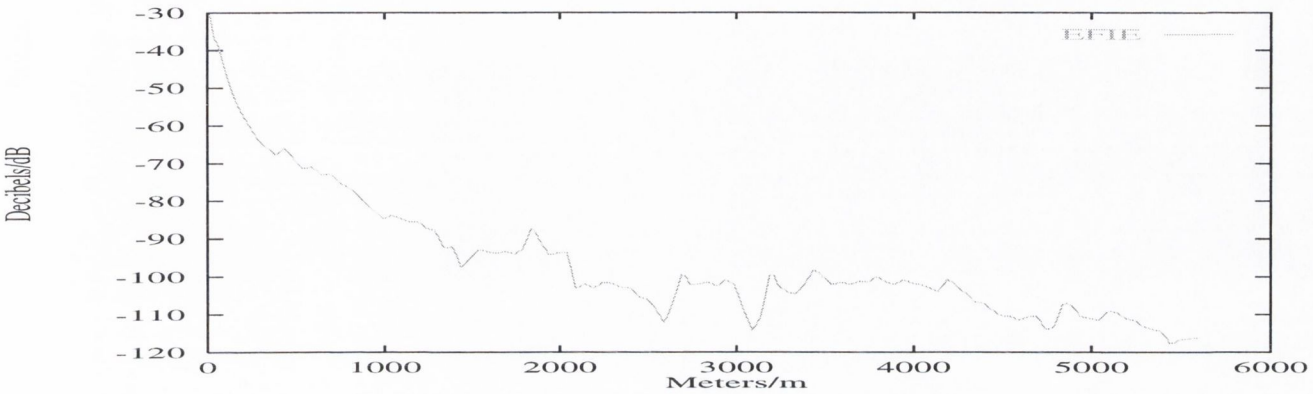

Figure 6.1: Electric Field coverage at 144MHz over the Jerslev profile.

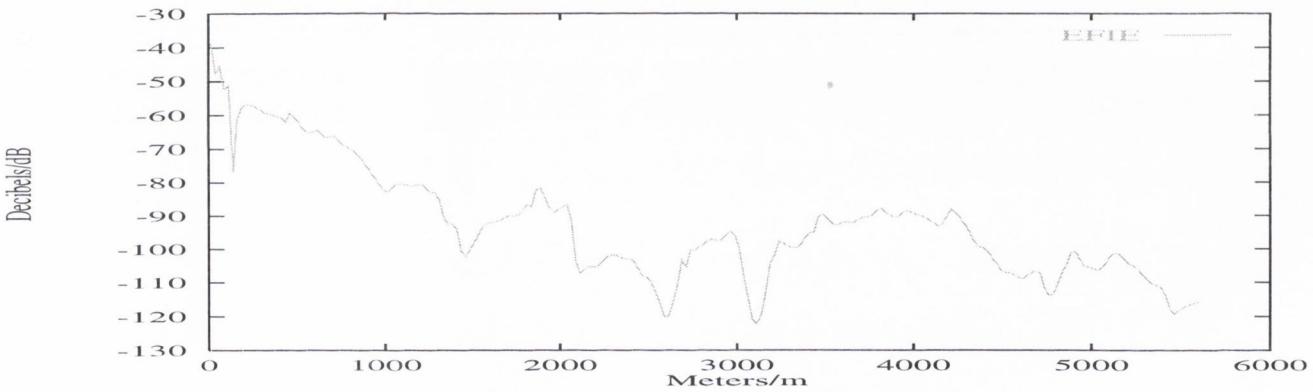

Figure 6.2: Electric Field coverage at 970MHz over the Jerslev profile.

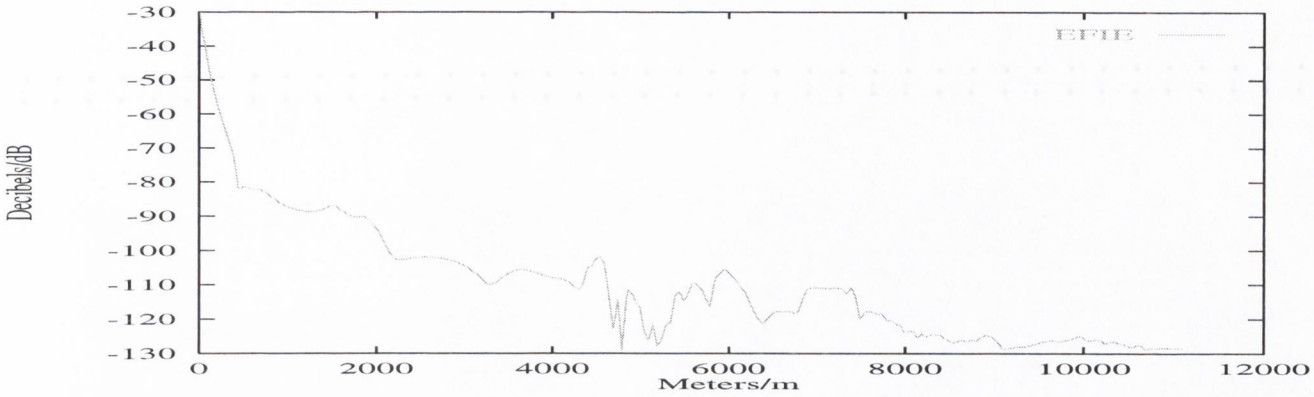

Figure 6.3: Electric Field coverage at 144MHz over the Hjorring profile.

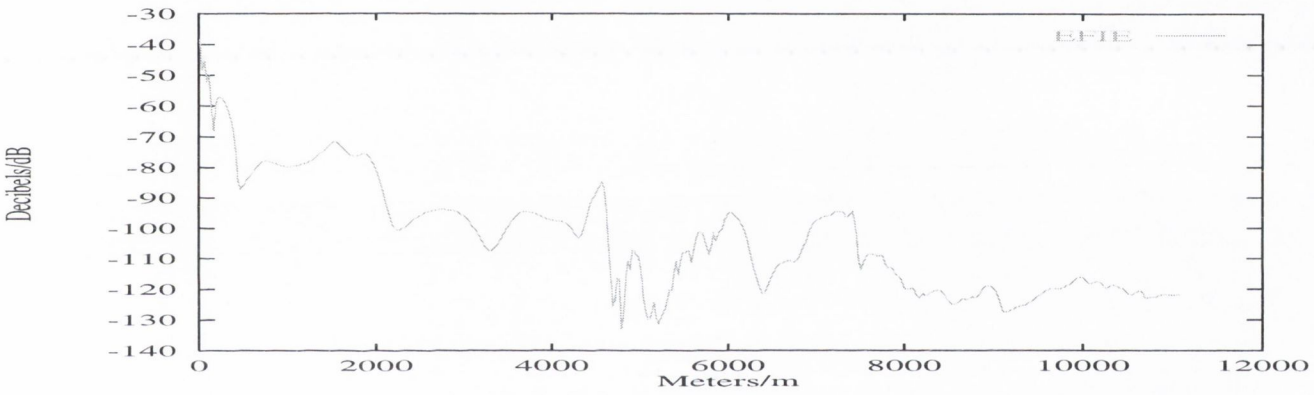

Figure 6.4: Electric Field coverage at 970MHz over the Hjorring profile.

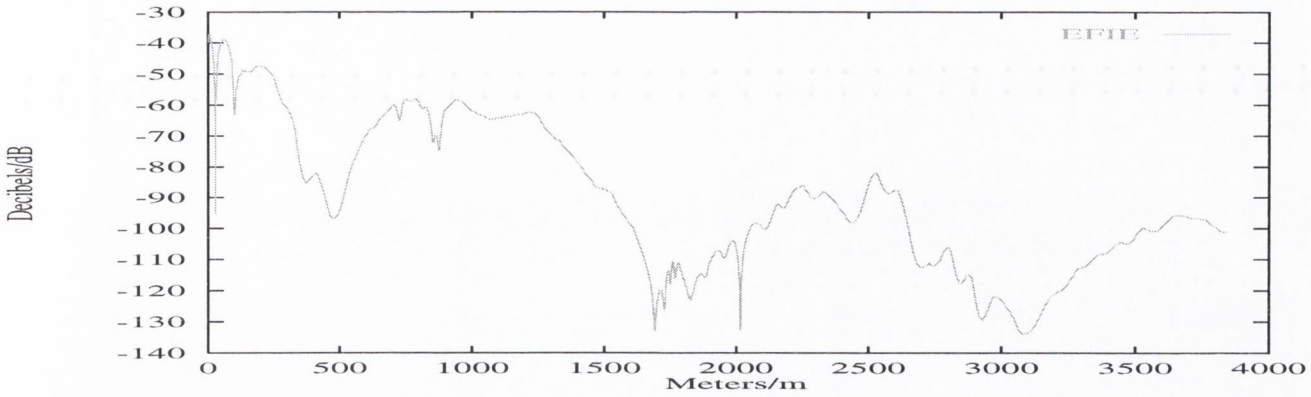

Figure 6.5: Electric Field coverage at 144MHz over the German profile.

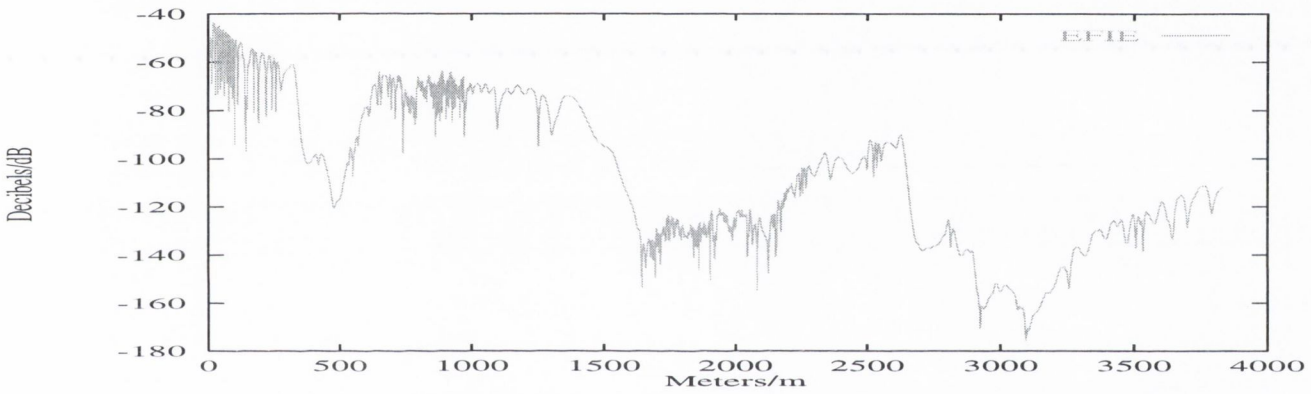

Figure 6.6: Electric Field coverage at 970MHz over the German profile.

FAST INTEGRAL EQUATION METHODS

This chapter is the central focus of this thesis.
Here fast computational methods based on the EFIE are examined.
This chapter provides the basis for the assertion that the Field Extrapolation Method is the fastest and most efficient method yet developed for the terrain scattering problem.
The fast integral equation methods are discussed in the following order:

1) The Natural Basis (NBS).
2) The Green's Function Perturbation Method (GFPM).
3) The Fast Multipole Method (FMM)/Fast Far-Field Approximation (FAFFA).
4) The Tabulated Interaction Method (TIM).
5) The Field Extrapolation Method (FEM).

3) to **5)** are methods which evaluate the scattered field by grouping terrain segments. For the Danish profiles groups of 100λ are taken whereas for the more demanding German profile the groups are 3λ.
Henceforth the results generated by the EFIE for a PEC surface will be referred to as the 'Exact' results.

7.1 The Natural Basis Method (NBS)

7.1.1 Theory

The Method of Moments gives us the freedom to choose basis functions.

The closer the basis function chosen approximates the solution of the integral equation, the quicker the inversion of the impedance matrix.

One such assumption [57] is that the phase of the surface current is dominated by, and is, $\pi/2$ radians out of phase with the field incident on the surface from the source.

This follows from Faraday's Law.

The assumption is reasonable for slowly undulating surfaces (because for an infinite flat surface it would be exact) at a distance along the surface from the source where the amplitude of the scattered field is small in comparison to the field incident from the source.

This will occur due to scattering into the atmosphere and absorption of scattered radiation by the surface.

The beauty of the NBS is its simplicity and the statement it makes; that it is possible, *a priori*, to make assumptions about the nature of the solution.

As we shall see all the methods in this chapter can be interpreted as 'basis methods', more sophisticated than the NBS in that a basis set is calculated dynamically.

The following table gives the salient data for the NBS followed by the results for the Danish and German Profiles, supplied courtesy of Teltec Ireland. 'C' represents an arbitrary constant.

7.1.2 Analysis of Results

The NBS clearly gives excellent results for the Jerslev profile. This is accounted for by the fact that this is a smooth and relatively flat profile and importantly, all of it is irradiated directly by the source so the resultant total field coverage is dominated by the field incident from the source.

This is not true for the German profile and so significant deviation from the exact results occur especially in the second trough which is the steepest and is not illuminated directly by the source.

The results are somewhat better in the first and third troughs. The reason for this is that these troughs are partially illuminated by the source.

7.1.3 Tabulated Characteristic Data

Computational Cost	Memory Requirement	Complexity of Code
$O(N/C)^2$	$O(N/C)$	Simple

Table 7.1: Computational Features of the NBS

Jerslev	German
8	50

Table 7.2: Computation times for Electric Field Coverage at 970MHz over the Jerslev (Danish) and German profiles.

7.1.4 Results

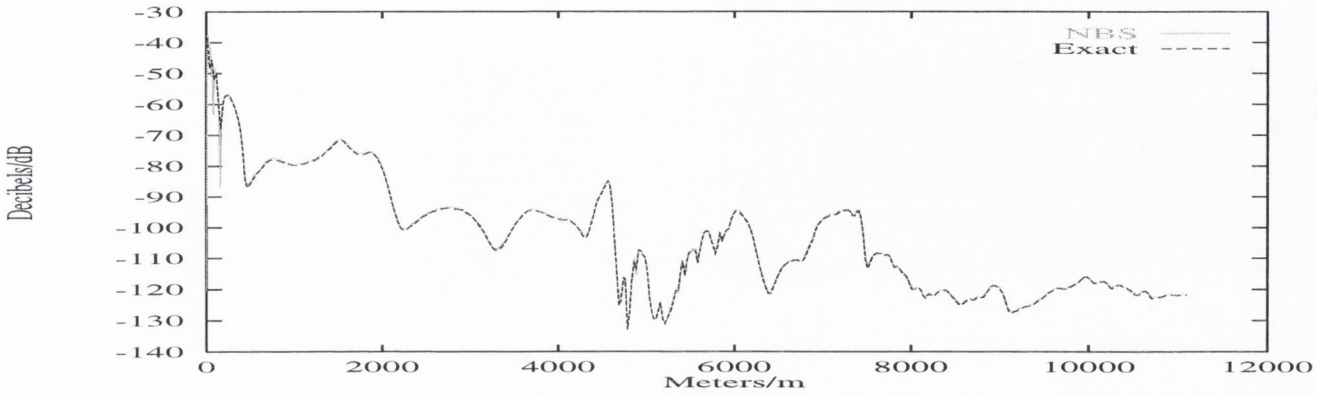

Figure 7.1: Comparative Plot of the Electric Field Coverage at 970MHz over Danish (Jerslev) Terrain.

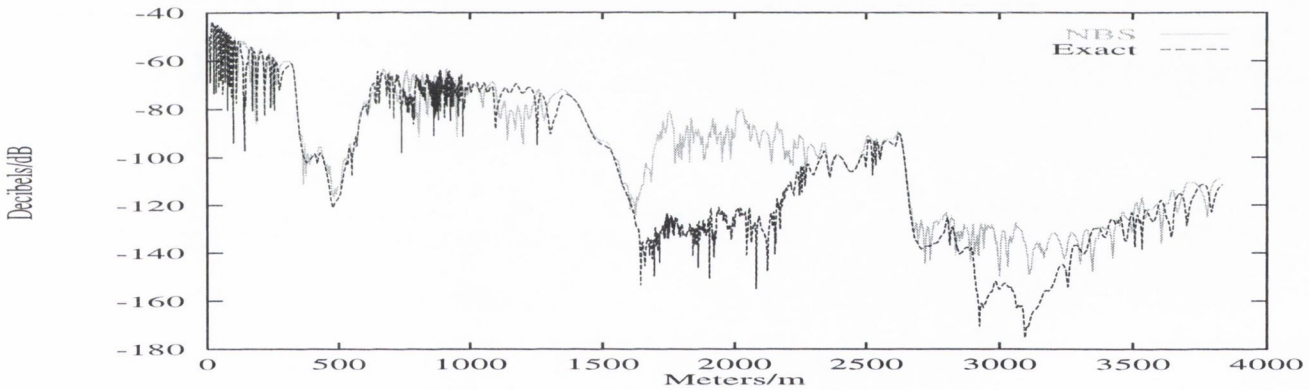

Figure 7.2: Comparative Plot of the Electric Field Coverage at 970MHz over German Terrain.

7.2 The Greens Function Perturbation Method (GFPM)

7.2.1 Theory

This method developed by Moroney and Cullen [58] [59] [60] approximates the RHS of the EFIE with a convolution.

A convolution can be inverted using an inverse FFT algorithm.

This is less computationally intensive than the MOM.

Consider the EFIE for a PEC:

$$E^I(\rho) = \int_S J(\rho')\mathcal{H}_0^{(2)}(\beta|\rho - \rho'|)d\rho' \tag{7.1}$$

Now we introduce the change of variable central to the desired conversion.

Through the arc-length relation with the independent variable x,

$$s = \int_0^x \sqrt{1 + \left(\frac{d\zeta(x)}{dx}\right)^2} dx \tag{7.2}$$

the distance between the source and observation points on the surface:

$$|\rho - \rho'| = \sqrt{(x - x')^2 + (\zeta(x) - \zeta(x'))^2} \tag{7.3}$$

becomes

$$\begin{aligned} d(s, s') &= \sqrt{(f(\rho) - f(\rho'))^2 + (\zeta(f(\rho)) - \zeta(f(\rho')))^2} \\ &\simeq g(s - s') \end{aligned} \tag{7.4}$$

- where $d(s, s')$ and $g(s - s')$ are the Euclidean distance and distance along the surface trajectory respectively, between the points s and s'.

We now write:

$$\mathcal{H}_0^2(\beta \mid \rho - \rho' \mid) = \mathcal{H}_0^2\left(\beta g(s - s')\sqrt{1 + T(s, s')}\right) \tag{7.5}$$

where:

$$T(s, s') = -1 + \left(\frac{f(\rho) - f(\rho')}{g(s - s')}\right)^2 + \left(\frac{\zeta(f(\rho)) - \zeta(f(\rho'))}{g(s - s')}\right)^2 \tag{7.6}$$

and

$$| T | < 1 \tag{7.7}$$

which will be satisfied when:

$$g(s - s') > \frac{d(s, s')}{2} \tag{7.8}$$

Hence (7.5) can be expanded using the Binomial Theorem giving:

$$\mathcal{H}_0^{(2)}(\beta \mid \rho - \rho' \mid) = \mathcal{H}_0^{(2)}(\beta g(s - s') + B(s, s')\beta g(s - s')) \tag{7.9}$$

where:

$$B(s, s') = \sum_{m=1}^{\infty} \binom{\frac{1}{2}}{m} T^m \tag{7.10}$$

$$= \sqrt{1 + T} - 1 \tag{7.11}$$

(7.9) can now be expanded as a Taylor series about $\beta g(s - s')$ giving:

$$\mathcal{H}_0^{(2)}(\beta \mid \rho - \rho' \mid) = \mathcal{H}_0^{(2)}(\beta g(s - s')) + \sum_{n=1}^{\infty} \frac{[\beta g(s - s')B]^n}{n!} \mathcal{H}_{(0)}^{(2)^n}(\beta g(s - s')) \tag{7.12}$$

where:

$$\mathcal{H}_0^{(2)^n}(x) = \frac{d^n}{dx^n} \mathcal{H}_0^{(2)}(x) \tag{7.13}$$

Replacing the Hankel function in (7.1) we have:

$$E^I(\rho) = -\frac{\beta\eta}{4} \int_S J(\rho') \mathcal{H}_0^{(2)}(\beta g(s - s'))ds' \tag{7.14}$$

$$- \frac{\beta\eta}{4} \int_S J(\rho') \sum_{n=1}^{\infty} \frac{[\beta g(s - s')B]^n}{n!} \mathcal{H}_0^{(2)^n}(\beta g(s - s'))ds'$$

Approximating (7.1) with the first integral - which is a convolution in s, we can solve for the current using an FFT.

Then:

$$J(\rho') \approx \mathcal{F}^{-1}\left(\frac{\mathcal{F}[E^I(\rho)]}{\mathcal{F}[\mathcal{H}_0^{(2)}(\beta g(\rho'))]}\right) \tag{7.15}$$

- from which the scattered field can be calculated using (2.40).

A CC reduction to $O(Nlog(N))$ is given by inversion using the FFT.

The method should be used only on slowly undulating terrain because the Euclidean distance and the distance along the surface trajectory have been approximated as being equal.

The salient data regarding GFPM is given in the table below followed by the results for the Danish and German profiles.

7.2.2 Analysis of Results

The following results given by the GFPM show very good agreement with the exact results for the Danish profiles. This is to be expected because these profiles do not undulate rapidly or to any great degree. Hence the approximation of arc-length with Euclidean distance is shown to hold well enough to give good results for these profiles. The same does not hold true for the German profile which is mountainous. Here the GFPM results are so poor they indicate only an approximate average coverage and a decay in field intensity with distance from the source. Clearly GFPM is limited in its application to terrain profiles giving good results for smooth and slowly undulating profiles only. The reduction on order of complexity of the algorithm from $O(N^2)$ to $O(N \log N)$, though an improvement, does not represent a speedy solution (a matter of seconds). Hence the GFPM like the NBS, though able to give good results for the Danish profiles, are not sufficient in terms of speed and range of application to different type terrain profiles to justify use of integral equation methods to estimate field coverage over suburban terrain.

7.2.3 Tabulated Characteristic Data

Computational Cost	Memory Requirement	Complexity of Code
$O(Nlog(N))$	$O(N)$	Complex

Table 7.3: Computational Features of the GFPM

Jerslev	Hjorring	German
6	20	12

Table 7.4: Computation times for Electric Field Coverage at 144MHz over the Jerslev (Danish), Hjorring (Danish) and German profiles.

Jerslev	Hjorring	German
25	100	50

Table 7.5: Computation times for Electric Field Coverage at 970MHz over the Jerslev (Danish), Hjorring (Danish) and German profiles.

7.2.4 Results

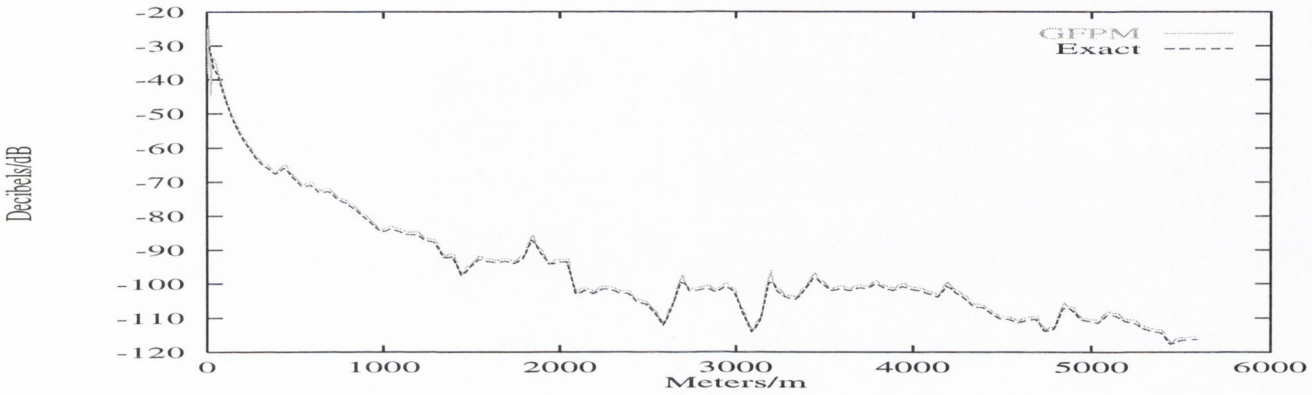

Figure 7.3: Electric Field Coverage at 144MHz over the Jerslev profile.

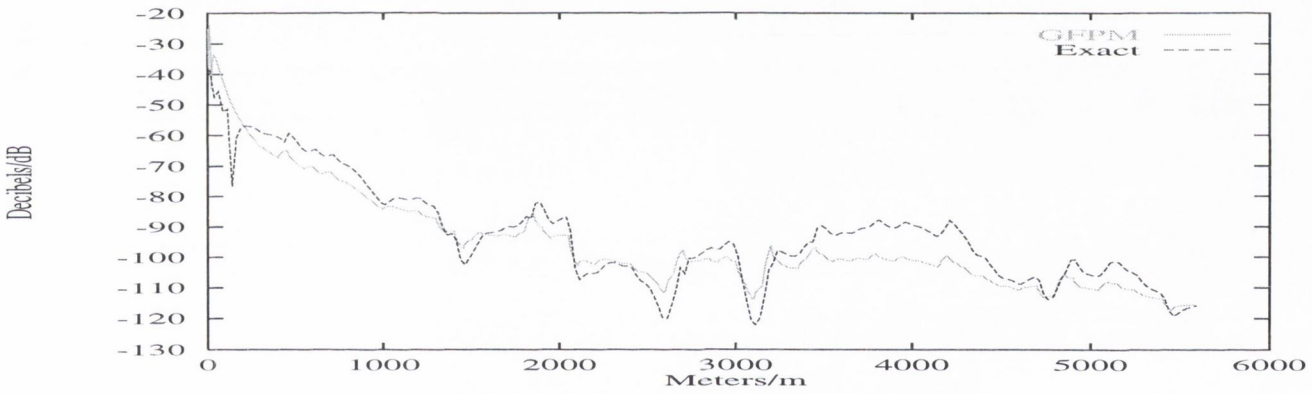

Figure 7.4: Electric Field Coverage at 970MHz over the Jerslev profile.

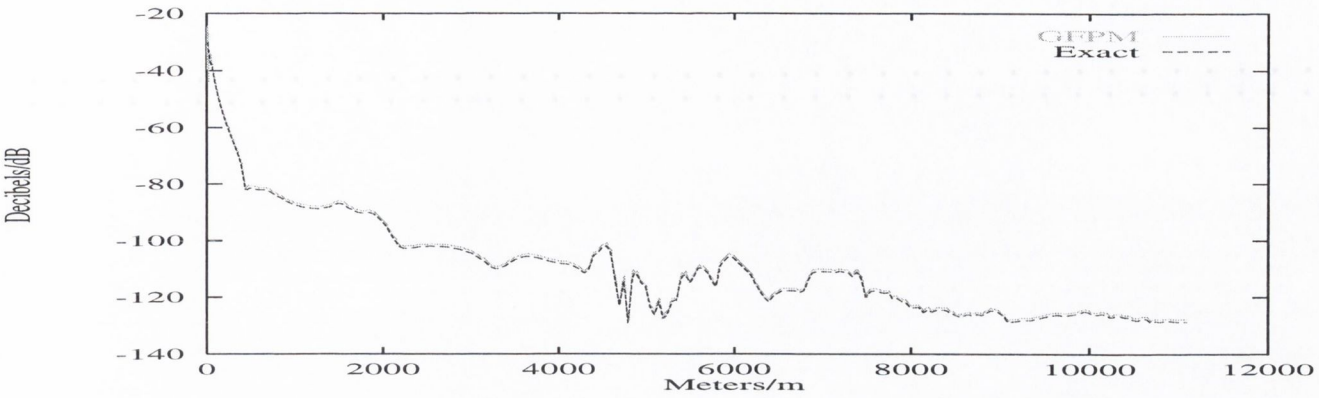

Figure 7.5: Electric Field Coverage at 144MHz over the Hjorring profile.

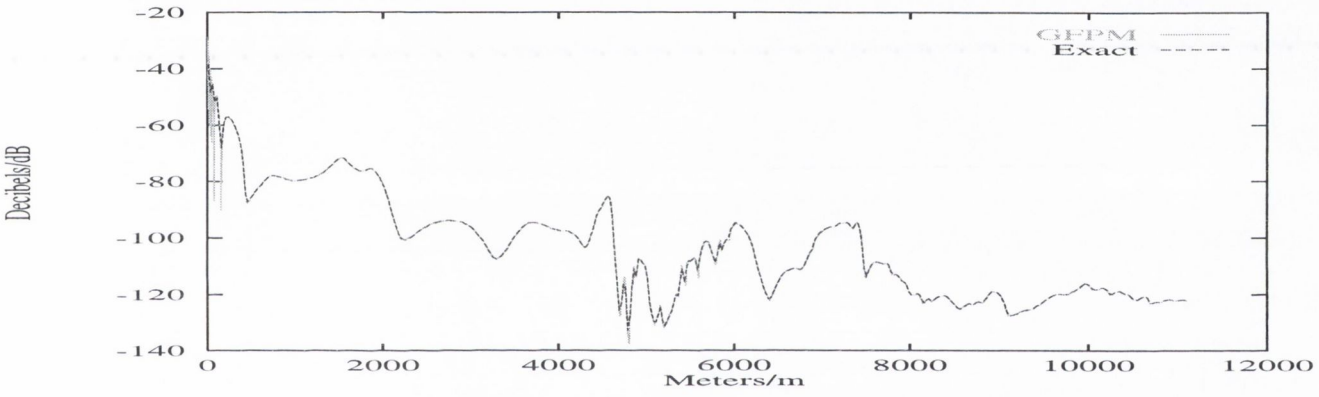

Figure 7.6: Electric Field Coverage at 970MHz over the Hjorring profile.

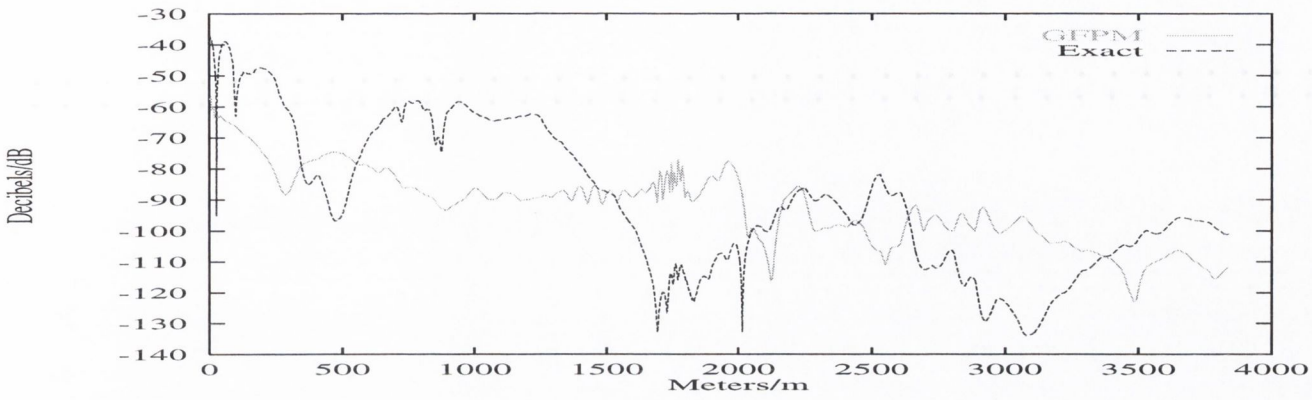

Figure 7.7: Electric Field Coverage at 144MHz over the German profile.

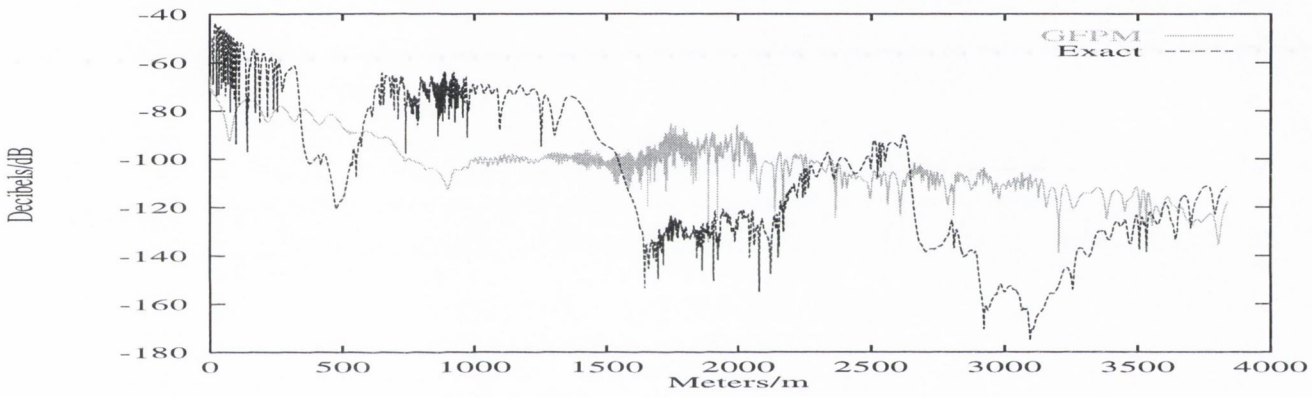

Figure 7.8: Electric Field Coverage at 970MHz over the German profile.

7.3 Fast Multipole Method/Fast Far Field Approximation

7.3.1 Theory (FMM)

Developed by Rokhlin[61], the FMM or variations thereof, according to Peterson[16], 'appear to offer the most efficient possibilities yet proposed for the accurate numerical analysis of electrically large geometries, where N may be far greater than 10^4'.

It was the first method to propose dividing the scatterer into groups of integration intervals.

The FFFA [8], TIM [25] and my own method, the FEM [62], take this approach.

This subsection gives the derivation of the FMM for the 2-D EM scattering case for a PEC according to [9].

I will relate the FFFA , TIM and FEM to the FMM on the basis of this derivation which will provide the mathematical insight necessary to determine the range of application of the fast methods which follow, as well as a means of comparison.

Consider the EFIE in matrix form with unit pulse basis and weighting functions:

$$(E) = (Z)(J) \tag{7.16}$$

The scattering surface of N, $\frac{\lambda}{4}$ integration intervals, is divided into M sub-scatterers or groups.

For interactions between groups G_l and $G_{l'}$ the impedance matrix can be rewritten:

$$[Z] = [B]^T[A][B] \tag{7.17}$$

where $[B]^T, [A]$ and $[B]$ are $1 \times P, P \times P$ and $P \times 1$ matrices respectively.

The entries in $[A]$ and $[B]$ are:

$$a_{nm}(l, l') = \mathcal{H}^{(2)}_{n-m}(\beta \mid \rho_l - \rho_{l'} \mid)e^{-i(n-m)\phi_{ll'}} \tag{7.18}$$

and

$$b_j(j, l') = \mathcal{J}_j(\beta \mid \rho_l - \rho_{l'} \mid)e^{-in\phi_{l'j}} \tag{7.19}$$

- where $\phi_{ll'}$ is the angle $\rho_l - \rho_{l'}$ makes with the horizontal and similarly for $\phi_{l'j}$.

$$E^I(\rho_j) = \frac{\beta\eta}{4} b^T_{l'j} \sum_{l=1, l\neq l'}^{N/M} a_{ll'} \sum_{i \in G_l} b_{il} J(\rho_i)\Delta s_i \tag{7.20}$$

- where $j \in G_{l'}$ and $l' = 1 \ldots \frac{N}{M}$.

For interactions between elements of the same group (7.16)is used. For (7.20) to be accurate $P \approx cM$ where c is a constant.

Hence the computational cost of the outer summation of (7.20) is $O(N^2)$ and so there is no advantage at this point in this formulation of the EFIE.

However the CC of (7.20) can be substantially reduced if $[A]$ can be diagonalized.

To this end we substitute the definitions for a and b given in Chew [7] [11] [12] [13] in (7.20) so it becomes:

$$\mathcal{H}_0^{(2)}(\beta \mid \rho_i - \rho_j \mid) = \sum_{m=-\infty}^{\infty} \mathcal{J}_m(\beta\rho_{jl'}) e^{im(\phi_{jl'} - \pi)} \sum_{n=-\infty}^{\infty} \mathcal{H}_{m-n}^{(2)}(\beta\rho_{l'l}) e^{-i(m-n)\phi_{l'l}} \times \mathcal{J}_n(\beta\rho_{il}) e^{-in\phi_{il}} \tag{7.21}$$

Referring to (7.22), even though $\mathcal{H}_{m-n}^{(2)}(x) \to \infty$ when $\mid m-n \mid \to \infty$, the above summations will converge because $\mathcal{J}_n(x) \to 0$ when $\mid n \mid \to \infty$.

The inner summation is the convolution of two DFTs and hence can be expressed as the product of two functions if their DFTs are known.

The DFT of $\mathcal{H}_n^{(2)}(x)e^{in\phi}$ does not exist since $\mathcal{H}_n^{(2)}(x) \to \infty$ when $\mid n \mid \to \infty$.

However we can truncate the inner summation since it converges and write (7.22) as:

$$\mathcal{H}_0^{(2)}(\beta \mid \rho_i - \rho_j \mid) = \sum_{m=-\infty}^{\infty} \mathcal{J}_m(\beta\rho_{l'j}) e^{im(\phi_{jl'} - \pi)} \sum_{n=m-P}^{m+P} \mathcal{H}_{m-n}^{(2)}(\beta\rho_{ll'}) e^{-i(m-n)\phi_{l'l}} \times \mathcal{J}_n(\beta\rho_{il}) e^{-in\phi_{il}} \tag{7.22}$$

Via the identity [6]:

$$\mathcal{J}_m(\beta\rho_{l'j}) e^{im\phi_{l'j}} = \frac{1}{2\pi} \int_0^{2\pi} e^{i\beta\rho_{l'j}\cos(\alpha - \phi_{l'j}) + im(\alpha - \frac{\pi}{2})} d\alpha \tag{7.23}$$

and similarly for $\mathcal{J}_i(\beta\rho_{il})e^{in\phi_{il}}$ we can write:

$$\mathcal{H}_0^{(2)}(\beta\rho_{ij}) = \frac{1}{2\pi} \int_0^{2\pi} b_{l'j}(\alpha) a_{ll'}(\alpha) b_{il}(\alpha) d\alpha \tag{7.24}$$

where:

$$a_{ll'}(\alpha) = \sum_{p=-P}^{P} \mathcal{H}_p^{(2)}(\beta\rho_{ll'}) e^{-ip(\phi_{ll'} + \alpha - \frac{\pi}{2})} \tag{7.25}$$

$$b_{l'j}(\alpha) = e^{i\beta\rho_{l'j}\cos(\alpha-\phi_{l'j})} \tag{7.26}$$

and

$$b_{il}(\alpha) = e^{i\beta\rho_{il}\cos(\alpha-\phi_{il})} \tag{7.27}$$

where now the cylindrical waves of (7.22) appear as plane waves in the integrand of (7.24) and a is replaced by the diagonal operator $a_{ll'}(\alpha)$.
Now using (7.24) in (7.20) we have:

$$E^I(\rho_j) = \frac{\beta\eta}{8\pi}\int_0^{2\pi} b_{l'j}(\alpha)\sum_{i=1,i\neq l'}^{\frac{N}{M}} a_{ll'}(\alpha)\sum_{i\in G_l} b_{il}(\alpha)J_i\Delta s_i \tag{7.28}$$

which replaced by a Q point summation yields:

$$E^I(\rho_j) = \frac{\omega\mu_0}{4Q}\sum_{q=1}^{Q} b_{l'j}(\alpha_q)\sum_{i=1,i\neq l'}^{N/M} a_{ll'}(\alpha_q)\sum_{i\in G_l} b_{il}(\alpha_q)J_i\Delta s_i \tag{7.29}$$

This is the FMM formulation.

7.3.2 Theory (FAFFA)

The FAFFA developed by Chew [8] [9] is derived from the FMM. It can be considered to be a form of the FMM.

Considering (7.24), the FFFA can be derived from the FMM in the following way:

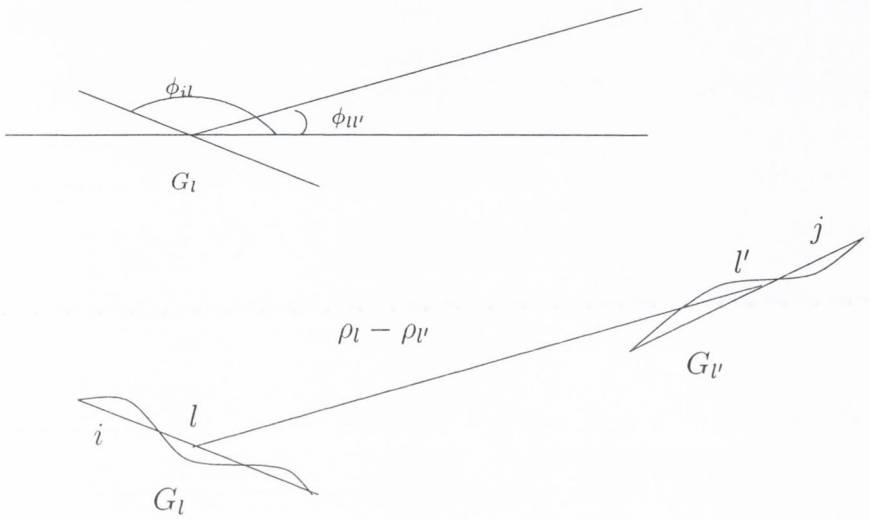

Figure 7.9: FAFFA scattering geometry. The upper diagram shows the angles ϕ_{il} and $\phi_{ll'}$ subtended by group G_l with the horizontal. The lower diagram shows groups G_l and $G_{l'}$ of $\lambda/4$ discretisations of the surface, their centrepoints l and l', the position vector $\rho_l - \rho_{l'}$ connecting them and arbitrary points i and j on the respective groups.

$$\mathcal{H}_0^{(2)}(\beta\rho_{ij}) = \frac{1}{2\pi}\int_0^{2\pi} b_{l'j}(\alpha)a_{ll'}(\alpha)b_{il}(\alpha)d\alpha \tag{7.30}$$

where:

$$a_{ll'}(\alpha) = \sum_{p=-P}^{P} \mathcal{H}_p^{(2)}(\beta\rho_{ll'})e^{-ip(\phi_{ll'}+\alpha-\frac{\pi}{2})} \tag{7.31}$$

$$b_{l'j}(\alpha) = e^{i\beta\rho_{l'j}\cos(\alpha-\phi_{l'j})} \tag{7.32}$$

and

$$b_{il}(\alpha) = e^{i\beta\rho_{il}\cos(\alpha-\phi_{il})} \tag{7.33}$$

$a_{ll'}(\alpha)$ above diverges as $P \to \infty$, which does not occur if we use the far-field approximation to the p^{th} order Hankel function:

$$\bar{\mathcal{H}}_p^{(2)}(x) = \sqrt{\frac{2i}{\pi x}}e^{-i(x-p\frac{\pi}{2}))} \tag{7.34}$$

which allows us to write (7.31) as:

$$a_{ll'}(\alpha) \simeq \sqrt{\frac{2i}{\pi\beta\rho_{ll'}}} e^{-i\beta\rho_{ll'}} \sum_{p=-P}^{P} e^{-ip(\phi_{ll'}-\alpha)} \tag{7.35}$$

$$= \sqrt{\frac{2i}{\pi\beta\rho_{ll'}}} e^{-i\beta\rho_{ll'}} \frac{\sin((P+\frac{1}{2})(\phi_{ll'}-\alpha))}{\sin(\frac{1}{2}(\phi_{ll'}-\alpha))}$$

As $P \to \infty$:

$$\sqrt{\frac{2i}{\pi\beta\rho_{ll'}}} e^{-i\beta\rho_{ll'}} \frac{\sin((P+\frac{1}{2})(\phi_{ll'}-\alpha))}{\sin(\frac{1}{2}(\phi_{ll'}-\alpha))} \to \frac{\pi(\alpha-\phi_{ll'})}{\sin(\frac{1}{2}(\alpha-\phi_{ll'}))}\delta(\alpha-\phi_{ll'}) \tag{7.36}$$

where:

$$\lim_{a\to\infty} \frac{\sin(ax)}{\pi x} = \delta(x) \tag{7.37}$$

- $\delta(x)$ is the Dirac-delta function.

Hence:

$$a_{ll'}(\alpha) = \sqrt{\frac{2i}{\pi\beta\rho_{ll'}}} e^{-i\beta\rho_{ll'}} \frac{\pi(\alpha-\phi_{ll'})}{\sin(\frac{1}{2}(\alpha-\phi_{ll'}))}\delta(\alpha-\phi_{ll'}) \tag{7.38}$$

for $P \to \infty$.

With this definition of $a_{ll'}(\alpha)$ (7.30) becomes:

$$\mathcal{H}_0^{(2)}(\beta\rho_{ij}) \simeq \frac{1}{2\pi}\sqrt{\frac{2i}{\pi\beta\rho_{ll'}}} e^{-i\beta\rho_{ll'}} \int_0^{2\pi} b_{l'j} \frac{\pi(\alpha-\phi_{ll'})}{\sin(\frac{1}{2}(\alpha-\phi_{ll'}))}\delta(\alpha-\phi_{ll'}) b_{il}(\alpha) d\alpha \tag{7.39}$$

which from L'Hopital's rule:

$$\lim_{x\to 0} \frac{x}{\sin(\frac{x}{a})} = a \tag{7.40}$$

becomes:

$$\mathcal{H}_0^{(2)}(\beta\rho_{ij}) \simeq \sqrt{\frac{2i}{\tau\beta\rho_{ll'}}} e^{-i\beta\rho_{ll'}} b_{l'j}(\phi_{ll'}) b_{il}(\phi_{ll'}) \tag{7.41}$$

- which with $b_{l'j}$ and b_{il} in there above defined form gives:

$$\mathcal{H}_0^{(2)}(\beta\rho_{ij}) \simeq \sqrt{\frac{2i}{\pi\beta\rho_{ll'}}} e^{-i\beta\rho_{ll'}} e^{i\beta\rho_{l'j}\cos(\phi_{ll'}-\phi_{l'j})} e^{i\beta\rho_{il}\cos(\phi_{ll'}-\phi_{il})} \tag{7.42}$$

which substituted into the discrete form of the EFIE yields:

$$E^I(\rho_j) = \sum_{j \in G_{l'} \in FF}^{G_l < G_{l'}} \bar{\mathcal{H}}_0^{(2)}(\beta \rho_{ll'}) e^{i\beta \Delta_{il} \cos(\phi_{ll'} - \phi_{l'j})} \sum_{i \in G_l \in FF} J(\rho_i) e^{i\beta \Delta_{il} \cos(\phi_{ll'} - \phi_{il})} \Delta s_i' \quad (7.43)$$
$$+ \sum_{i \in G_l \in NF}^{i<j} \mathcal{H}_0^{(2)}(\beta \rho_{ll'}) J(\rho_i) \Delta s'$$

- which is the Fast Far-Field Approximation.

This formulation amounts to assuming ρ in the amplitude component of the far-field approximation to the Hankel function is constant:

$$\rho_{ij} \simeq \rho_{ll'} \quad (7.44)$$

and in the phase component:

$$\rho_{ij} \simeq \hat{\rho}_{ll'} \cdot \rho_{l'j} + \rho_{ll'} + \hat{\rho}_{ll'} \cdot \rho_{il} \quad (7.45)$$

Note as with (7.29) reduction in complexity is achieved because the following sum can be reused:

$$\sum_{i \in G_l \in FF} J(\rho_i) e^{i\beta \Delta_{il} \cos(\phi_{ll'} - \phi_{il})} \Delta s_i' \quad (7.46)$$

Lu and Chew [8] propose further reduction in complexity by performing the above summation for a number of values of the argument of the exponential in the range $[-\pi, \pi]$ and using an interpolation procedure to arrive at an approximation for the complete sum. This brings the CC to $O(N^{1.33})$.

[47] propose nesting the algorithm (a multilevel algorithm) which in the limiting case brings the CC to $O(N \log N)$.

[14] also develops a variation to the FMM $\rightarrow$ FFFA progression above.

It is what he terms a 'Ray Propagation Fast Multipole Algorithm'.

Like the FFFA it is based on the FMM.

In contrast with the FFFA, $P \not\to \infty$ in (7.36) above but takes a large value giving $\alpha_{ll'}$ a spiked oscillatory form.

This is termed a 'ray' and interactions between groups take the form of this ray with

side-lobes filtered out.

It is a lucid formulation of an idea tackled by Canning [43] [44] [45] [46] - introducing sparsity to the impedance matrix by defining a radiation pattern.

The salient facts about the FAFFA are given in the table, followed by results for the Danish and German profiles.

7.3.3 Analysis of Results

the results given by the FAFFA show excellent agreement with the exact results for the Danish profiles. For the more demanding German profile the results deteriorate somewhat from the exact most noticeably in the troughs where the distance approximation is less accurate due to the greater surface curvature.

This can be overcome by choosing a smaller groupsize. Indeed a groupsize of one quarter the radiation wavelength leads to an numerically exact implementation of the EFIE.

The FAFFA is a clear improvement on the NBS and GFPM producing good results for the demanding German profile where the NBS and GFPM failed and doing so with a reduced order of complexity in the algorithm.

7.3.4 Tabulated Characteristic Data

Computational Cost	Memory Requirement	Complexity of Code
$O(C_1N^2/M + C_2NM)$	$O(N/M)$	Complex

Table 7.6: Computational Features of the FAFFA

Jerslev	Hjorring	German
80	300	25

Table 7.7: Computation times for Electric Field Coverage at 144MHz over the Jerslev (Danish), Hjorring (Danish) and German profiles.

Jerslev	Hjorring	German
4000	15000	1200

Table 7.8: Computation times for Electric Field Coverage at 970MHz over the Jerslev (Danish), Hjorring (Danish) and German profiles.

7.3.5 Results

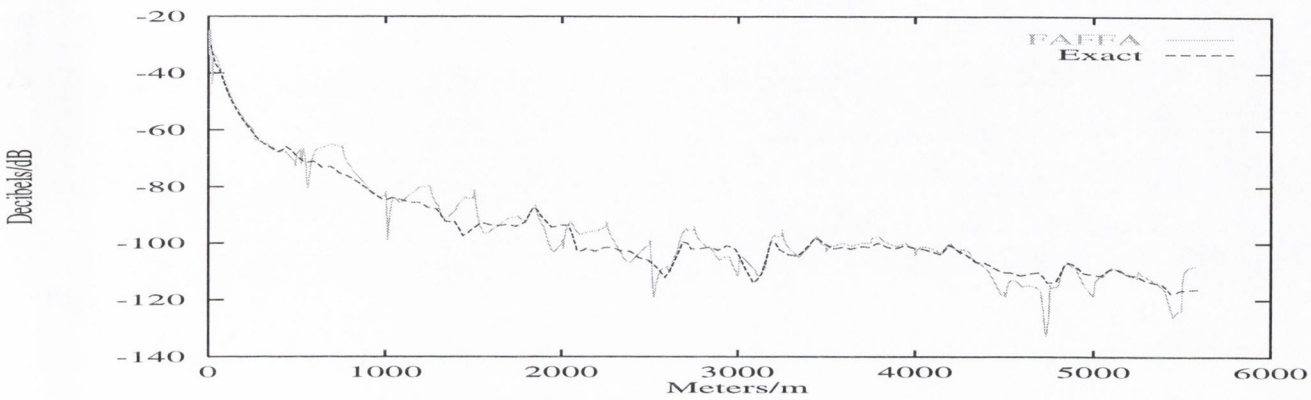

Figure 7.10: Electric Field Coverage at 144MHz over the Jerslev profile.

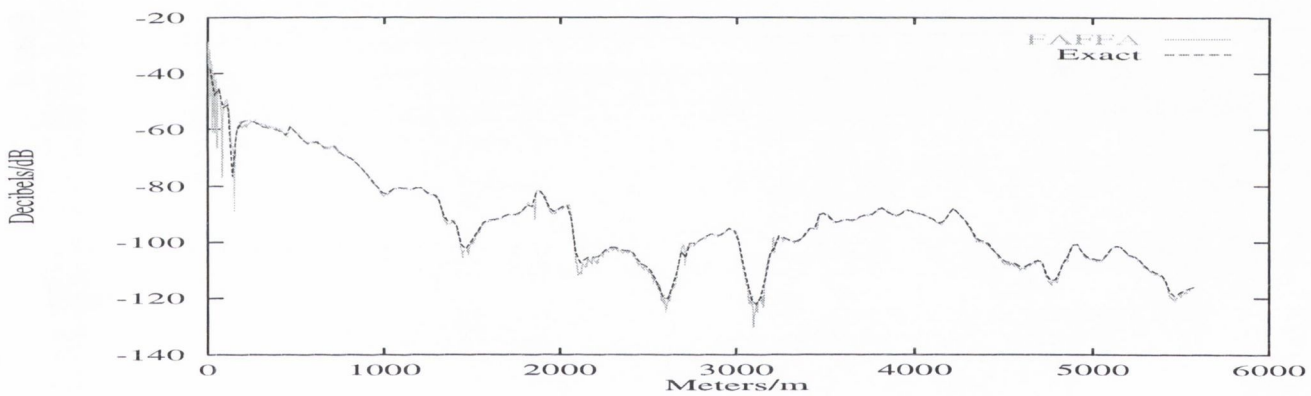

Figure 7.11: Comparative Plot of the Electric Field Coverage at 970MHz over the Jerslev profile.

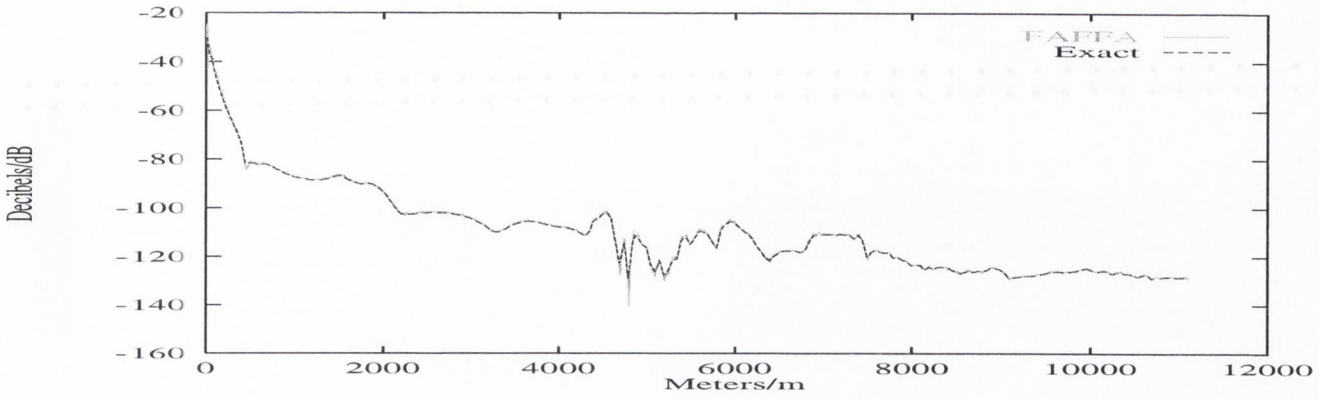

Figure 7.12: Comparative Plot of the Electric Field Coverage at 144MHz over the Hjorring profile.

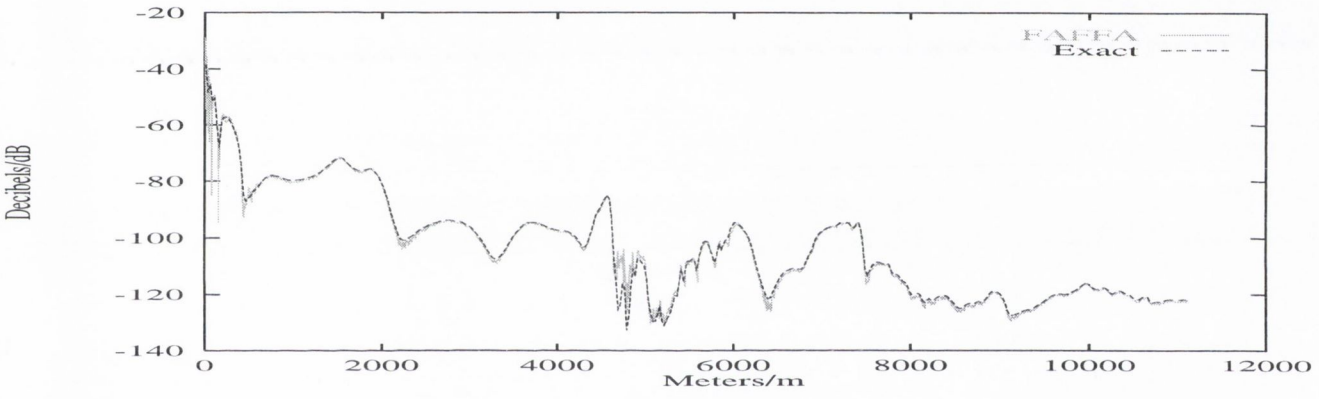

Figure 7.13: Comparative Plot of the Electric Field Coverage at 970MHz over the Hjorring profile.

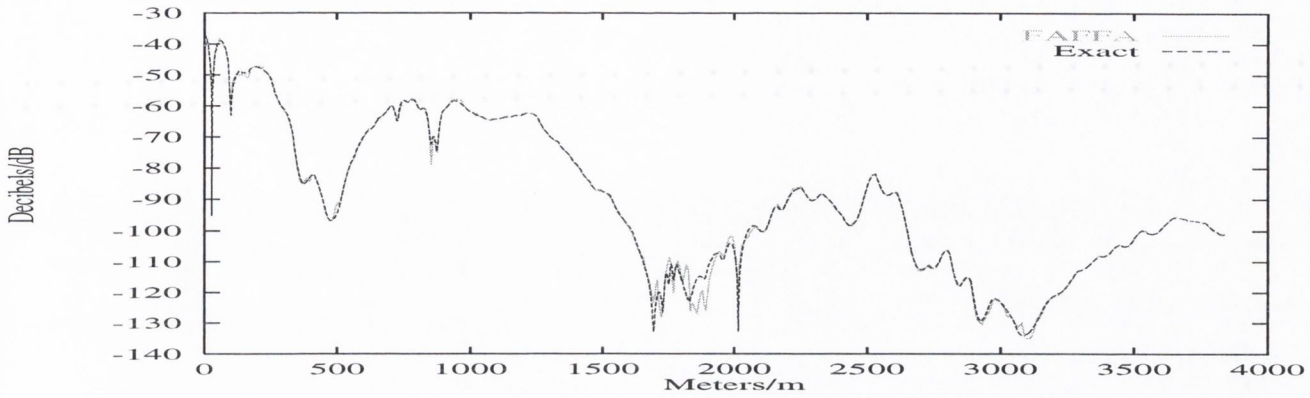

Figure 7.14: Comparative Plot of the Electric Field Coverage at 144MHz over the German profile.

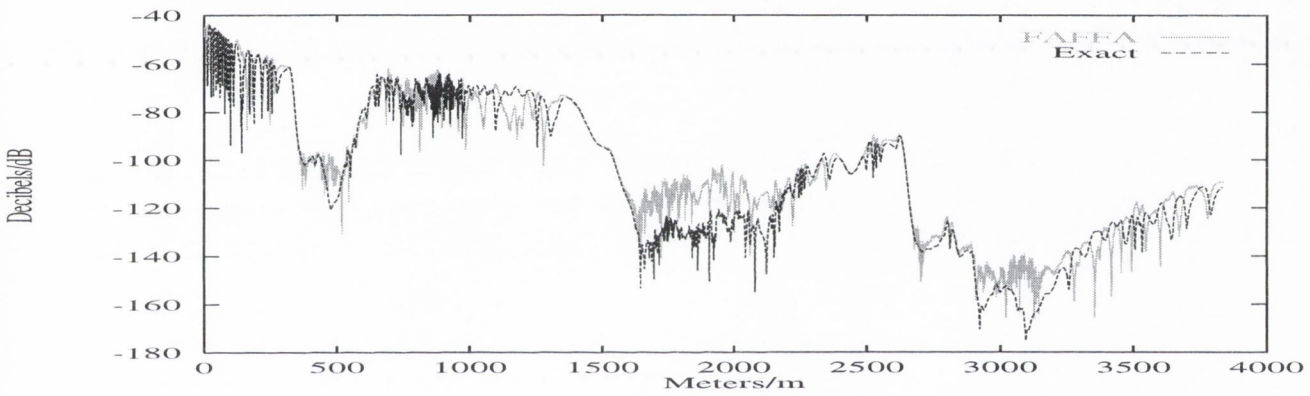

Figure 7.15: Comparative Plot of the Electric Field Coverage at 970MHz over the German profile.

7.4 The Tabulated Interaction Method (TIM)

7.4.1 Theory

Brennan and Cullen [25] ... [41] propose a separate program to precompute and store the summation in (7.46) for a range of incident and scattering angles $\phi_{ll'} - \phi_{l'j}$ and $\phi_{ll'} - \phi_{il}$ respectively.

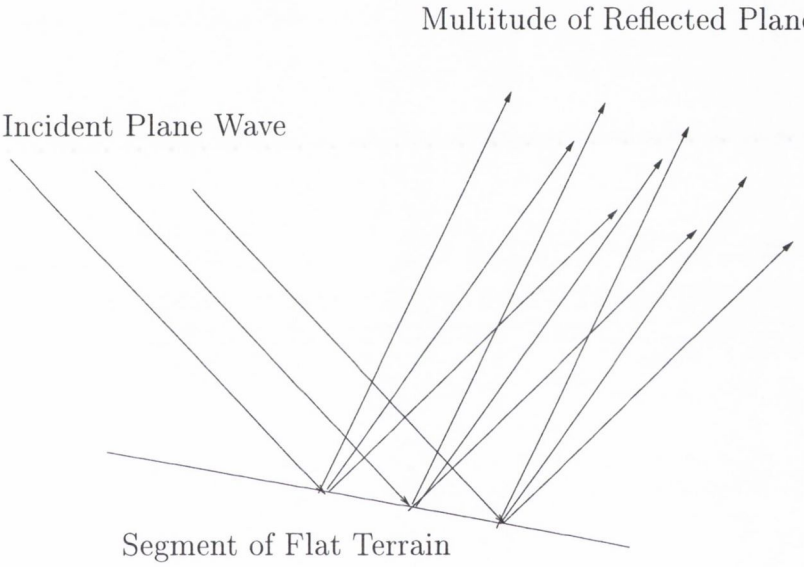

Figure 7.16: TIM scattering geometry showing an incident plane wave on a flat segment of surface being considered to scatter a multitude of plane waves.

From (7.44) and (2.40):

$$\begin{aligned} E^I(\rho_{l'}) &= E^T(\rho_{l'}) \\ &- \sum_{G_{l'}=0}^{G_l<G_{l'}} \mathcal{H}_0^{(2)}(\beta\rho_{ll'}) \sum_{i=0}^{i<M} e^{(i\beta\Delta_{l'j}\cos(\phi_{ll'}-\phi_{l'j})} e^{(i\beta\Delta_{il}\cos(\phi_{ll'}-\phi il)} J(\rho_i)\Delta s_i' \end{aligned} \tag{7.47}$$

Where the groups can be taken to be flat plates without too much distortion of the surface, (7.48) can be written locally (i.e. over a plate) to a good approximation:

$$
\begin{aligned}
E^I(\rho_{l'}) &= E^T(\rho_{l'}) \\
&- \sum_{G_{l'}=0}^{G_l<G_{l'}} \mathcal{H}_0^{(2)}(\beta\rho_{ll'})E(\rho_{l'}) \sum_{i=0}^{i<M} e^{(i\beta\Delta_{l'j}\cos(\phi_{ll'}-\phi l'j)} e^{(i\beta\Delta_{il}\cos(\phi_{ll'}-\phi il)} \\
&\times J_{Plane}(\rho_i, \phi_{ll'} - \phi_{il})\Delta s_i'
\end{aligned}
\tag{7.48}
$$

- where J_{Plane} is obtained from the EFIE with incident field a unit amplitude plane wave. The functional dependence of the summation over the current on angle of incident and scattered radiation can be established by creating a lookup table for this summation tabulated w.r.t. $\phi_{ll'} - \phi_{il}$ and $\phi_{ll'} - \phi_{l'j}$.

$E^T(l)$ is the total field incident at point l on the lth plate. As such it is the sum of the radiation incident on the lth plate over a range of angles of incidence $\phi_{ll'} - \phi_{il}$.

Hence:

$$
\begin{aligned}
E^I(\rho_j) &= E^T(\rho_j) \\
&- \sum_{G_l=0}^{G_l<G_{l'}} \mathcal{H}_0^{(2)}(\beta\rho_{ll'}) \sum_{\phi=(\phi_{ll'}-\phi_{il})_{min}}^{\phi=(\phi_{ll'}-\phi_{il})_{max}} E^T(l, \phi_{ll'} - \phi_{il}) \\
&\times \sum_{i=0}^{i<M} e^{(i\beta\Delta_{l'j}\cos(\phi_{ll'}-\phi_{l'j})} e^{(i\beta\Delta_{il}\cos(\phi_{ll'}-\phi_{il})} J_{Plane}(\rho_i, \phi_{ll'} - \phi_{il})\Delta s_i'
\end{aligned}
\tag{7.49}
$$

- from which $E^T(\rho_l)$ is determined.

The total field above the surface is then:

$$
\begin{aligned}
E(\rho'') &= E^I(\rho'') \\
&- \sum_{G_l=0}^{G_l<G_{l'}} \mathcal{H}_0^{(2)}(\beta \mid \rho_{l'} - \rho'' \mid)E(\rho_l) \sum_{i=0}^{i<M} e^{(i\beta\Delta_{l'j}\cos(\phi_{ll'}-\phi_{l'j})} e^{(i\beta\Delta_{il}\cos(\phi_{ll'}-\phi_{il})} \\
&\times J_{Plane}(\rho_i, \phi_{ll'} - \phi_{il})\Delta s_i'
\end{aligned}
\tag{7.50}
$$

The salient facts about TIM are given in the table followed by results for the Danish and German profiles.

7.4.2 Analysis of Results

The results given by the TIM are similar to those given by the FAFFA illustrating that it is possible to obtain good results with tabulation via a plane wave approximation.
This yields no computational advantage in itself but where a number of trials are performed, computation times are much improved because it is necessary to create the table only once.
This is the useful feature of TIM and would come into play where one is investigating coverage over different terrain profiles where the same groupsize would be used.
Were coverage at different frequencies to be investigated it would be disadvantageous to use TIM since the table would have to be re-evaluated for each frequency.
TIM suffers from the disadvantage that unlike the FAFFA, this algorithm does not converge to the EFIE with decreasing groupsize. The reason for this is that edge effects become significant in the results generated for the table (from finite length plates) giving rise to greater inaccuracies as the groupsize gets smaller.
This means TIM unlike the FAFFA and the FEM (which is introduced presently) is limited in the types of terrain for which it can produce good results.
This limitation is illustrated in the following results where the groupsize is taken to be one wavelength.
Here the results obtained, instead of converging to the exact, break down.

7.4.3 Tabulated Characteristic Data

Computational Cost	Memory Requirement	Complexity of Code
$O(C(N/M)^2 + N/M)$	$O(N/M)$	Complex
$O(CM^2)$	$O(C)$	Simple

Table 7.9: Computational Features of the TIM (Main Program/Tabulation Program)

Jerslev	Hjorring	German
0.5	1.5	1

Table 7.10: Computation times for Electric Field Coverage at 144MHz over the Jerslev (Danish), Hjorring (Danish) and German profiles.

Jerslev	Hjorring	German
25	80	50

Table 7.11: Computation times for Electric Field Coverage at 970MHz over the Jerslev (Danish), Hjorring (Danish) and German profiles.

7.4.4 Results

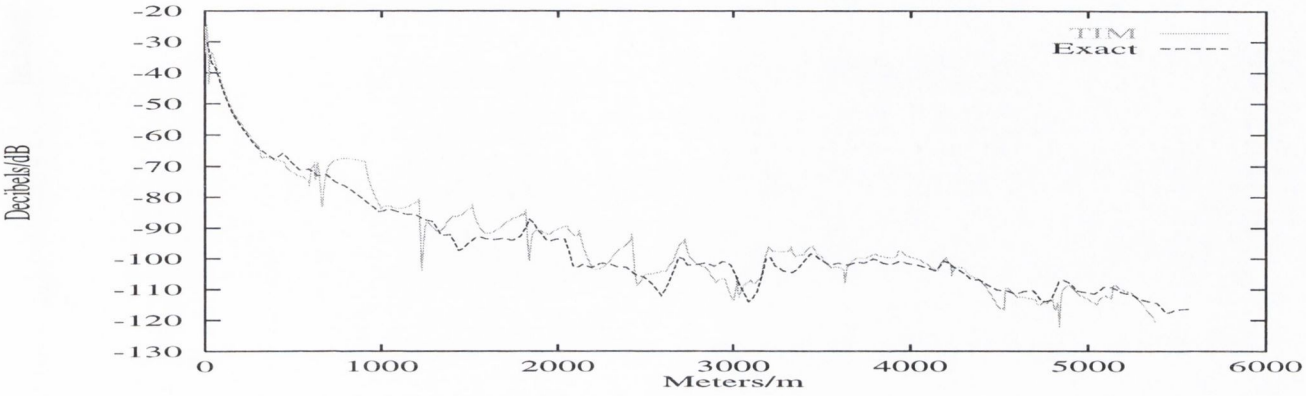

Figure 7.17: Comparative Plot of the Electric Field Coverage at 144MHz over the Jerslev profile.

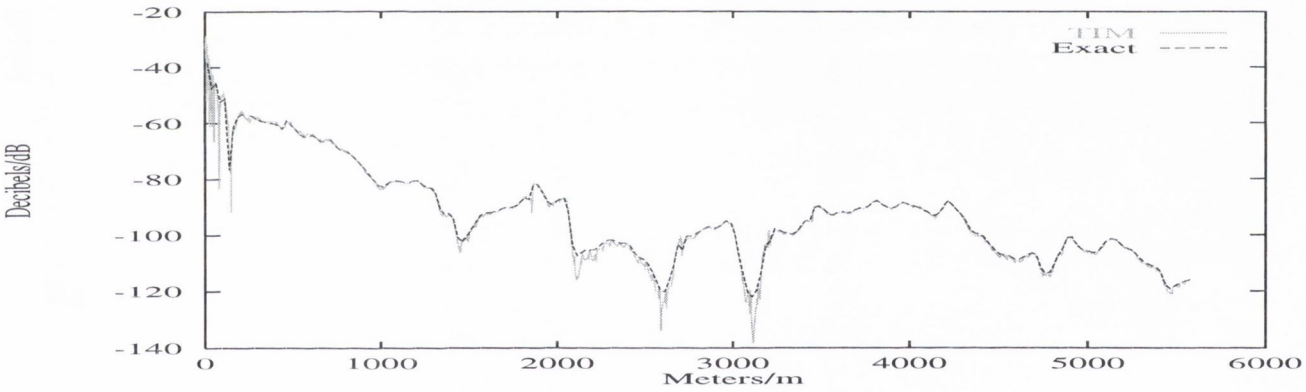

Figure 7.18: Comparative Plot of the Electric Field Coverage at 970MHz over the Jerslev profile.

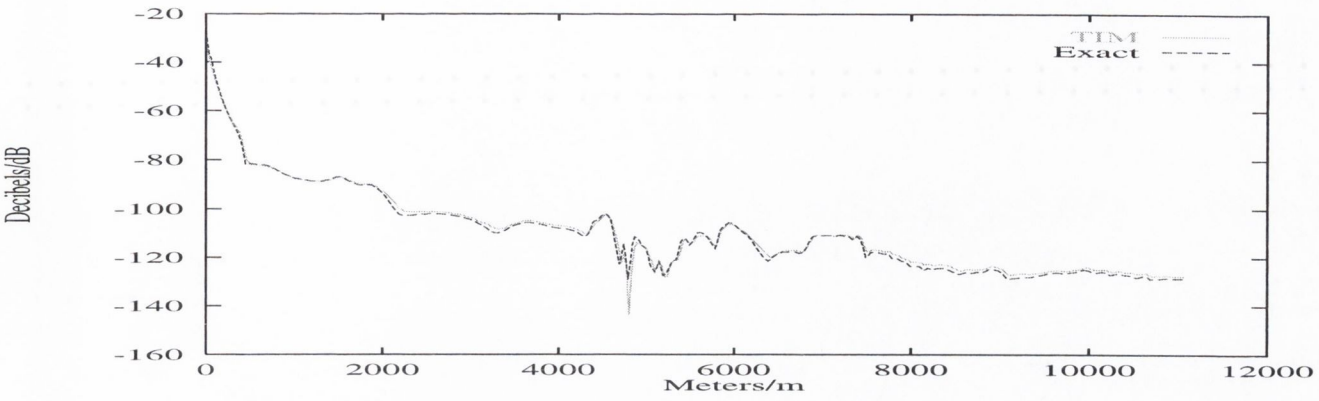

Figure 7.19: Comparative Plot of the Electric Field Coverage at 144MHz over the Hjorring profile.

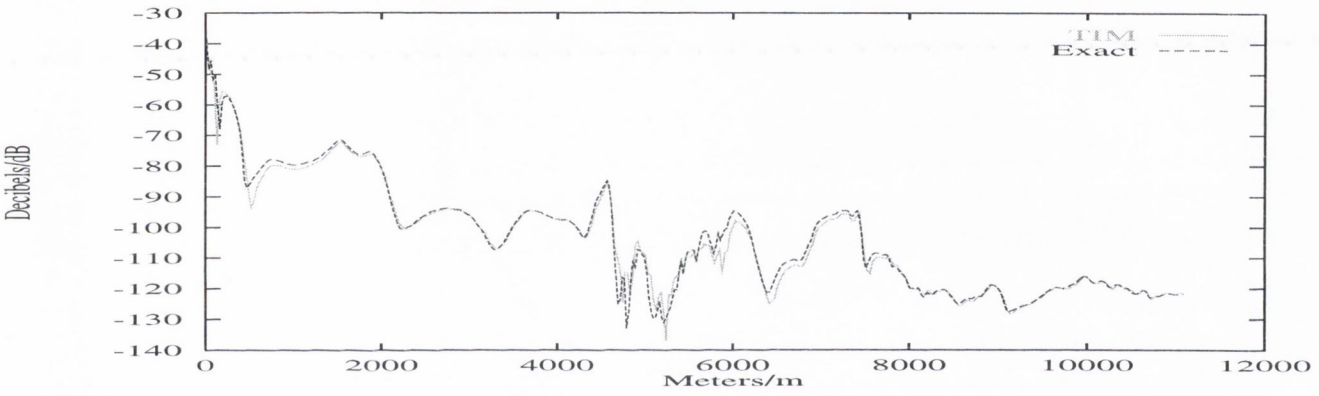

Figure 7.20: Comparative Plot of the Electric Field Coverage at 970MHz over the Hjorring profile.

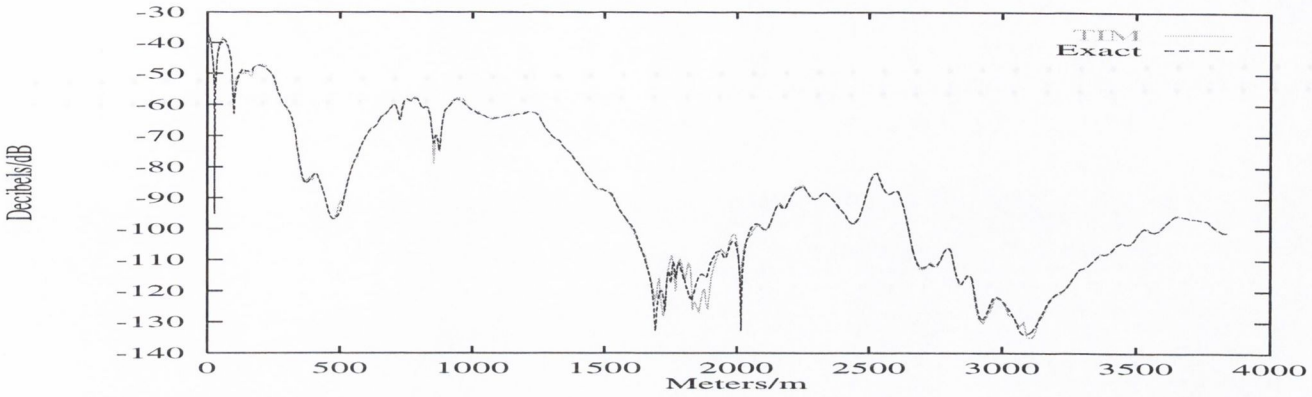

Figure 7.21: Comparative Plot of the Electric Field Coverage at 144MHz over the German profile.

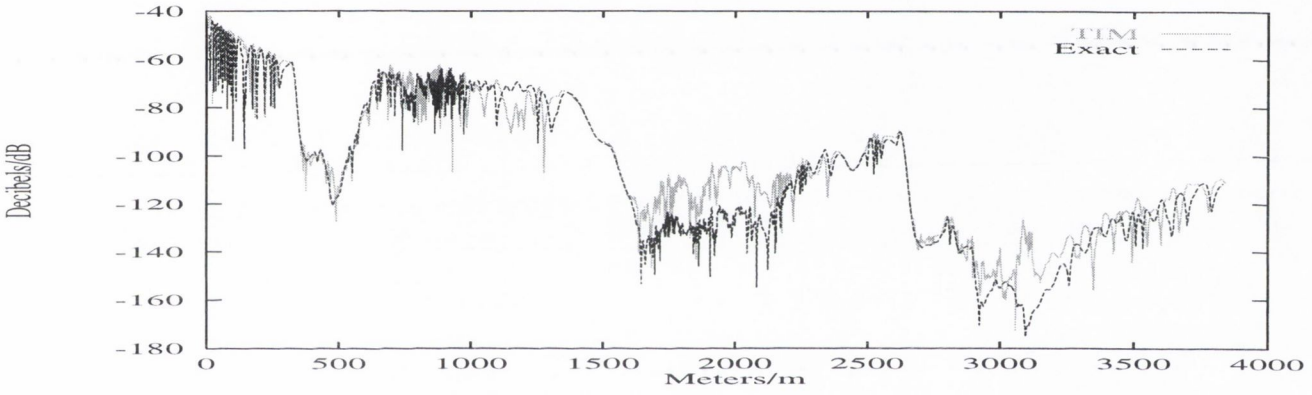

Figure 7.22: Comparative Plot of the Electric Field Coverage at 970MHz over the German profile.

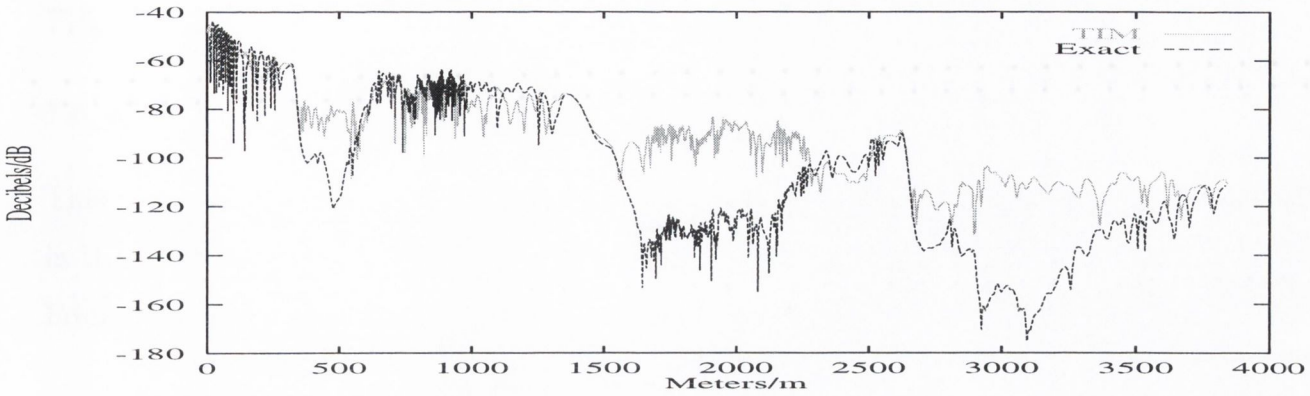

Figure 7.23: Comparative Plot of the Electric Field Coverage at 970MHz over the German profile with plate length of 1λ.

7.5 The Field Extrapolation Method (FEM)

7.5.1 Theory

This method eliminates the need to calculate or look up the summation over the current in the FAFFA formulation.

From (7.1):

$$J(\rho_i) = \frac{E(\rho_i)}{Z_{Self}} \tag{7.51}$$

$$E^I(l') = \sum_{G_l=0}^{G_l<G_{l'}} \mathcal{H}_0^{(2)}(\beta\rho_{ll'}) \sum_{i\in G_l} \frac{E(\rho_i)}{Z_{Self}} \mathcal{H}_0^{(2)}(\beta\rho_{il})\Delta s' \tag{7.52}$$

- where $J(\rho_i)$ has been replaced by the first term of the discrete form of the EFIE - $E(\rho_i)/Z_{Self}$.

l, l' refer now to the last segment in the scattering and receiving groups (this is a matter of convenience which will become apparent).

The formulation of (7.52) thus amounts to considering interactions between the last segment in each group.

The contribution of the other segments to the solution is considered by their interaction with the last segment.

Now I assume:

1) The total field over a segment or group of segments takes the form of the field incident from the source.

2) All groups refer to approximately flat (but not necessarily horizontal) terrain.

3) Group - group interactions are characterised by very oblique angles of incidence (Forward Scattering Model).

The Green's function is taken here as the far-field form of the Hankel function which is easy to manipulate algebraically.

These assumptions allow me write:

$$E(\rho_i) = A\mathcal{H}_0^{(2)}(\beta\rho_i) \tag{7.53}$$

as the form of the field incident on any group, where A is a constant.

Were we to consider a flat plate of finite length in free space illuminated by the source the total field incident on the last segment (due to the source and forward propagation from previous segments) would be:

$$\begin{aligned} E^T(\rho_l) &= A\sum_{i\in G_l} \frac{\mathcal{H}_0^{(2)}(\beta\rho_i)\mathcal{H}_0^{(2)}(\beta\rho_{il})}{Z_{Self}}\Delta s' \\ &= E(\rho_l)\sum_{i\in G_l} \frac{\mathcal{H}_0^{(2)}(\beta\rho_i)\mathcal{H}_0^{(2)}(\beta\rho_{il})}{Z_{Self}\mathcal{H}_0^{(2)}(\beta\rho_l)}\Delta s' \\ &\simeq E(\rho_l)\sum_{i=0}^{N/M} \frac{\mathcal{H}_0^{(2)}(\beta\rho_i)\mathcal{H}_0^{(2)}(\beta\rho_{il})}{Z_{Self}\mathcal{H}_0^{(2)}(\beta\rho_l)}\Delta s' \end{aligned} \tag{7.54}$$

Hence:

$$\sum_{i\in G_l} \frac{E(\rho_i)}{Z_{Self}}\mathcal{H}_0{}^{(2)}(\beta\rho_{il})\Delta s' = C\frac{E(\rho_l)}{Z_{Self}}\Delta s' \tag{7.55}$$

where

$$C = \sum_{i=0}^{N/M} \frac{\mathcal{H}_0^{(2)}(\beta\rho_i)\mathcal{H}_0^{(2)}(\beta\rho_{il})}{Z_{Self}\mathcal{H}_0^{(2)}(\beta\rho_l)}\Delta s' \tag{7.56}$$

Now (7.52) can be written:

$$E^I(\rho_{l'}) = \frac{C}{Z_{Self}} \sum_{G_l=0}^{G_l<G_{l'}} \mathcal{H}_0^{(2)}(\beta\rho_{ll'})E(\rho_l)\Delta s' \tag{7.57}$$

- which is the FEM formulation.

It should be noted that 'C' needs to be evaluated only once throughout the program. Hence the summation of (7.55) has been eliminated from (7.52).

This is analogous to eliminating (7.46) from the FAFFA and TIM.

From (2.40) the scattered field above the surface is then:

$$E^S(\rho'') = \frac{C}{Z_{Self}} \sum_{G_l=0}^{G_l<G_{l'}} E(\rho_l)\mathcal{H}_0^{(2)}(\beta \mid \rho_l - \rho'' \mid)\Delta s' \tag{7.58}$$

- where C appears here having the same value as before.

The FEM is adaptive in that groups of unequal size may be used.

As a 'grouping' algorithm the relationship between the FEM and the FMM based solutions (FMM, FFFA, TIM) is clear.

However from equations (7.24), (7.44) and (7.50) the FMM, FAFFA and TIM are N/M-point EFIE algorithms with unit pulse basis functions and weights $b_{l'j}$ and b_{il} applied about the group centre-points as part of a dynamic algorithm (as opposed to a 'fixed' algorithm such as the Natural Basis Method [57] which we have seen proposes a basis function of $e^{-i\beta\Phi(E^I(\rho_l))}$ along the terrain).

The FEM distinguishes itself from these algorithms in that it cannot be interpreted so.

The solution for the surface current is assumed in (7.55).

The salient facts for the FEM are given in the table followed by results for the Danish and German profiles.

7.5.2 Analysis of Results

The results given by the FEM show excellent agreement with the exact results.
Again in the German profile there is some deviation from the exact, most noticeably in the second (steepest) trough, though not to the extent of any of the previous methods.
Unlike the FAFFA and TIM, the FEM completely obviates the summation over the current, replacing it instead with a constant.
Unlike the TIM and like the FAFFA, the FEM converges to the EFIE for smaller group sizes.

7.5.3 Tabulated Characteristic Data

Computational Cost	Memory Requirement	Complexity of Code
$O(N/M)^2)$	$O(N/M)$	Very Simple

Table 7.12: Computational Features of the FEM

Jerslev	Hjorring	German
0.0008	0.04	0.7

Table 7.13: Computation times for Electric Field Coverage at 144MHz over the Jerslev (Danish), Hjorring (Danish) and German profiles.

Jerslev	Hjorring	German
0.04	0.2	35

Table 7.14: Computation times for Electric Field Coverage at 970MHz over the Jerslev (Danish), Hjorring (Danish) and German profiles.

7.5.4 Results

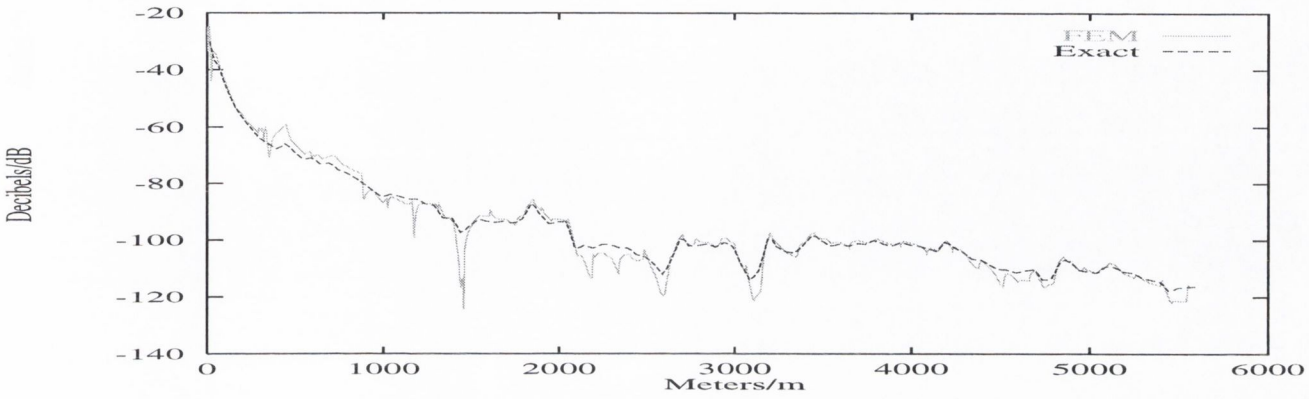

Figure 7.24: Electric Field Coverage at 144MHz over the Jerslev profile.

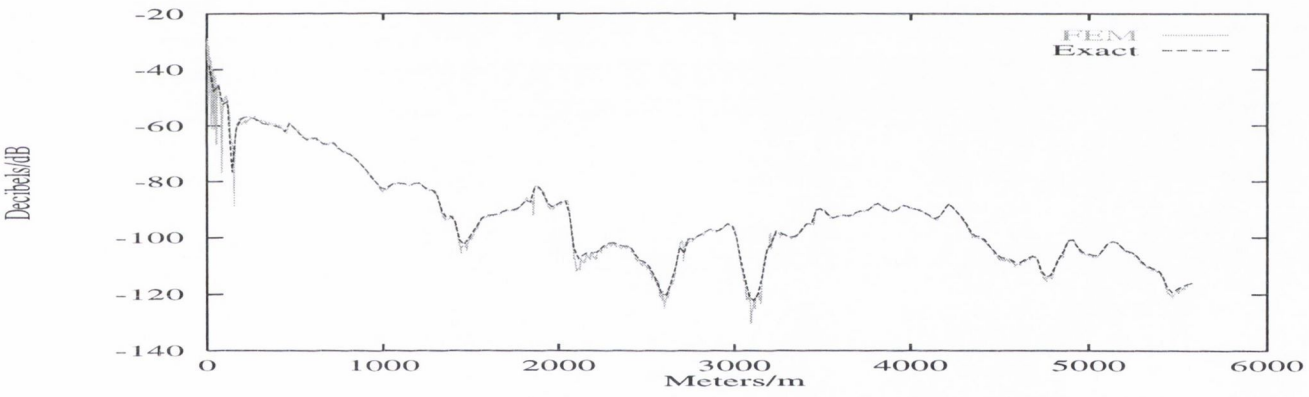

Figure 7.25: Comparative Plot of the Electric Field Coverage at 970MHz over the Jerslev profile.

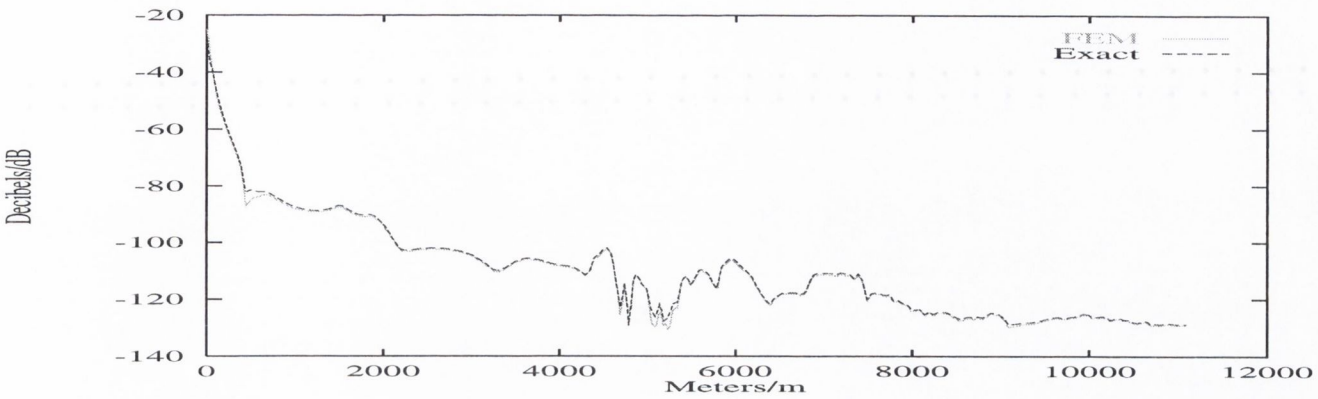

Figure 7.26: Comparative Plot of the Electric Field Coverage at 144MHz over the Hjorring profile.

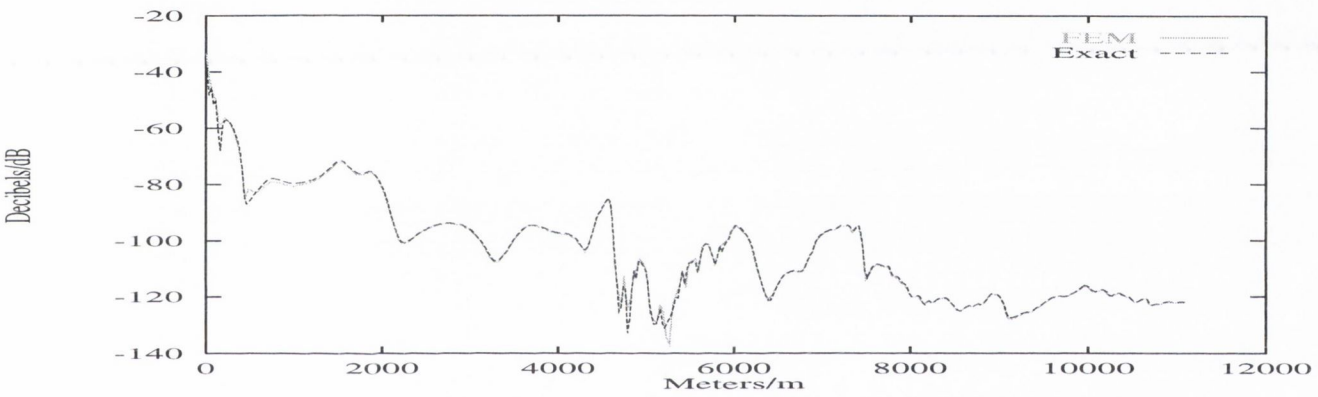

Figure 7.27: Comparative Plot of the Electric Field Coverage at 970MHz over the Hjorring profile.

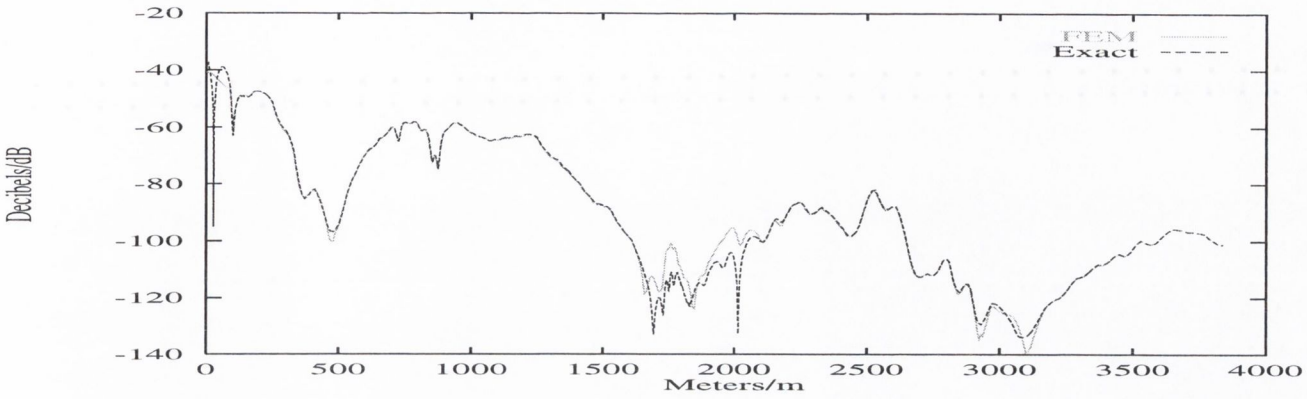

Figure 7.28: Comparative Plot of the Electric Field Coverage at 144MHz over the German profile.

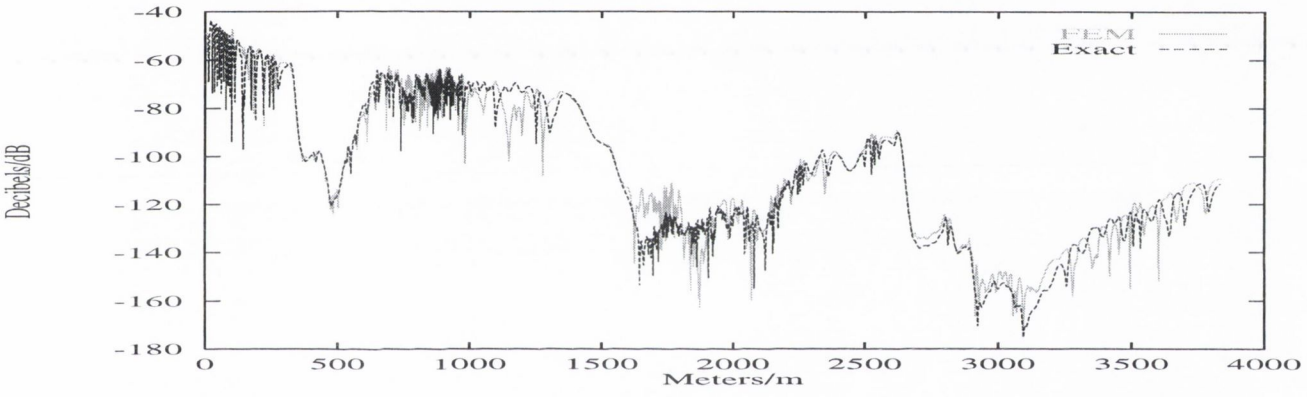

Figure 7.29: Comparative Plot of the Electric Field Coverage at 970MHz over the German profile.

7.6 Comparison of PEC Methods

7.6.1 Introduction

Here I will compare results given in this section. The purpose of this comparison is to advise the reader on the applicability of each method to the sub-urban scattering problem and also as a means of highlighting the effectiveness of the FEM.

GFPM and the Natural Basis have been ignored because they break down on the German profile.

It is clear there is little difference in the results given by the FAFFA, TIM and the FEM except at the second and third troughs of the German profile where the approximate methods diverge somewhat from the exact.

The second trough is the deepest in the German profile and so is the most demanding. The problem can be overcome by reducing the group-size in the FAFFA and FEM.

The order of complexity and memory requirements of the FEM are smaller than the FAFFA and the TIM. The code is very simple in comparison with the FAFFA and TIM. The FEM is thus the most appropriate fast integral equation algorithm to calculate field coverage over terrain.

The following tables are a compilation of the salient data for the above methods.

7.6.2 Tabulated Characteristic Data

Method	CC	Memory	Code Complexity
FAFFA	$O(C_1N^2/M + C_2NM)$	$O(N/M)$	Complex
TIM	$O(C(N/M)^2 + N/M)$	$O(N/M)$	Complex
TIM(Tab)	$O(CM^2)$	$O(M)$	Simple
FEM	$O(N/M)^2)$	$O(N/M)$	Very Simple

Table 7.15: Computational Features of the FAFFA, TIM and FEM.

Method	Jerslev	Hjorring	German
Exact	900/45000	3400/170000	410/20500
FAFFA	80/4000	300/15000	25/1200
TIM	0.5/25	1.6/80	1/50
TIM(Tab)	250/400	1000/1800	6500/8000
FEM	0.0008/0.04	0.004/0.2	0.7/35

Table 7.16: Computation times for Electric Field Coverage at 144/970MHz over the Jerslev (Danish), Hjorring (Danish) and German profiles.

7.6.3 Results

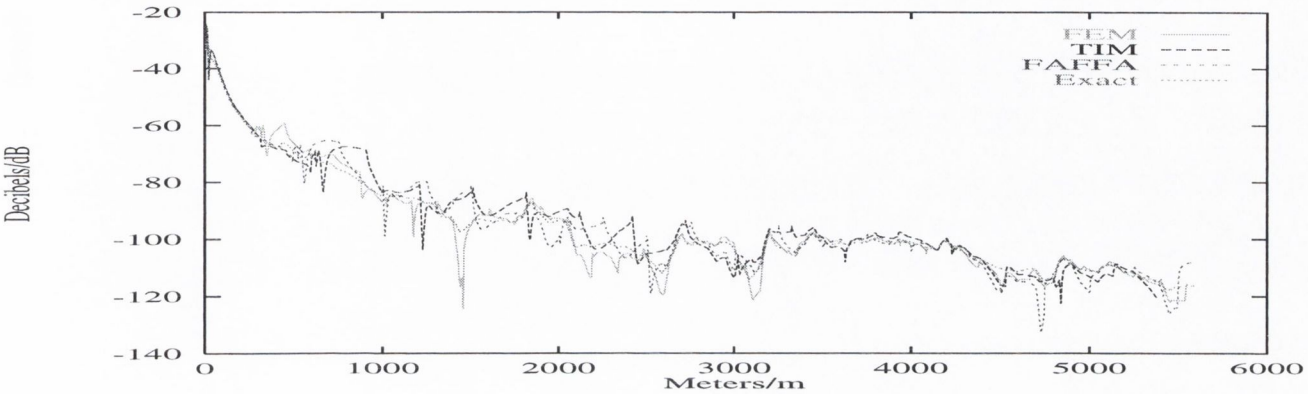

Figure 7.30: Comparative Plot of the Electric Field Coverage at 144MHz over the Jerslev profile.

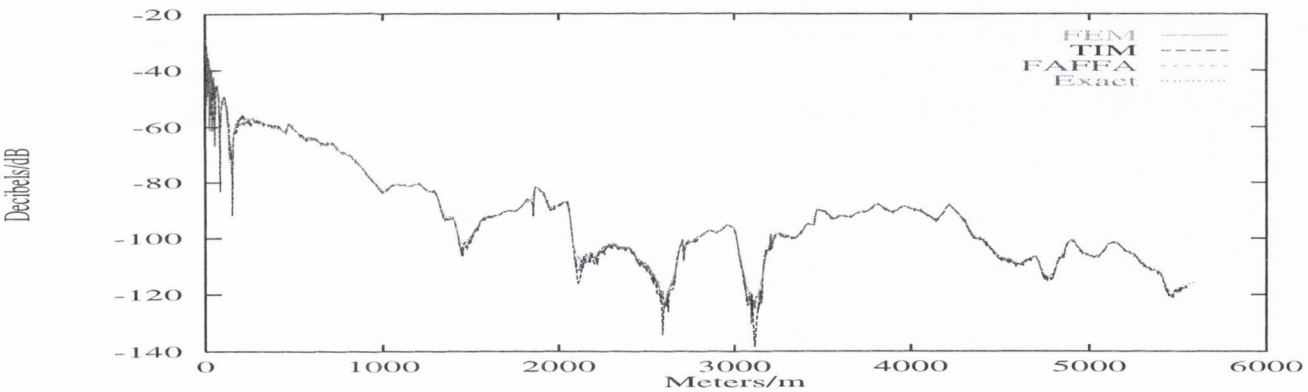

Figure 7.31: Comparative Plot of the Electric Field Coverage at 970MHz over the Jerslev profile.

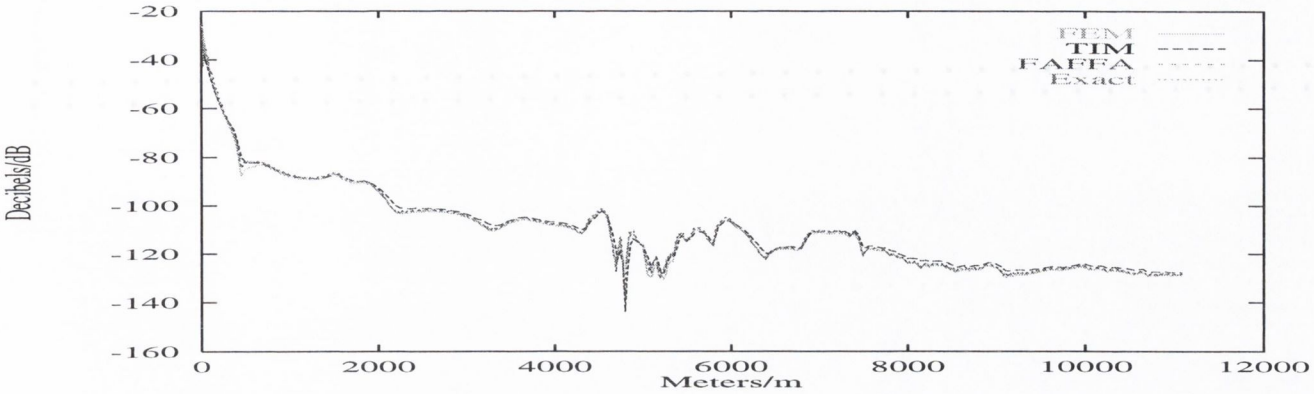

Figure 7.32: Comparative Plot of the Electric Field Coverage at 144MHz over the Hjorring profile.

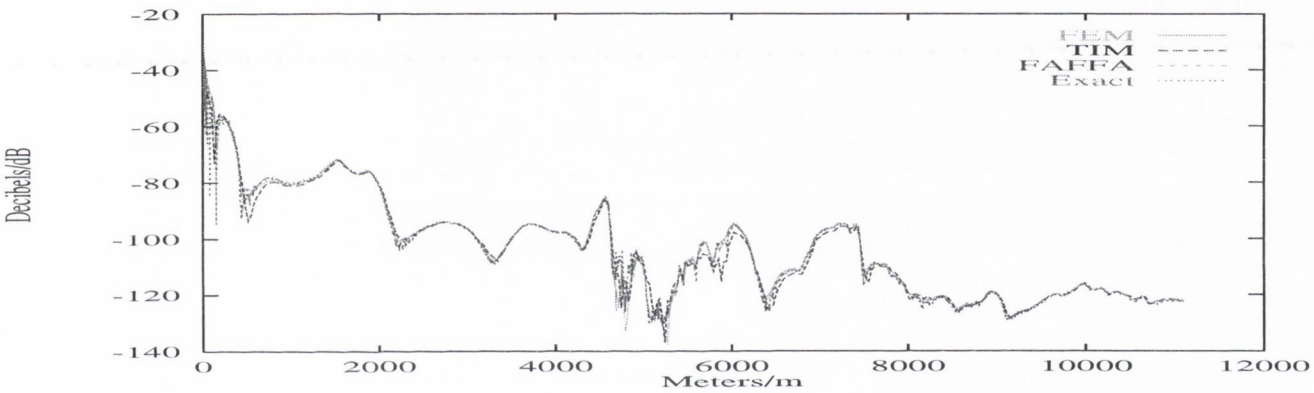

Figure 7.33: Comparative Plot of the Electric Field Coverage at 970MHz over the Hjorring profile.

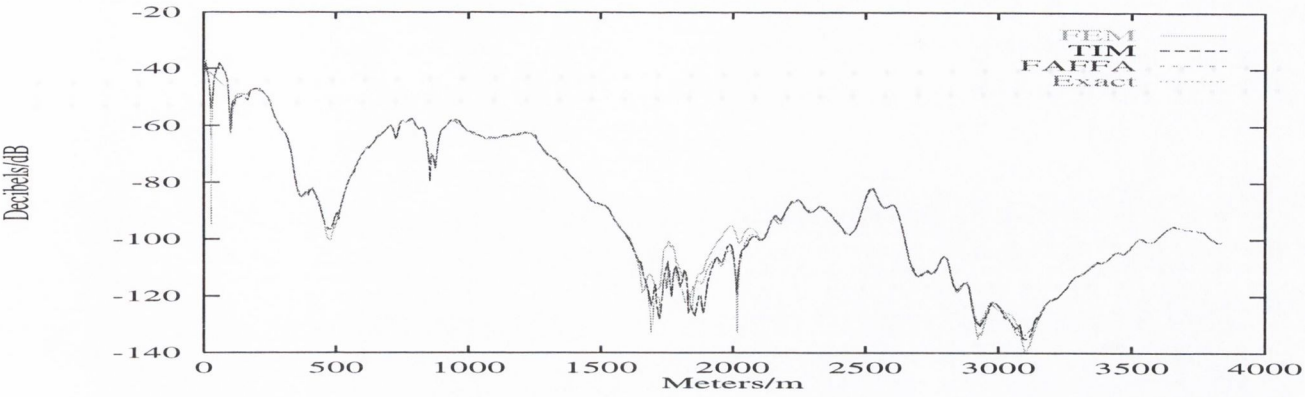

Figure 7.34: Comparative Plot of the Electric Field Coverage at 144MHz over the German profile.

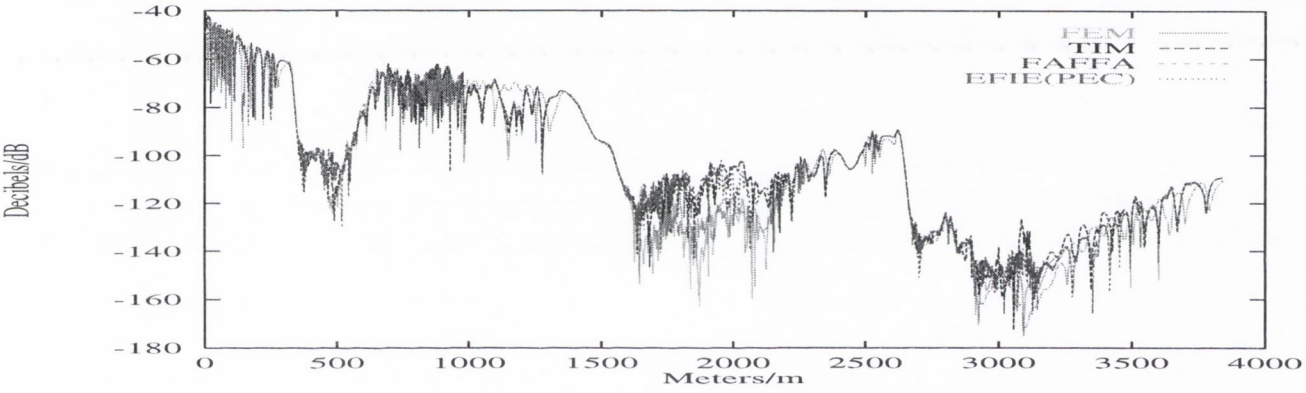

Figure 7.35: Comparative Plot of the Electric Field Coverage at 970MHz over the German profile.

FEM APPLIED TO ROUGH SURFACES

8.1 Introduction

The terrain profiles used throughout this thesis are two dimensional coordinates given at every $50M$ and $10M$ along the $'X'$ axis for the Danish and German profiles respectively. As a consequence of this the terrain profiles are composed of flat segments and the results for field coverage have been based on these profiles.

In reality however perturbations will exist on the surface which will not be accounted for by profile data. It is the purpose of this chapter to investigate whether such small-scale perturbations (clutter) will have a significant effect on coverage and on the FEM algorithm.

In the FEM algorithm (7.56) will be used on a sample of rough surface. Following discussion on the generation of a rough surface profile, the modified FEM algorithm will be tested for convergence with the exact solution.

8.2 A Model for Clutter

The model for clutter developed here is a statistical model. Here I will use a Gaussian distribution to represent variations in surface height not included in the original profile.

I correlate this distribution with a *Sinc* function to give an undulating effect. This is achieved by virtue of the sinusoidal form of the *Sinc* function and also due to the fact that as a correlation function it acts to filter out high frequency undulations giving a realistic model for perturbations of the surface profile.

To see exactly how this is achieved I first present the procedure used to generate the model. It is generated independently and superimposed on the original profile.

This procedure to generate the clutter model is general so arbitrary probability density functions and correlation functions can be used.

1) Generate a uniformly distributed random process 'y'.

(This is done using the standard 'C' library function 'rand()'.)

2) Apply the mapping y $\rightarrow$ f(y) where:

$$f(y) = \sqrt{2}\sigma erf^{-1}(y) \tag{8.1}$$

3) Obtain the FT of f(y) and the desired correlation function.

4) Obtain the inverse FT of the product.

The result is a correlated stationary stochastic process with a Gaussian p.d.f..

The theory behind this procedure is as follows:

Consider the random variable 'y' representing surface height. Its probability distribution function $P(y)$ is defined as:

$$P(y) = Prob[y < \alpha] \tag{8.2}$$

- i.e. the probability that the random variable y assumes a value less than some given number α.

The probability density function is then defined as:

$$p(y) = \frac{dP(y)}{dy} \tag{8.3}$$

which has the obvious property that:

$$\int p(y)dy = 1 \tag{8.4}$$

The autocorrelation (or the function with which the probability distribution is correlated) is defined as:

$$\rho(\tau) = \int y(x)y(x+\tau)dx \tag{8.5}$$

- where x represents horizontal distance.

A stochastic process is said to be strictly stationary if all its statistical properties are

independent of time. Perturbations of the surface are clearly a strictly stationary process. Taking the Fourier Transform of both sides we obtain the well known Wiener-Kintchine relation which is:

$$\begin{aligned} \mathcal{F}[\rho(\tau)] &= \mathcal{E}(\omega) \\ &= \mid F(\omega) \mid^2 \end{aligned} \tag{8.6}$$

- where $\mathcal{E}(\omega)$ is referred to as the power spectral density.

If $\mathcal{E}(\omega)$ is constant over ω then the random process is termed 'white noise'.

White noise is where a random variable distribution is uncorrelated (see below) and exists at all sampling frequencies.

The uniformly distributed process obtained in **1**) is taken to be white which implies its auto correlation function is the Dirac delta function - $\delta(\tau)$.

As a uniformly distributed random variable its probability density function is a constant (say unity) over a finite range. To determine a random variable $f(y)$ which has a Gaussian probability density function given the uniformly distributed random variable y, is to evaluate the function $'f'$ given via the identity:

$$\int dy = \frac{1}{\sqrt{2\pi}} \int exp^{-\frac{f(y)^2}{2}} df(y) \tag{8.7}$$

- which gives the mapping in **2**).

Because the *Sinc* function is a pulse in the frequency domain, it acts as a low-pass filter. This rids us of the high-frequency (grassy) components.

The product of the Fourier Transforms of $f(y)$ and the *Sinc* function performs this filtering which is step **3**) above.

The inverse Fourier Transform of the result (step **4**))then gives the spatial domain randomly distributed variable with a Gaussian distribution correlated with the *Sinc* function.

I have used the term 'Fourier Transform' loosely above. Specifically, I have used the Discrete Fourier Transform.

The Fourier Transform of a signal is defined as:

$$\begin{aligned} \mathcal{F}(f(y)) &= F(\omega) \\ &= \int f(y) e^{-i\omega y} dy \end{aligned} \tag{8.8}$$

The Discrete Time Fourier Transform is the Fourier Transform of a sampled signal and it follows that it is defined by:

$$\begin{aligned} \mathcal{F}_{DTFT}(f(y)) &= \mathcal{F}(f(y)) \\ &= \frac{1}{T}\sum_{n=-\infty}^{n=+\infty} F(\omega - n\omega_0) \end{aligned} \tag{8.9}$$

The Discrete Fourier Transform is then a sampled Fourier Transform of a truncated sampled signal.

It follows from this that it is defined by:

$$\begin{aligned} \mathcal{F}_{DFT} &= \mathcal{F}_s(f_s^{trunc}(y)) \\ &= \sum_{k=0}^{N-1} f(ky)e^{-i2\pi nk/N} \end{aligned} \tag{8.10}$$

- where $n = 0....N-1$, from which one period of the output is taken.

The subscript 's' denotes sampling and the superscript '$trunc$' truncation.

The algorithm used throughout this thesis where Fourier Transforms are encountered is the Fast Fourier Transform. A derivation of this algorithm and the latter two identities are given in the appendix.

Because the FEM is the most efficient method for evaluating field coverage over terrain, I now use it to estimate coverage over rough terrain using (7.56) on a sample of rough surface equal in length to the group-size. This effectivley models the distorted signal strength on rough surfaces as evinced by the following comparative plots at 144MHz and 970MHz on the German profile.

8.2.1 Analysis of Results

Correlation of a Gaussian distribution with the *Sinc* function gives a realistic model for surface perturbations. The results show that with increased roughness due either to increased amplitude or frequency of the perturbations or both is mirrored by the results obtained for the field coverage, but as with the smooth profile itself, the field results for the smooth profile remain the mean. The FEM algorithm does not break down when applied to rough surfaces and internal resonance does not occur within the surface perturbations to the extent that they effect the overall results.

8.2.2 Results

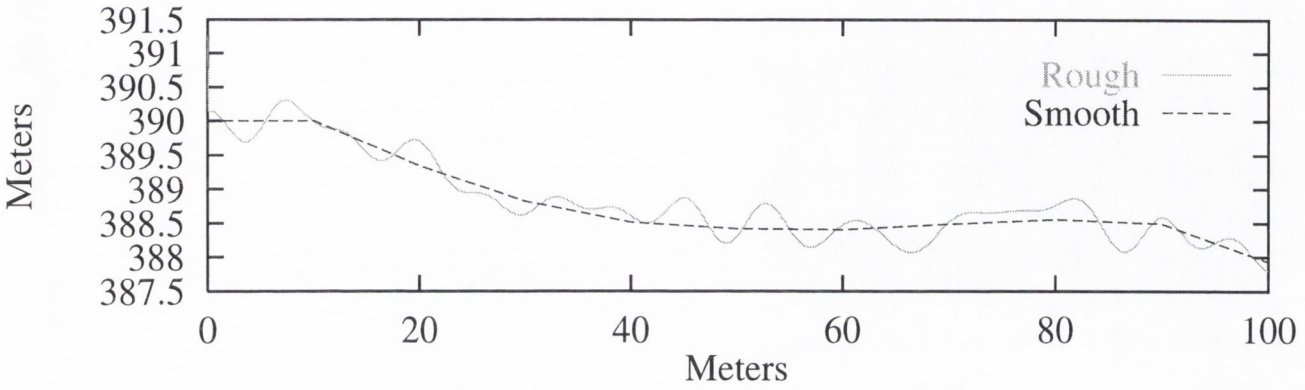

Figure 8.1: 100M of Smooth and Rough German Terrain. Amplitude and frequency of the '*Sinc*' function are 1.0M and 1.0 rad/s respectively.

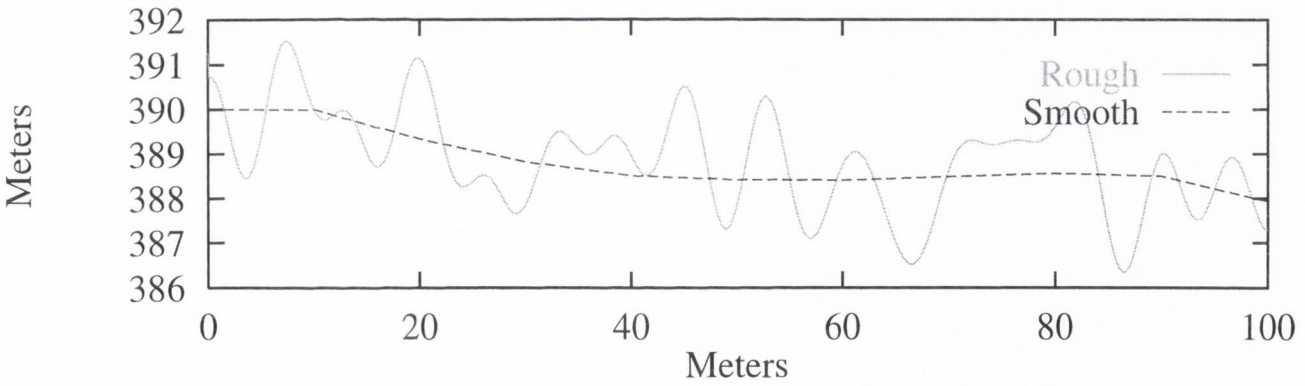

Figure 8.2: 100M of Smooth and Rough German Terrain. Amplitude and frequency of the 'Sinc' function are 5.0M and 1.0 rad/s respectively.

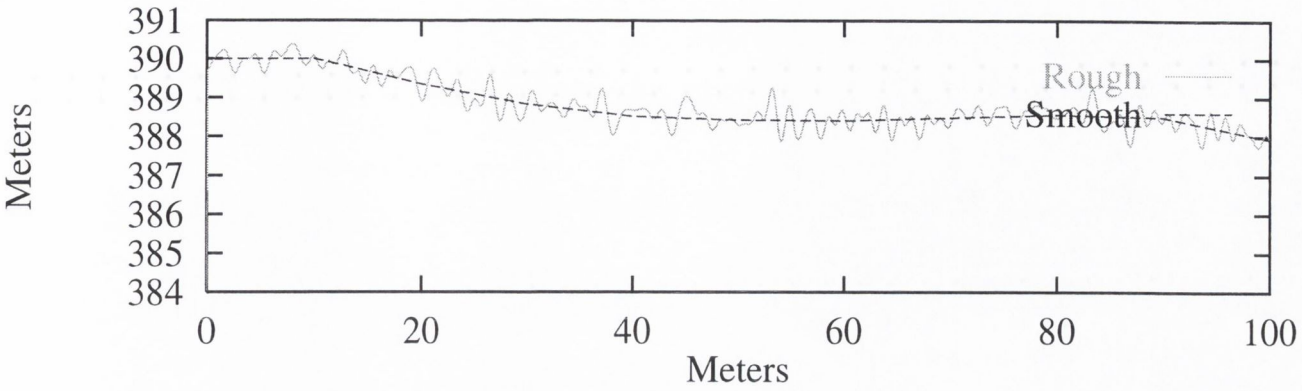

Figure 8.3: 100M of Smooth and Rough German Terrain. Amplitude and frequency of the 'Sinc' function are 1.0M and 5.0 rad/s respectively.

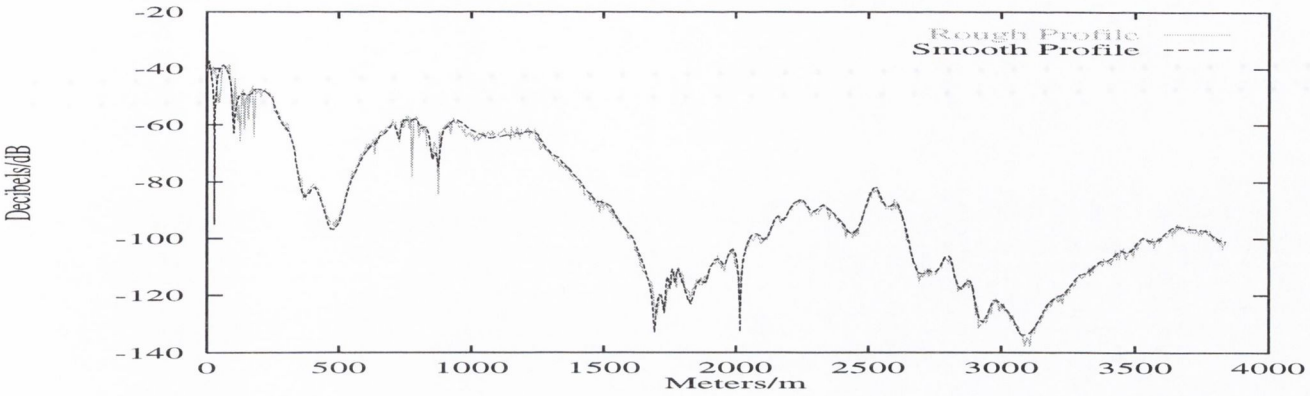

Figure 8.4: Comparative Plot of the Electric Field coverage at 144MHz over the rough German profile. Amplitude and frequency of the '*Sinc*' function are $1M$ and $1rad/s$ respectively.

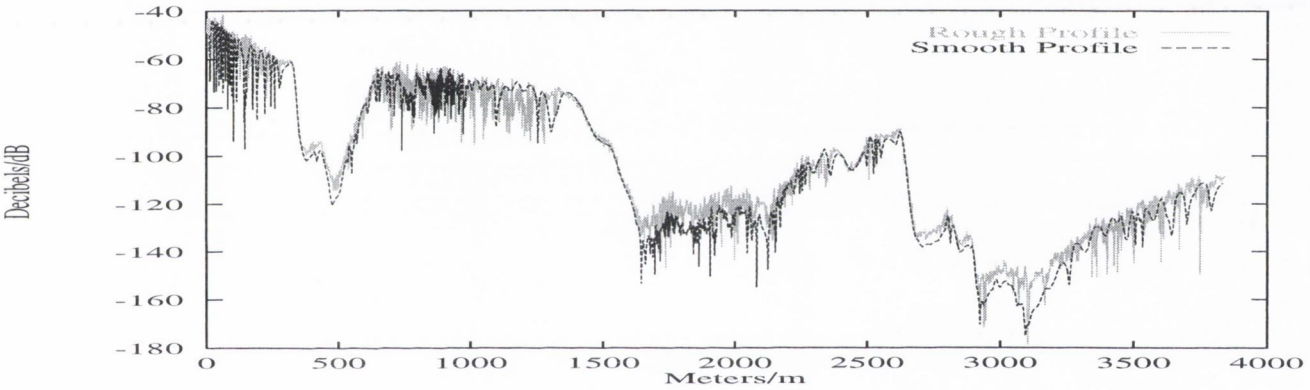

Figure 8.5: Comparative Plot of the Electric Field coverage at 970MHz over the rough German profile.

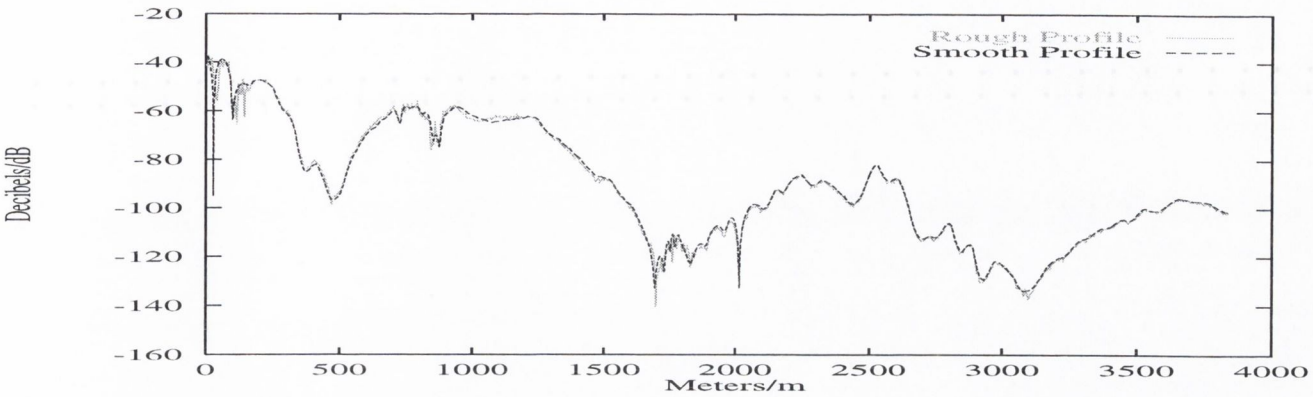

Figure 8.6: Comparative Plot of the Electric Field coverage at 144MHz over the rough German profile. Amplitude and frequency of the '*Sinc*' function are $1M$ and $5rad/s$ respectively.

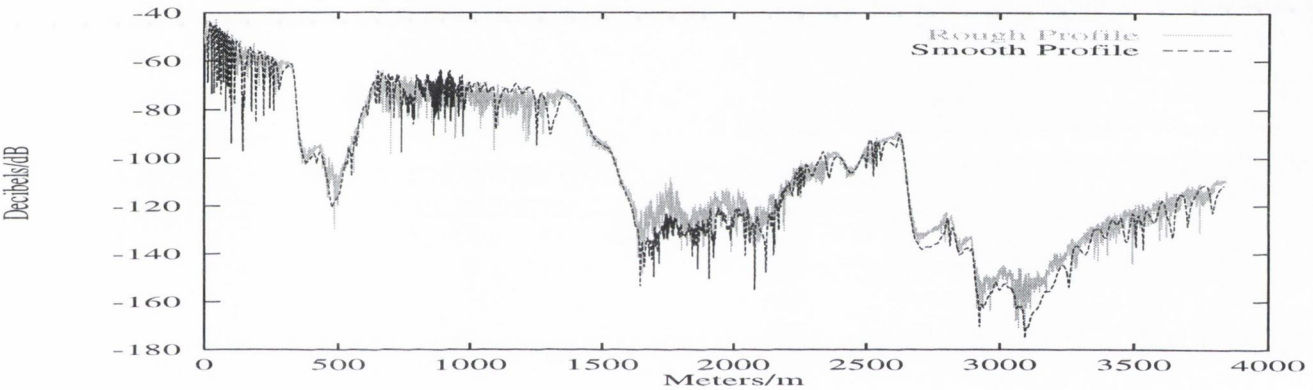

Figure 8.7: Comparative Plot of the Electric Field coverage at 970MHz over the rough German profile. Amplitude and frequency of the '*Sinc*' function are $1M$ and $5rad/s$ respectively.

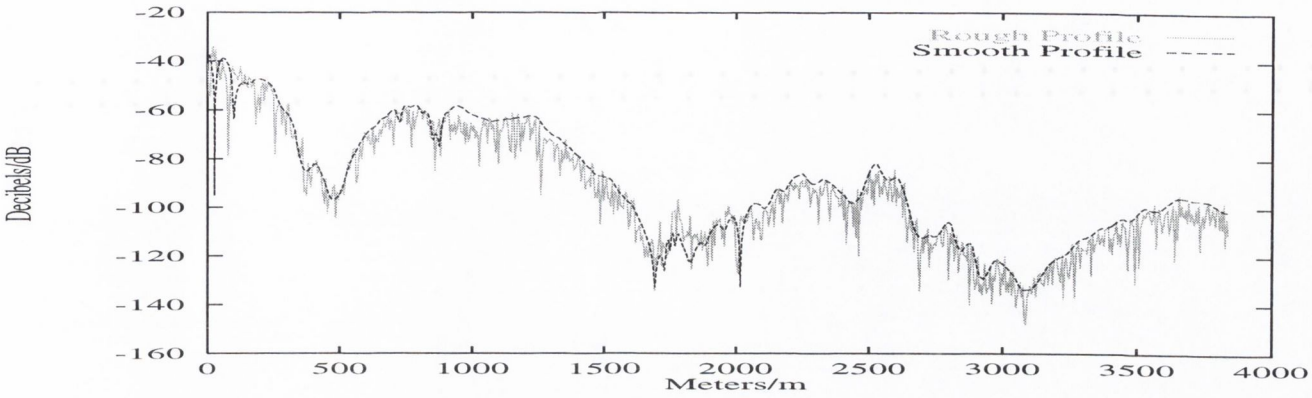

Figure 8.8: Comparative Plot of the Electric Field coverage at 144MHz over the rough German profile. Amplitude and frequency of the '*Sinc*' function are $5M$ and $1rad/s$ respectively.

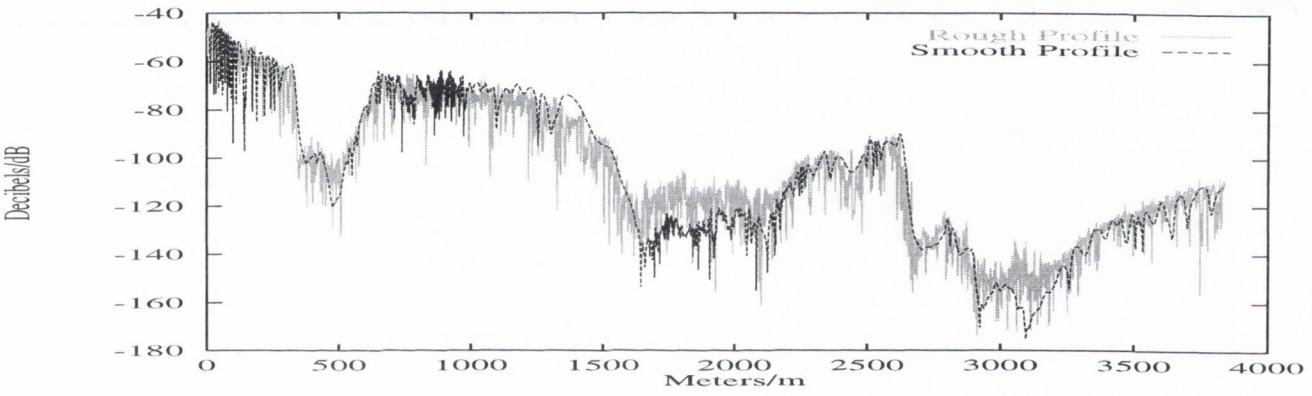

Figure 8.9: Comparative Plot of the Electric Field coverage at 970MHz over the rough German profile. Amplitude and frequency of the '*Sinc*' function are $5M$ and $1rad/s$ respectively.

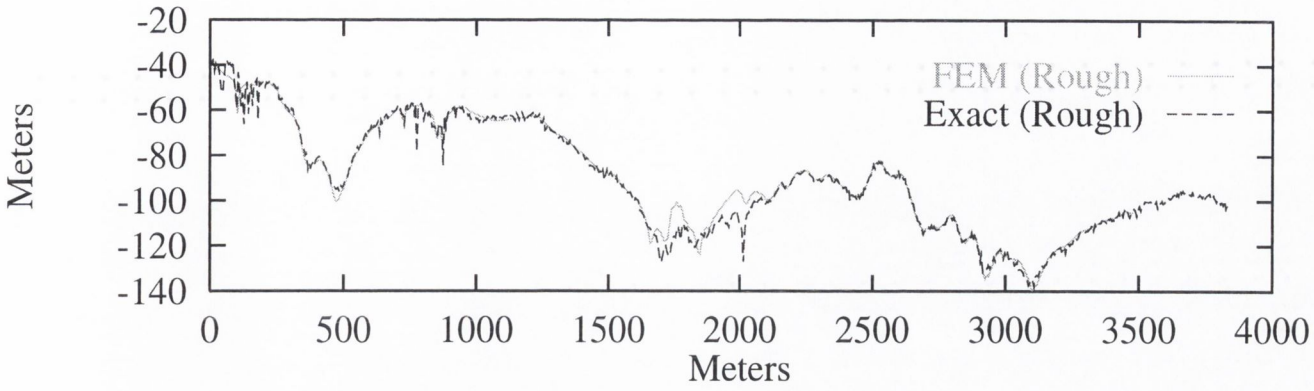

Figure 8.10: Comparative Plot of the Field Coverage at 144MHz over Rough German Terrain. Amplitude and frequency of the $'Sinc'$ function are $1M$ and $1rad/s$ respectively.

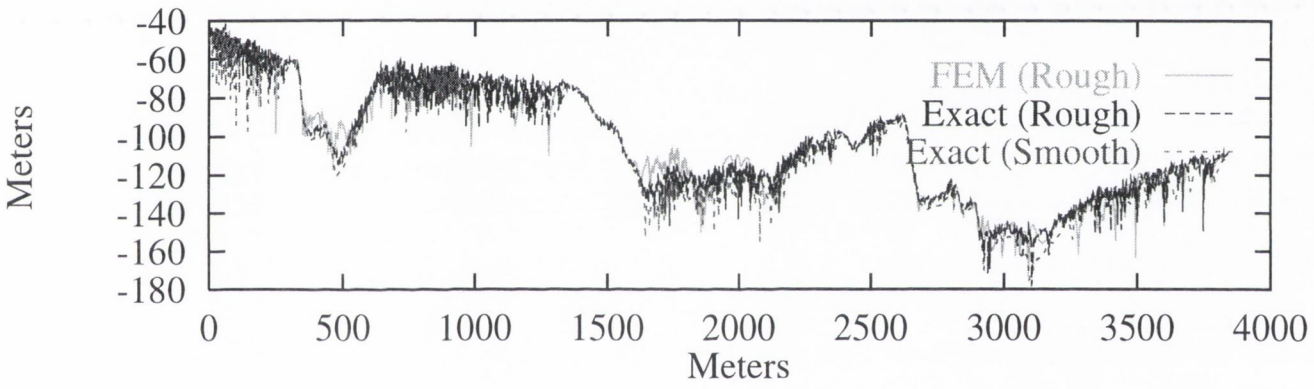

Figure 8.11: Comparative Plot of the Field Coverage at 970MHz over Rough German Terrain. Amplitude and frequency of the $'Sinc'$ function are $1M$ and $1rad/s$ respectively.

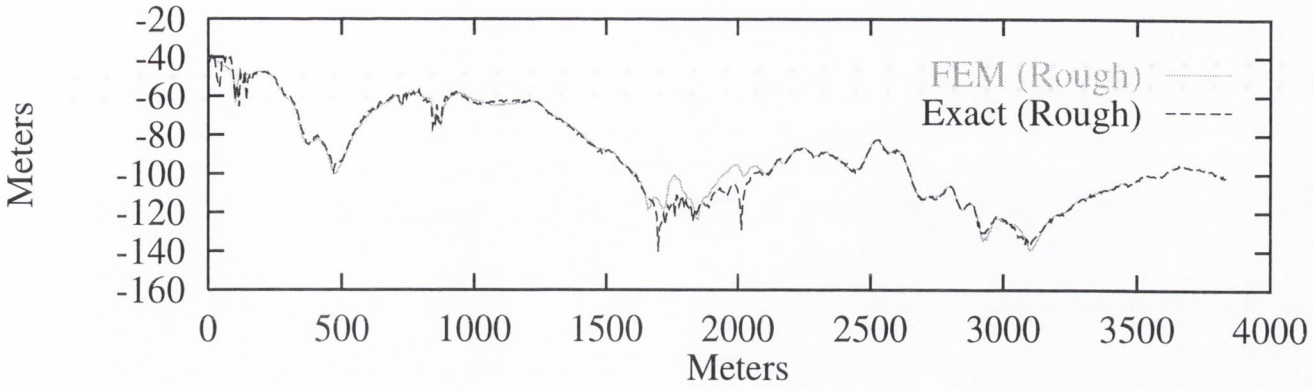

Figure 8.12: Comparative Plot of the Field Coverage at 144MHz over Rough German Terrain. Amplitude and frequency of the '*Sinc*' function are $1M$ and $5rad/s$ respectively.

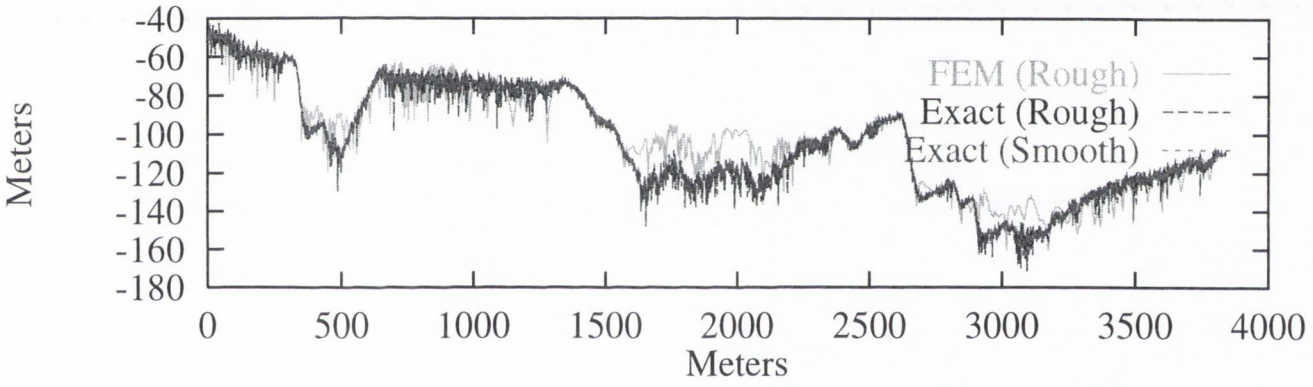

Figure 8.13: Comparative Plot of the Field Coverage at 970MHz over Rough German Terrain. Amplitude and frequency of the '*Sinc*' function are $1M$ and $5rad/s$ respectively.

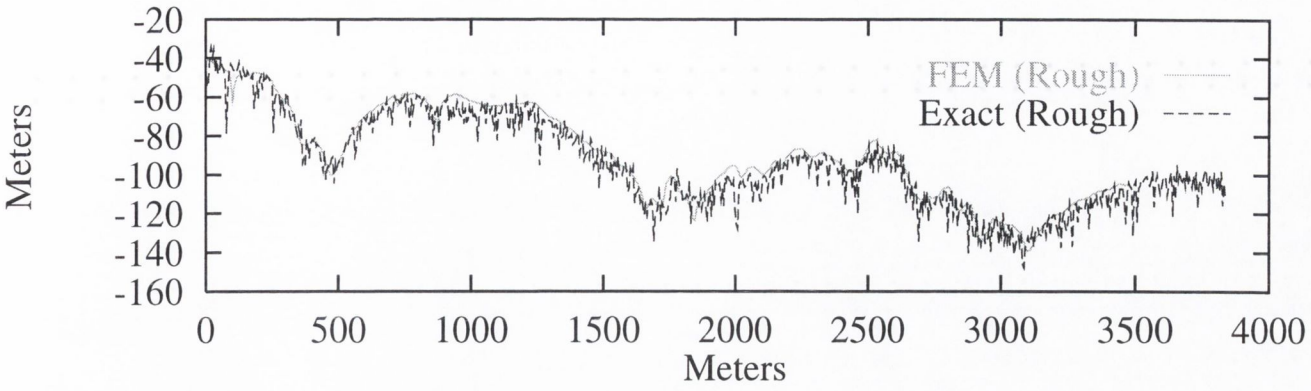

Figure 8.14: Comparative Plot of the Field Coverage at 144MHz over Rough German Terrain. Amplitude and frequency of the '*Sinc*' function are $5M$ and $1rad/s$ respectively.

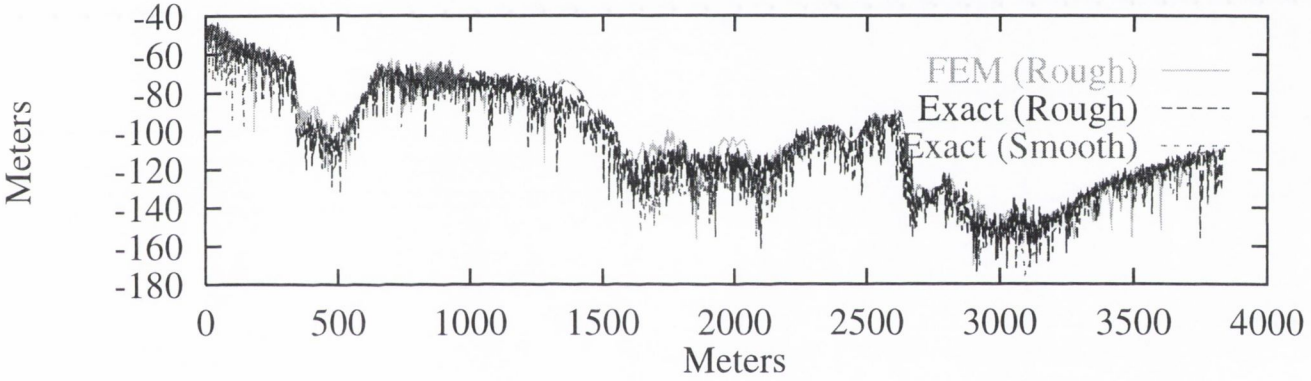

Figure 8.15: Comparative Plot of the Field Coverage at 970MHz over Rough German Terrain. Amplitude and frequency of the '*Sinc*' function are $5M$ and $1rad/s$ respectively.

REVIEW OF SCATTERING METHODS

Here I will discuss briefly five non-integral equation methods that may be used to calculate the scattered field and importantly point out the advantages and disadvantages of each. The purpose of this section is to prepare the reader for the conclusion to this thesis.

9.1 The Physical Optics Approximation (PO)

The Physical Optics approximation (PO) or Fresnel/Kirchoff theory is the fastest approximate means with which to determine the field scattered by a surface, having $O(N)$ as its order of complexity. This feature of the PO has led to algorithms which model diffraction effects given by undulations on the surface with those effects given by flat screens placed perpendicular to a flat surface. These results are then used in conjunction with the PO to build up a canonical solution for the scattered field. The PO is easily explained by examining the MFIE:

$$\hat{n} \times H^I(\rho) = \frac{1}{2}(\hat{n} \times H(\rho')) - \int_S (\hat{n} \times H(\rho')) \times \nabla' \times G(\rho, \rho') ds' \tag{9.1}$$

- where the above integral is a Cauchy integral. If the surface is infinite, flat and irradiated by a ubiquitous plane wave, the surface current is determined exactly from:

$$\frac{1}{2}(\hat{n} \times H(\rho')) \tag{9.2}$$

The reason for this is that the Cauchy integral is zero because the radiation scattered to a point from either side cancels completely. The approximation breaks down for finite and/or rough surfaces and where the source does not give ubiquitous near-plane wave coverage.

Advantages:

- The PO gives the fastest obtainable results for the scattered field.
- The PO algorithm is the simplest available.

Disadvantage:

- The PO gives reasonable results only where the surface is long and almost flat and the field incident on the surface is approximately plane.

9.2 The Impedance Boundary Condition (IBC)

The Impedance Boundary Condition relates the Surface Electric and Magnetic Currents. It can be written:

$$M_s(t) = \eta_s J_s(t) \times \hat{n}(t) \tag{9.3}$$

- where η_s is the surface impedance - Peterson [16].

As a consequence of this relation, an Electric Field Integral Equation for a dielectric can be written entirely in terms of the equivalent surface electric current.

This allows the EFIE for a dielectric to be stated as:

$$E_z^I(t) + \eta_s(t) J_z(t) + i\beta\eta_0 A_z + \left(\frac{\partial F_y}{\partial x} - \frac{\partial F_x}{\partial y} \right)_{S+} \tag{9.4}$$

where:

$$A_z(t) = \frac{1}{4i} \int J_z(t') \mathcal{H}_0^{(2)}(\beta R) dt' \tag{9.5}$$

$$F_z(t) = \frac{1}{4i} \int \hat{t}\eta_s(t') J_z(t) \mathcal{H}_0^{(2)}(\beta R) dt' \tag{9.6}$$

$$R = \sqrt{(x(t) - x(t'))^2 + (y(t) + y(t'))^2} \tag{9.7}$$

and η_0 is the intrinsic impedance of free space.

Advantage:

• IBC simplifies the calculation of the field scattered by a dielectric surface by reducing coupled integral equations to an integral equation in one unknown.

Disdvantages:

• η_s is an empirically derived constant and it is not uniform over an arbitrary surface. In fact η_s can depend strongly on angle of incidence for some materials - Hoppe [21]. It is suitable for application to materials with a high permittivity or permeability whose reflection characteristics do not depend strongly on the angle of incidence - Peterson [16].

9.3 The Parabolic Equation Method (PE)

The Parabolic Equation [22] for fields is an approximation to the elliptic Helmholtz equation.

The Parabolic equation has as its solution an inverse Fourier Transform.

In cylindrical coordinates the Helmholtz equation is:

$$\frac{\partial^2\psi}{\partial r^2} + \frac{\partial^2\psi}{\partial y^2} + \frac{1}{r}\frac{\partial^2\psi}{\partial\theta^2} + \frac{1}{r}\frac{\partial\psi}{\partial r} + \beta^2\eta^2(r,y,\theta)\psi = 0 \tag{9.8}$$

Substituting:

$$\psi(r,y) = u(r,y)\frac{e^i\beta r}{\sqrt{\beta r}} \tag{9.9}$$

we get the following equation in u:

$$\frac{\partial^2 u}{\partial r^2} + \frac{\partial^2 u}{\partial y^2} - 2i\beta\frac{\partial u}{\partial r} + +\beta^2\left(\eta^2 - 1 + \frac{1}{(2\beta r)^2}\right)u = 0 \tag{9.10}$$

Assuming further that $u/4r^2 \rightarrow 0$ and $\mid \frac{\partial^2 u}{\partial r^2} \mid \ll 2\beta \mid \frac{\partial u}{\partial r} \mid$ yields:

$$\frac{\partial^2 u}{\partial y^2} - 2i\beta\frac{\partial u}{\partial r} + +\beta^2\left(\eta^2 - 1\right)u = 0 \tag{9.11}$$

- which is the desired parabolic form.

Advantage:

- Coded FFT algorithms are widely available.

Disadvantages:

- Having as its solution an inverse Fourier Transform, the Parabolic Equation Method, like GFPM, suffers from the same restrictions giving poor results for uneven surfaces.
- The inverse transforms are taken along vertical domains.

In theory this domain is infinite. To counteract this the field is forced to taper to zero a distance above the surface.

This introduces a further approximation and added coding complexity.

9.4 The Impedance Matrix Localisation Method (IML)

The aim of this method [43] [44] [45] [46] is to generate a sparse impedance matrix which is cheaper to store and invert. This is done by choosing basis functions, which when used with the Green's function, force points on the surface to radiate in a non-isotropic fashion. In other words, the basis functions, chosen give mathematical expression to 'shining' yielding an impedance matrix with magnified and reduced entries corresponding to points on the surface which interact strongly and weakly respectively.
Those entries below a certain threshold can be set to zero producing a sparse matrix.

Advantage:

- This idea is useful for scatterers with a regular shape or where the geometry of the problem can be expressed simply in canonical form.

Disadvantages:

- Not suitable for rural terrain which is not easily reduced to a canonical form.
- Choice of the appropriate basis function to model interactions must be specific to the interaction being described.

Given there are many different types of interactions even for simple geometries, it would be difficult to generate good results.

9.5 The Geometrical/Uniform Theory of Diffraction (GTD/UTD)

As very high frequencies, the field can be described by geometrical optics.
That is:

$$E(\rho) = E(0)e^{-i\beta|\rho|} \tag{9.12}$$

This expression for the field contains no diffraction effect.
GTD [54] is an extension of the above to include diffraction effects based on the following postulates:

1) Fermat's Principle [53] can be applied to diffracted rays. (For an homogeneous medium this means diffracted rays follow straight lines).
2) The magnitude of the diffracted ray depends on the incident field and the nature of the boundary in the neighbourhood of the point of diffraction.
3) The phase of the diffracted ray is proportional to the optical length of the ray.

According to these postulates the diffracted field is proportional to the product of the incident field and a diffraction coefficient in the same way as the reflected field is proportional to a reflection coefficient in geometrical optics [5].
The diffraction coefficient is determined by taking the asymptotic form of the exact solution of the canonical problem.
The complete solution for the scattered field is obtained by superposition of reflected and diffracted rays.
In GTD diffraction coefficients are singular at the boundary.
UTD [55] overcomes these by assuming the incident field is plane, giving less accurate but robust diffraction coefficients.
Diffraction coefficients for various type boundaries are derived based on GTD and UTD in various texts, [5] [52].

Advantages:

- Very suitable for modelling propagation in urban environments because such a problem is easily reduced to a canonical form because of the generally regular shape of buildings.
- Calculation of field coverage due to reflected rays is an easy matter.

Disadvantages:

- Not suitable for rural terrain which is not easily reduced to a canonical form.
- To obtain good results, selection of the appropriate diffraction coefficient is necessary.

CONCLUSION

The conclusions this thesis makes are as follows:

• The PEC Model is a suitable model for terrain scattering problems.
Results obtained for the German profile where the terrain is considered to be composed of clay, sand or loam, superimposed on the result for the PEC Model are similar.
It is thus clear the PEC Model is valid for undulating terrain.
The reason for this is that at grazing incidence most of the radiation is reflected from the surface i.e. the phenomenon of Total Internal Reflection [52].

• Terrain scattering does not present resonance problems.
Comparison of results generated by the Coupled EFIEs and CFIE being virtually identical means resonance, which would manifest itself in poor results with the Coupled EFIE [16], is absent.

• Common terrain materials (clay, sand, loam) yield similar results for the scattered field.

• The FEM is the most appropriate algorithm to solve the terrain scattering problem.
By comparison it is clear the FEM algorithm has the lowest order of complexity of all integral equation methods presented in this thesis.
It is also the simplest algorithm and is easily adapted to include variable group sizes.
The speed at which the FEM produces good coverage results for terrain is unrivalled.
The simplicity of the algorithm and that it converges to the exact solution with smaller group sizes suggest no reason why this algorithm cannot be applied to the urban scattering problem.

• Small-scale clutter (amplitude $< 5M$) has a minor distortion effect on coverage.
The FEM converges to the exact solution on the rough terrain model.

• The results presented in this thesis justify the use of integral equations for sub-urban environments.
Further research based on the FEM should yield acceptable results for urban environments, up to now the domain of GTD/UTD and Ray-Tracing algorithms.
This is evinced by the fact that the FEM gives accurate results in a fraction of the time taken by other fast integral equation methods for the German profile which is mountainous.

APPENDIX A

The Surface Equivalence Principle

Consider the situation depicted in the figure below. Here we have two regions of space separated by a mathematical surface S. One of the regions is unbounded. Region 1 is homogeneous with electric and magnetic permeabilities ϵ_1 and μ_1 where Region 2 contains inhomogeneities that may include perfectly conducting materials.

A source electric and magnetic current (J_2, M_2) is located in Region 2 and radiating in

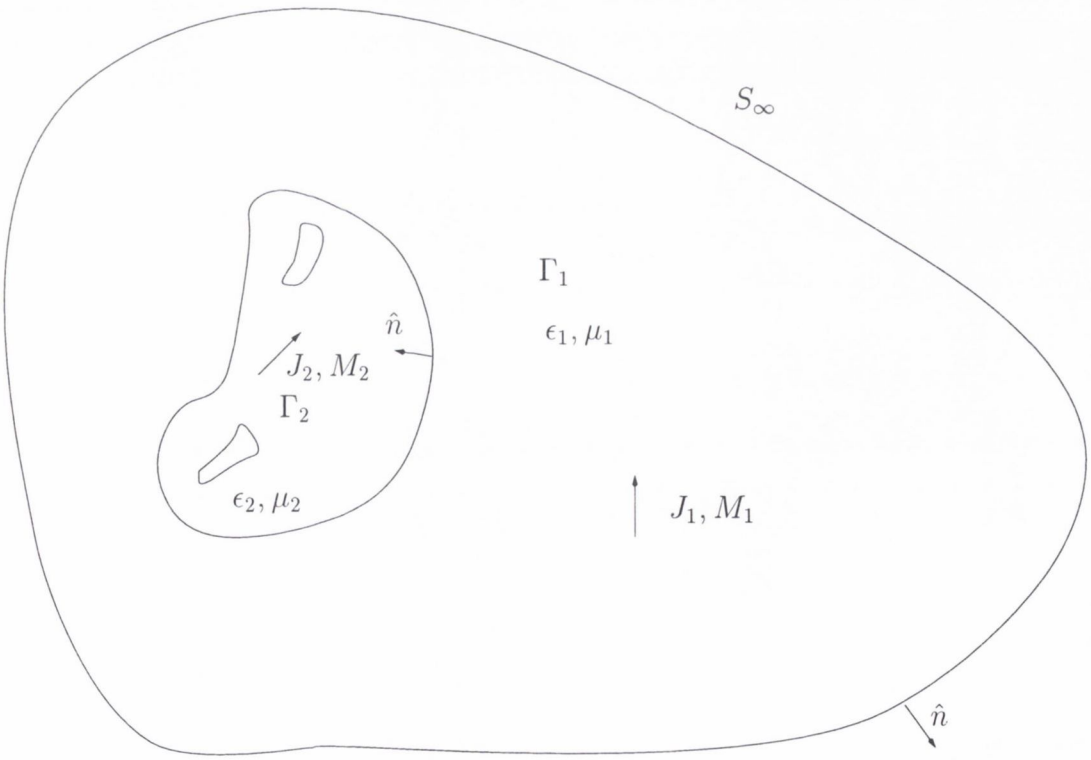

Figure 10.1: Two regions of space Γ_1 and Γ_2 separated by a mathematical surface S. Region 1 is homogeneous with (ϵ_1, μ_1) and Region 2 contains inhomogeneities that may include perfectly conducting materials. A source (J_2, M_2) in Region 2 produces fields (E_2, H_2) throughout Region 1. A second source (J_1, M_1) located in Region 1 radiates fields (E_1, H_1) throughout Region 1.

the presence of the inhomogeneities produces fields E_2 and H_2 throughout Region 1.

We postulate also a second source (J_1, M_1) located in Region 1 but radiating fields E_1 and H_1 in an homogeneous space having constitutive parameters ϵ_1 and μ_1.

The fields of both sources satisfy the Sommerfeld radiation condition [4] on the boundary at infinity (S_∞).

Throughout Region 1, Maxwell's equations can be written:

$$\nabla \times E_1 = -i\omega\mu_1 H_1 - M_1 \tag{10.1}$$

$$\nabla \times H_1 = -i\omega\epsilon_1 E_1 - J_1 \tag{10.2}$$

$$\nabla \times E_2 = -i\omega\mu_1 H_1 \tag{10.3}$$

$$\nabla \times H_2 = -i\omega\epsilon_1 E_2 \tag{10.4}$$

Therefore in Region 1 we can construct the following equations:

$$H_2 \cdot (\nabla \times E_1) = -i\omega\mu_1 H_2 \cdot H_1 - H_2 \cdot M_1 \tag{10.5}$$

$$E_2 \cdot (\nabla \times H_1) = i\omega\epsilon_1 E_2 \cdot E_1 + E_2 \cdot J_1 \tag{10.6}$$

$$H_1 \cdot \nabla \times E_2 = -i\omega\mu_1 H_1 \cdot H_2 \tag{10.7}$$

$$E_1 \cdot \nabla \times H_2 = i\omega\epsilon_1 E_1 \cdot E_2 \tag{10.8}$$

Combining these equations we get:

$$H_2 \cdot \nabla \times E_1 - E_1 \cdot \nabla \times H_2 + E_2 \cdot \nabla \times H_1 - H_1 \cdot \nabla \times E_2 = E_2 \cdot J_1 - H_2 \cdot M_1 \tag{10.9}$$

which is equivalent to:

$$\nabla \cdot (E_1 \times H_2 - E_2 \times H_1) = E_2 \cdot J_1 - H_2 \cdot M_1 \tag{10.10}$$

This is a statement of the Lorentz Reciprocity Theorem.

Integrating both sides over Region 1 and applying the divergence theorem:

$$\int\int\int_{\Gamma_1} \nabla \cdot Q dv = \int\int_S Q \cdot \hat{n} dS + \int\int_{S_\infty} Q \cdot \hat{n} dS \tag{10.11}$$

- where $\hat{n}$ is the normal vector on the surface pointing out of Region 1.

Then:

$$\int\int_S (E_1 \times H_2 - E_2 \times H_1) \cdot \hat{n} dS = \int\int\int_\Gamma (E_2 \cdot J_1 - H_2 \cdot M_1) dv \tag{10.12}$$

- where the integral over the surface at infinity vanishes as a result of the radiation condition.

Vector identities dictate that:

$$E_1 \times H_2 \cdot \hat{n} = -E_1 \cdot (\hat{n} \times H_2) \tag{10.13}$$

and

$$E_2 \times H_1 \cdot \hat{n} = -H_1 \cdot (E_2 \times \hat{n}) \tag{10.14}$$

Hence:

$$\int\int_S E_1 \cdot (-\hat{n} \times H_2) - H_1 \cdot (-E_2 \times \hat{n}) dS = \int\int\int_\Gamma (E_2 \cdot J_1 - H_2 \cdot M_1) dv \tag{10.15}$$

- which is a general statement of reciprocity.

Let us suppose that sources in Region 1 are described :

$$J_1 = \hat{u}\delta(\rho - \rho') \tag{10.16}$$

and

$$M_1 = 0 \tag{10.17}$$

- where ρ denotes the source point in Region 1 and ρ' represents the integration variable.

Then:

$$\hat{u} \cdot E_2 \mid_\rho = \int\int_S E_1 \cdot (-\hat{n} \times H_2) - H_1 \cdot (-E_2 \times \hat{n}) dS' \tag{10.18}$$

- where E_1 and H_1 are the fields produced at location ρ' in an infinite homogeneous space by sources J_1 and M_1 located at ρ.

These fields can be expressed as:

$$E_1(\rho') = \frac{\nabla'\nabla' + \beta^2}{i\omega\epsilon_1} \left(\hat{u} \frac{e^{-i\beta|\rho - \rho'|}}{4\pi \mid \rho - \rho' \mid} \right) \tag{10.19}$$

and

$$H_1(\rho') = \nabla' \times \left(\hat{u} \frac{e^{-i\beta|\rho-\rho'|}}{4\pi \mid \rho - \rho' \mid} \right) \tag{10.20}$$

-where the derivatives are taken w.r.t. the primed coordinates.

Because of the symmetry of the Green's function:

$$\nabla'\nabla' \cdot \left(\hat{u} \frac{e^{-i\beta|\rho-\rho'|}}{4\pi \mid \rho - \rho' \mid} \right) = \nabla\nabla \cdot \left(\hat{u} \frac{e^{-i\beta|\rho-\rho'|}}{4\pi \mid \rho - \rho' \mid} \right) \tag{10.21}$$

and

$$\nabla' \times \left(\hat{u} \frac{e^{-i\beta|\rho-\rho'|}}{4\pi \mid \rho - \rho' \mid} \right) = -\nabla \times \left(\hat{u} \frac{e^{-i\beta|\rho-\rho'|}}{4\pi \mid \rho - \rho' \mid} \right) \tag{10.22}$$

Hence:

$$\begin{aligned} \hat{u} \cdot E_2 \mid_\rho = \int\int_S \Bigg(& \frac{\nabla\nabla \cdot + \beta^2}{i\omega\epsilon_1} \left(\hat{u} \frac{e^{-i\beta|\rho-\rho'|}}{4\pi \mid \rho - \rho' \mid} \right) \cdot (-\hat{n} \times H_2) \\ & + \nabla \times \left(\hat{u} \frac{e^{-i\beta|\rho-\rho'|}}{4\pi \mid \rho - \rho' \mid} \right) \cdot (-E_2 \times \hat{n}) \Bigg) dS' \end{aligned} \tag{10.23}$$

- where the integration is performed in primed coordinates over the surface S.

The first term in the preceding equation can be modified using:

$$\begin{aligned} (-\hat{n} \times H_2) \cdot \nabla\nabla \cdot \left(\hat{u} \frac{e^{-i\beta|\rho-\rho'|}}{4\pi \mid \rho - \rho' \mid} \right) &= \sum_{i=1}^{3} \hat{x_i} \cdot (-\hat{n} \times H_2) \frac{\partial}{\partial x_i} \frac{\partial}{\partial u} \left(\frac{e^{-i\beta|\rho-\rho'|}}{4\pi \mid \rho - \rho' \mid} \right) \\ &= \frac{\partial}{\partial u} \sum_{i=1}^{3} \frac{\partial}{\partial x_i} \left(x_i \cdot (-\hat{n} \times H_2) \frac{e^{-i\beta|\rho-\rho'}}{4\pi \mid \rho - \rho' \mid} \right) \\ &= \hat{u} \cdot \nabla\nabla \cdot \left((-\hat{n} \times H_2) \frac{e^{-i\beta|\rho-\rho'|}}{4\pi \mid \rho - \rho' \mid} \right) \end{aligned} \tag{10.24}$$

- where x_i denote the three Cartesian variables and u is a variable defined along $\hat{u}$.

Furthermore:

$$\nabla \times \left(\hat{u} \frac{e^{-i\beta|\rho-\rho'|}}{4\pi \mid \rho - \rho' \mid} \right) \cdot (-E_2 \times \hat{n}) = \nabla \left(\hat{u} \frac{e^{-i\beta|\rho-\rho'|}}{4\pi \mid \rho - \rho' \mid} \right) \times \hat{u} \cdot (-E_2 \times \hat{n})$$

$$= -\hat{u} \cdot \nabla \left(\hat{u} \frac{e^{-i\beta|\rho-\rho'|}}{4\pi \mid \rho - \rho' \mid} \right) \times (-E_2 \times \hat{n})$$

$$= -\hat{u} \cdot \nabla \times \left((-E_2 \times \hat{n}) \hat{u} \frac{e^{-i\beta|\rho-\rho'|}}{4\pi \mid \rho - \rho' \mid} \right) \quad (10.25)$$

- which allows us to write:

$$\hat{u} \cdot E_2 \mid_\rho = \hat{u} \cdot \frac{\nabla\nabla \cdot + \beta^2}{i\omega\epsilon_1} \int\int_S (-\hat{n} \times H_2) \frac{e^{-i\beta|\rho-\rho'|}}{4\pi \mid \rho - \rho' \mid} dS' \quad (10.26)$$

$$-\hat{u} \cdot \nabla \times \int\int_S (-\hat{n} \times E_2) \frac{e^{-i\beta|\rho-\rho'|}}{4\pi \mid \rho - \rho' \mid} dS'$$

- which is the Surface Equivalence Principle.

APPENDIX B

Fourier Series and Transforms

The Fourier Series of a periodic signal f(t) is defined as:

$$FS(f(t)) = \sum_{-\infty}^{+\infty} C_k E^{ik\frac{2\pi}{\Omega}t} \tag{10.27}$$

where

$$C_k = \frac{1}{\Omega}\int_{\frac{-\Omega}{2}}^{\frac{\Omega}{2}} f(t)e^{-ik\frac{2\pi}{\Omega}t}dt \tag{10.28}$$

- where k is integer and Ω the period of f(t).

For a non-periodic signal the Fourier Transform must be used.

Here we consider the complete signal (ie in the range $-\infty$ to $+\infty$) to be a single period of a periodic signal.

In other words we let T above tend to infinity.

The Fourier Transform is thus defined:

$$\begin{aligned} F(\omega) &= \mathcal{F}(f(t)) \\ &= \int_{-\infty}^{+\infty} f(t)e^{-i\omega t}dt \end{aligned} \tag{10.29}$$

Because integration of a continuous signal is impossible with a computer we define the Discrete Time Fourier Transform as:

$$\begin{aligned} DTFT(f(t)) &= \mathcal{F}(f_s(t)) \\ &= \frac{1}{T}\sum_{-\infty}^{+\infty} F(\omega - n\omega_0) \end{aligned} \tag{10.30}$$

where

$$f_s(t) = \sum_{-\infty}^{+\infty} f(t)\delta(t - nT) \tag{10.31}$$

- the sampled signal, where T is the sampling period.

The Fourier Transform itself will be a sampled quantity on a computer and we can only sample a truncated signal so we must define and use the Discrete Fourier Transform:

$$\begin{aligned} DFT(f(t)) &= \mathcal{F}_s(f_s^{trunc}(t)) \\ &= \sum_{k=0}^{N-1} f(kt)e^{-i2\pi nk/N} \end{aligned} \tag{10.32}$$

- where $k, n = 0.....N-1$.

Consider:

$$\begin{aligned} \mathcal{F}(\sum_{-\infty}^{+\infty} \delta(t-nT) &= \int \sum_{-\infty}^{+\infty} \delta(t-nT)e^{-i\omega t}dt \\ &= \sum_{-\infty}^{+\infty} e^{-i\omega nT} \\ &= \sum_{-\infty}^{+\infty} e^{i\omega nT} \\ &= \sum_{-\infty}^{+\infty} \left(\frac{1}{\omega_0} \int_{\frac{-\omega_0}{2}}^{\frac{\omega_0}{2}} \omega_0 \sum_{-\infty}^{+\infty} \delta(\omega - n\omega_0)e^{-ik\frac{2\pi}{\omega_0}\omega} \right) e^{i\omega n\frac{2\pi}{\omega_0}} \\ &= \omega_0 \sum_{-\infty}^{+\infty} \delta(\omega - n\omega_0) \end{aligned} \tag{10.33}$$

- by definition of the Fourier Series given above, where $\omega_0 = \frac{2\pi}{T}$.

But:

$$\begin{aligned} \mathcal{F}(f(t)\sum_{-\infty}^{+\infty} \delta(t-nT)) &= \frac{1}{2\pi}F(\omega) * \mathcal{F}(\sum_{-\infty}^{+\infty} \delta(\omega - n\omega_0) \\ &= \frac{1}{2\pi}F(\omega) * \omega_0 \sum_{-\infty}^{+\infty} \delta(\omega - n\omega_0) \\ &= \frac{1}{T}\sum_{-\infty}^{+\infty} F(\omega - n\omega_0) \end{aligned} \tag{10.34}$$

Hence:

$$\mathcal{F}(f_s(t)) = \frac{1}{T}\sum_{-\infty}^{+\infty} F(\omega - n\omega_0) \tag{10.35}$$

Also consider:

$$\begin{aligned}\mathcal{F}(f_s(t)) &= \int \sum_{-\infty}^{+\infty} f(t)\delta(t-nT)e^{-i\omega t}dt \\ &= \sum_{-\infty}^{+\infty} f(nT)e^{i\omega nT} \end{aligned} \tag{10.36}$$

So:

$$\mathcal{F}(f_s^{trunc}(t)) = \sum_{n=0}^{N-1} e^{-i\omega nT} \tag{10.37}$$

Hence:

$$\mathcal{F}_s(f_s^{trunc}(t)) = \int \sum_{n=0}^{N-1} e^{-i\omega nT}\delta(\omega - k\frac{\omega_0}{N})d\omega \tag{10.38}$$

- where $k = 0.....N-1$.

From which follows:

$$\begin{aligned}\mathcal{F}_s(f_s^{trunc}(t)) &= \sum_{n=0}^{N-1} f(nT)e^{-i\omega knT/N} \\ &= \sum_{n=0}^{N-1} f(nT)e^{-i\omega knT/N} \end{aligned} \tag{10.39}$$

- which is the DFT.

To simplify the following analysis of the Inverse DFT we define the following:

$$w = e^{\frac{i2\pi}{N}} \tag{10.40}$$

The existence of the variable T is assumed when referring to the integer k or n and F will denote the DFT of the signal f(t).

Then the DFT can be written:

$$F(k) = \sum_{n=0}^{N-1} f(n)w^{-nk} \tag{10.41}$$

- where $k = 0....N-1$.

Conversely the Inverse Discrete Fourier Transform is:

$$f(n) = \frac{1}{N} \sum_{k=0}^{N-1} F(k) w^{kn} \tag{10.42}$$

- where $n = 0....N-1$.

Hence:

$$\begin{aligned} f(n) = \frac{1}{N} \sum_{k=0}^{N-1} F(k) w^{kn} &= \frac{1}{N} \sum_{k=0}^{N-1} w^{kn} \sum_{m=0}^{N-1} f(m) w^{-km} \\ &= \frac{1}{N} \sum m = 0^{N-1} f(m) \left(\sum_{k=0}^{N-1} w^{(n-m)k} \right) \end{aligned}$$

But:

$$\sum_{k=0}^{N-1} w^{(n-m)k} = \frac{1 - w^{(n-m)N}}{1 - w^{(n-m)}} \tag{10.43}$$

and

$$\begin{aligned} w^N &= e^{i2\pi} \\ &= 1 \end{aligned} \tag{10.44}$$

we have:

$$\frac{1 - w^{(n-m)N}}{1 - w^{(n-m)}} = N \tag{10.45}$$

- $IFF\ n = m$.

So:

$$\begin{aligned} \frac{1}{N} \sum_{k=0}^{N-1} F(k) w^{kn} &= \frac{1}{N} f(n) N \\ &= f(n) \end{aligned} \tag{10.46}$$

The Fast Fourier Transform

The Fast Fourier transform is an algorithm designed to speed up the computation time of the discrete Fourier Transform.

By definition the DFT and IDFT can be written in matrix form thus:

$$\begin{pmatrix} F(0) \\ F(1) \\ F(2) \\ \vdots \\ F(N-1) \end{pmatrix} = \begin{pmatrix} 1 & 1 & 1 & \dots & 1 \\ 1 & w^{-1} & w^{-2} & \dots & w^{-(N-1)} \\ 1 & w^{-2} & w^{-4} & \dots & w^{-2(N-1)} \\ \vdots & \vdots & \vdots & \dots & \vdots \\ 1 & w^{-(N-1)} & w^{-2(N-1)} & \dots & w^{-(N-1)^2} \end{pmatrix} \begin{pmatrix} f(0) \\ f(1) \\ f(2) \\ \vdots \\ f(N-1) \end{pmatrix} \quad (10.47)$$

$\equiv$

$$[F] = [\hat{W}_N][f] \quad (10.48)$$

In the same manner the Inverse FFT can be expressed as:

$$[f] = \frac{1}{N}[W_N][F] \quad (10.49)$$

- where $[W_N]$ is obtained from $[\hat{W}_N]$ by replacing w^{-k} with w^k.

Where N is a power of '2' we then decompose the sequence $f(n)$ into two interleaved sequences, one with even arguments and the other with odd arguments.

Using this decomposition we can write the first $\frac{N}{2}$ members of the transform sequence $F(k)$ as:

$$\begin{pmatrix} F(0) \\ F(1) \\ F(2) \\ \vdots \\ F(\frac{N}{2}-1) \end{pmatrix} = \begin{pmatrix} 1 & 1 & \dots & 1 \\ 1 & w^{-2} \dots w^{-2(\frac{N}{2}-1)} & & \\ 1 & w^{-4} \dots w^{-4(\frac{N}{2}-1)} & & \\ \vdots & \vdots & \dots & \vdots \\ 1 & w^{-2(\frac{N}{2}-1)} & \dots & w^{-2(\frac{N}{2}-1)^2} \end{pmatrix} \begin{pmatrix} f(0) \\ f(2) \\ f(3) \\ \vdots \\ f(N-2) \end{pmatrix} \quad (10.50)$$

$$+\begin{pmatrix} 1 & 1 & \dots & 1 \\ 1 & w^{-1} & \dots & w^{-(N-1)} \\ 1 & w^{-2} & \dots & w^{-2(N-1)} \\ \vdots & \vdots & \dots & \vdots \\ w^{(-(\frac{N}{2}-1)} & w^{-3(\frac{N}{2}-1)} \dots w^{-(\frac{N}{2}-1)(N-1)} & & \end{pmatrix} \begin{pmatrix} f(1) \\ f(3) \\ f(4) \\ \vdots \\ f(N-1) \end{pmatrix}$$

The two latter argument matrices, $[\hat{\hat{W}}/2]$ and $[\hat{W}/2]$ are related by:

$$[\hat{\hat{W}}/2] = \begin{pmatrix} 1 & 0 & 0 & 0 \\ 0 & w^{-1} & 0 & 0 \\ 0 & 0 & w^{-2} & 0 \\ 0 & 0 & 0 & w^{-(\frac{N}{2}-1)} \end{pmatrix} [\hat{W}_{N/2}] \tag{10.51}$$

$\equiv$

$$[\hat{\hat{W}}_{N/2}] = [\hat{W}_d][\hat{W}_{N/2}] \tag{10.52}$$

and so:

$$\begin{pmatrix} F(0) \\ F(1) \\ F(2) \\ \vdots \\ F(\frac{N}{2}-1) \end{pmatrix} = [\hat{W}_{N/2}] \begin{pmatrix} f(0) \\ f(2) \\ f(4) \\ \vdots \\ f(N-2) \end{pmatrix} + [\hat{W}_d][\hat{W}_{N/2}] \begin{pmatrix} f(1) \\ f(3) \\ f(5) \\ \vdots \\ f(N-1) \end{pmatrix} \tag{10.53}$$

In a similar manner the last $\frac{N}{2}$ members of the sequence $F(k)$ can be written as:

$$\begin{pmatrix} F(\frac{N}{2}) \\ F(\frac{N}{2}+1) \\ F(\frac{N}{2}+2) \\ \vdots \\ F(N-1) \end{pmatrix} = [\hat{W}_{N/2}] \begin{pmatrix} f(0) \\ f(2) \\ f(4) \\ \vdots \\ f(N-2) \end{pmatrix} - [\hat{W}_d][\hat{W}_{N/2}] \begin{pmatrix} f(1) \\ f(3) \\ f(5) \\ \vdots \\ f(N-1) \end{pmatrix} \tag{10.54}$$

Clearly the calculations of $F(k)(k = 0; N/2 - 1)$ are identical to the calculations of

$F(k)(k = N/2; N - 1)$ except for the sign change.

Thus we have succeeded in reducing the calculation of an N-point Fourier Transform to the calculation of two N/2-point transforms.

If this process is repeated a number of steps equal to:

$$\log N - 1 = \log_2(\frac{N}{2}) \tag{10.55}$$

- then we arrive at transforms of order two.

Each of these two-point transforms has:

$$[\hat{W}_2] = \begin{pmatrix} 1 & 1 \\ 1 & -1 \end{pmatrix} \tag{10.56}$$

- and no multiplications are needed.

Each stage of the reduction requires $\frac{N}{2}$ multiplications, therefore the total number of (complex) multiplications required for the calculation of the complete transform is:

$$M = (\frac{N}{2}) \log_2(\frac{N}{2}) \tag{10.57}$$

and the total number of (complex) additions requires is:

$$A = N \log_2 N \tag{10.58}$$

which compares with $(N - 1)^2$ multiplications and $N(N - 1)$ additions were the direct method to be used.

BIBLIOGRAPHY

[1] D. Livingston, 'The physics of Microwave Propagation' Prentice-Hall Electrical Engineering Series, 1970.

[2] T.G. Kyle,'Atmospheric Transmission Emission and Scattering' Pergamon Press, 1991.

[3] M.P. Hail,'Effects of the Troposphere on Radio Communication' IEE Press, 1979.

[4] A. Sommerfeld,'Partial Differential Equations in Physics' New York: Academic Press, 1949.

[5] C. Balanis,'Advanced Engineering Electromagnetics' Wiley 1989.

[6] W. C. Chew, Waves and Fields in Inhomogeneous Media, ch. 1 Preliminary Background. IEEE Press, 1990.

[7] W.C. Chew, 'Waves and Fields in Inhomogeneous Media' New York, Van Nostrand Reinhold 1990.

[8] C.C. Lu and W.C. Chew,'Fast Far Field Approximation for Calculating the RCS of Large Objects' Micro. Opt. Tech. Lett. Vol. 8, No. 5, pp.238–241, 1995.

[9] C.C. Lu and W.C Chew,'Fast Algorithm for solving hybrid integral equations' IEE Proceedings-H Vol.140, No.6 pp.455–460, 1993.

[10] J. M. Song and W. C. Chew,'Multilevel fast multipole algorithm for solving combned field integral equations of electromagnetic scattering' Micro. Opt. Tech. Lett. Vol. 10, No. 1, pp.14–19, 1995.

[11] Y.M. Wang and W.C. Chew:'An Efficient Algorithm for the solution of a Scattering Problem', Micro Opt. Tech. Let., 1990 3,(3), pp 102-106.

[12] Y.M. Wang and W.C. Chew: 'A Fast Algorithm for the solution of a Scatering Problem using a Recursive Aggregate Matrix Method', Micro. Opt. Tech. Lett., 1990, 3, (5), pp 164 - 169.

[13] L. Gurel, Y.M. Wang, G, Otto, R.Wagner, Q.H. Liu and W.C. Chew: 'A Generalized Recursive Algorithm for Wave scattering Solutions in Two Dimensions'. IEEE Trans., 1992, MTT-40, (4), pp. 716-723.

[14] R. Wagner and W.C. Chew,'A Ray-Propagation Fast Multipole Method' Micro. Opt. Tech. Lett. Vol. 7 No. 10, pp. 435–438, 1994.

[15] H. Baher Analog and Digital Signal Processing. ch. 10 Stochastic Signals and Power Spectra. Wiley, 1990.

[16] A. F. Peterson, S. L. Ray, R. Mittra Computational Methods for Electromagnetics, ch. 1 Electromagnetic Theory. ch. 2 Integral Equation Methods for Scattering from Infinite Cylinders. IEEE Press, 1960.

[17] J. Van Bladel, Singular Electromagnetic fields and Sources, ch. 2 Concentrated Sources. Wiley, 1989.

[18] R. F. Harrington, Field Computation by Moment Methods, ch. 3 Two Dimensional Electromagnetic Fields. IEEE Press, 1968.

[19] R. F. Harrington, Time Harmonic Electromagnetic Fields, pp 18-19 McGraw-Hill 1961.

[20] K. Umashankar and A. Taflove, Computational Electromagnetics, ch. 5 Two Dimensional Homogeneous Dielectric Object: TM and TE Polarizations. Artech House, 1993.

[21] D. Hoppe and Y. Rahmat-Samii, Impedence Boundary Conditions in Electromagnetics, ch. 1 Introduction. Taylor and Francis, 1995.

[22] M.A. Leontovich and V.A Fock, 'Solution of the Problem of Propagation of Electromagnetic Waves along the Earth's Surface by the Method of the Parabolic Equation' J. Phys. of the USSR Vol. 10, pp. 13-24, 1946.

[23] E.Kenny, W.M. O'Brien, E.Kenny and P.Cullen, 'Fast numerical calculation of UHF propagation over two dimensional dielectric terrain using an integral equation method' Proceedings of IEEE Vehicular Technology Conference VTC 97 ISBN 0-7803-3659-3 pp.1118-1121 June 1997.

[24] C. Brennan, P. Cullen and L. Rossi,'A high speed adaptive methodology for calculating UHF propagation loss over terrain' PIMRC97, Helsinki, September 1997.

[25] C. Brennan and P. Cullen,'Tabulated Interaction Method for UHF terrain propagation problems' IEEE Trans. Ant. Prop. Vol.46 No.5 pp.738-739 1998.

[26] C.Brennan and P. Cullen, 'Application of the Fast far-field approximation to the computation of UHF path loss over irregular terrain' IEEE Transactions on Antennas and Propagation Vol. 46 N0. 6 1998.

[27] C. Brennan and P. Cullen, 'Multilevel Tabulated Interaction Method applied to UHF propagation over irregular terrain' IEEE Transactions on Antennas and Propagation Vol. 47 N0. 10 Oct' 1999.

[28] C.Brennan and P.Cullen, 'An MFIE based tabulated interaction method for UHF terrain propagation problems. To appear in IEEE Transactions on Antennas and Propagation.

[29] C.Brennan and P.Cullen, 'The use of integral equations in mobile radio planning' Journal de Societe Belge des Ingenieurs de Telecommunications et d'electronique (SITEL) No. 1 1997 pp. 21-36 ISSN 0035-3248.

[30] L.Rossi, C.Brennan and P.Cullen, 'An implementation of a multilevel fast far-field algorithm for solving electric field integral equations' To appear in IEE Proceedings-H

[31] C.Brennan and P.Cullen 'A method to speed up the iterative solutions of terrain scattering problems' Proceedings of the 10th International Conference on Antennas and Propagation ICAP 97 [ISBN 0 85296 685 7] pp. 294-298 Edinburgh, April 1997.

[32] C.Brennan and P.Cullen 'On the tabulated interaction method applied to UHF propagation over terrain' COST 259 Temporary Document TD(97) 005 Torino Italy, 1997.

[33] C.Brennan and P.Cullen 'Efficient techniques for the computation of UHF grazing incidence terrain scattering COST Temporary Document TD(97) 091 Lisbon, Sept' 1997.

[34] C.Brennan and P.Cullen 'An Integral Equation approach to long distance UHF terrain propagation' COST 259 Temporary Document TD(98) 064

[35] L.Rossi C.Brennan and P.Cullen 'A method for producing a sparse discretised integral operator allowing a priori determination of the interaction terms' International Conference on Electromagnetics in Advanced Applications' Torino Italy, Sept' 1999.

[36] L.Rossi C.Brennan and P.Cullen 'A high speed adaptive methodology for calculating UHF propagation loss over terrain' 8th IEEE int Symp. on Personal Indoor and Mobile Radio Communications Helsinki, Sept' 1997.

[37] L.Rossi C.Brennan and P.Cullen 'Extension of efficient integral equation methods to propagation over dielectric terrain' URSI General Assembly Toronto, Canada August 1999.

[38] C.Brennan and P.Cullen 'Efficient techniques for the computation of UHF grazing incidence terrain scattering (Invited Paper) International Conference on Electromagnetics in Advanced Applications ICEAA97, Torino, Sept' 1997, pp. 351-353.

[39] C.Brennan and P.Cullen 'Recent advances in the numerical solution of integral equations applied to EM scattering from terrain. Proceedings 14th Annual Review of Progress in Applied Computational Electromagnetics Naval Postgraduate School, Monterey California March 1998 Vol. 1 pp. 390-396.

[40] C.Brennan and P.Cullen and L.Rossi 'An analytical approximation of the TIM look-up table' COST 259 Temporary Document TD(99) 025 Thessaloniki, Greece, Jan' 1999.

[41] C.Brennan and P.Cullen and L.Rossi 'Efficient integral equation based analysis of plane wave scattering from infinite periodic perfectly conducting structures' International Conference on Electromagnetics in Advanced Applications ICEAA99 Torino Italy, Sept' 1999.

[42] O. Brigham, The Fast Fourier Transform' Prentice Hall 1988.

[43] F.X. Canning, 'The Impedance Matrix Localisation (IML) Method for Moment Method Calculations' IEEE Trans. Ant. and Prop. Magazine, October 1990 pp.18–30.

[44] F.X. Canning, 'Sparse Approximation for Solving Integral Equations with Oscillatory Kernels' SIAM J. Sci. Stat. Comput. Vol. 13,No. 1, pp. 71–87 Jan. 1992.

[45] F.X. Canning, 'Interaction Matrix Localisation (IML) permits solution of larger scattering problems' IEEE Trans. Magnetics. Vol. 27, No. 5 pp.4275–4278 1991.

[46] F.X. Canning, 'Improved Impedance Matrix Localisation Method' IEEE Trans. Ant. and Prop. Vol. 41, No. 5, May 1993.

[47] N. Engheta, W. D. Murphy, V. Rokhlin and M.S. Vassiliou,'The Fast Multipole Method (FMM) for Electromagnetic Scattering Problems' IEEE Trans. Ant. Prop. Vol 40, No 6 pp. 634-641, 1992.

[48] R.F.Harrington,'Field Computation by Moment Methods' MacMillan, New York, 1968.

[49] M. Hata,'Empirical Formula for Propagation Loss in Land Mobile Radio Services' IEEE Trans. Veh. Technol. Vol.29 No.3 pp.317–325, 1980.

[50] M.Hestenes and E. Stiefel,'Method of Conjugate Gradients for Solving Linear Systems' J. Res. Nat. Bur. Stand. Vol. 49 pp.409–436, 1952.

[51] J.T. Hviid, J. B. Andersen, J Toftgård and J. Bøjer, 'Terrain Based Propagation model for Rural Terrain - An Integral Equation Approach' IEEE Trans. Ant. Prop. Vol. 43 No. 1 pp. 41–46, 1995.

[52] A. Ishimaru,'Electromagnetic Wave Propagation, Radiation and Scattering' Prentice Hall, 1991.

[53] D.S. Jones,'Methods in Electromagnetic Wave Propagation' Clarendon Press, Oxford, 1994.

[54] J.B. Keller,'Geometric Theory of Diffraction' Jnl. Opt. Soc. Am. Vol.52, pp. 116–130, 1962.

[55] R.G. Kouyoumjian and P.H. Pathak, "A Uniform Geometric Theory of Diffraction for an Edge in a Perfectly Conduction Surface", Proc. IEEE, vol 62, no 11, pp. 1448-1461, November 1974.

[56] M.F.Levy,'Parabolic Equation Modelling of Propagation over Irregular Terrain' Elec. Letters Vol.26 No.15 pp.1153–1155, 1990.

[57] D. Moroney and P. J. Cullen,'A Fast Integral Equation Approach to UHF Coverage Estimation' in Mobile and Personal Communications pp. 343-350, edited E. del Re. 1995 Elsevier Press.

[58] D. Moroney and P. J. Cullen,'The Green's Function Perturbation Method for the solution of Electromagnetic Scattering Problems' Progress in Electromagnetic Research PIER 15 pp. 221–252 1997.

[59] P. MacSharry, D. Moroney and P. J. Cullen, 'Wave sacttering by a two-dimensional band-limited fractal surface based on a perturbation of the Green's function' Journal of Applied Physics, Vol. 78 No. 12 pp. 6490-6948 December 1995.

[60] P.MacSharry, D. Moroney and P. J. Cullen, 'Wave scattering by a two dimensional pressure release surface based on a perturbation of the Green's function' Journal of the Acoustical Society of America Vol. 98 N0. 3 pp. 1699-1716 September 1995.

[61] V. Rokhlin, 'Rapid Solution of integral equations of scattering theory in two dimensions' Jnl. Comp. Phys. Vol. 36,No. 2,pp. 414–439, 1990.

[62] E.P. O Nuallain, 'The Field Extrapolation Method' Internal Report, Dept. Electronic Engineering, Trinity College Dublin. Mar. 2000.